Computer Modelling and Polarimetric Studies of the Magnetic Field in the Crab Nebula Plasma

by

Amanda Jane Brace

Thesis submitted for the degree of Master of Science
to the Faculty of Science, University of Glasgow.

Department of Physics and Astronomy,
University of Glasgow,
University Avenue,
Glasgow,
G12 8QQ.

Acknowledgements

I would like to thank Professors John Brown and Ernest Laing for their supervision over the past two years. Many thanks are due to Professor Jim Hough for the last minute proof reading of some sections of this thesis and valuable moral support.

Thank you to Declan for his help with the frozen-in field equation, Carolyn for being able to spell, Big David, Wee David, Amarjit, Alan, Helen and Jim. A special thank you to Andrew for proof reading this thesis, helping with the IBM produced pictures, getting rid of my Mac viruses, mopping my fevered brow, being able to cook and many other things which are far too numerous to go into here! Thanks to J.F. for putting up with all the long phone calls and to all the people at Oxfam, Byres Road who helped to keep me sane. Thanks to my parents for not asking when I was going to get a "real job" too often and "Hello to everyone else who knows me!".

I would like to thank the Royal Observatory Edinburgh for provision of McLean, Aspin and Reitsema's data on computer tape, and Andy Sibbald at the Kelvin Laboratory for transferring the data onto the VAX computer at East Kilbride.

This project was sponsored by the Science and Engineering Research Council.

Contents

Abstract

In this thesis a study of polarimetric observations of the Crab nebula is presented. We also describe the development of a computer model which predicts the polarization pattern for a dipole magnetic field structure. The Crab nebula is a plasma and it's plasma behaviour is relevant to the development of a computer model of the nebular magnetic field. Therefore, we also examine in this thesis the basic plasma physics required for study of the Crab nebula.

Chapter 1 is an introduction to this thesis outlining the raison d'être of this project and presenting the relevant background information about the Crab nebula. Brief descriptions of the physical properties and history of the nebula are given, followed by a more detailed review of past theoretical works which have a bearing on this thesis.

In chapter 2 we outline the theory of polarization of electromagnetic waves. The polarization parameters used in this thesis, the Stokes intensities and Stokes parameters, are introduced. The expressions for degree and angle of polarization derived from the Stokes intensities or parameters are formulated and we discuss these quantities and the effects of depolarization with relevance to this work.

From the review in chapter 1 we find that it has long been known that the mechanism by which the observed radiation from the Crab nebula is produced is the synchrotron mechanism. Chapter 3 presents the theory of synchrotron radiation. In the latter sections of chapter 3 we examine the theory of polarization of synchrotron radiation and arrive at the equations required to calculate the Stokes intensities of synchrotron radiation for any given electron density distribution and magnetic field structure.

In chapter 4 we consider the plasma aspects of the Crab nebula. A consideration of the macroscopic magnetohydrodynamic equations, which are a generalised form of Ohm's law, the Maxwell curl equations for the electric and magnetic fields, the

equation of continuity, the equation of motion and the adiabatic equation for conservation of energy for the plasma, lead us to the concept of "frozen-in" magnetic fields. This has great relevance to the behaviour of the Crab nebula and we discuss recent papers in which attempts to solve the frozen-in field equation have been presented. We also include a discussion and a brief treatment of the frozen-in field equation which was made as a result of the study of recent work in this field.

Chapters 5 and 6 make up the body of original work in this thesis. Chapter 5 presents the methods and results of analysis of the polarimetric data of Woltjer and McLean, Aspin and Reitsema. These observations are separated by a period of 26 years and so we examined the data for changes in polarization angle, and thus magnetic field direction, which might have occurred during this time. We also searched the data for centres of polarization or intensity patterns by a method of symmetry testing.

Chapter 6 describes the development and presents the results of the computer generated model of a dipole magnetic field. We begin by considering special cases of the orientation of the dipole axis to the observer's line of sight and then move on to a model which allows any angle of inclination of the observer to the dipole axis. The final version of the model incorporates a component of magnetic field in the ϕ-direction of the dipole coordinate system. This model produced some interesting results.

The results of the data analysis and computer modelling are discussed in the relevant chapters, but chapter 7 contains some concluding remarks and an overview of the thesis. All computer programs written during the course of this project were written in Fortran and are included in the appendices at the back of the thesis.

Figure 1.1 (facing): A photograph of the Crab nebula taken by Baade in 1954 [9] at a wavelength of approximately 6000 angstroms. This photograph shows clearly the filamentary structure of the Crab nebula. The north direction is vertically upwards and east is to the left in this picture; thus, this photograph has the same orientation as the polarization maps of the Crab nebula which are presented in chapter 5 of this thesis. The extent of the nebula shown by this photograph is the same as that covered by the photometric polarization data taken by Baade, analysed and presented by Woltjer [1], which is used in this thesis. The CCD polarization data of McLean, Aspin and Reitsema [2], also used in this thesis, covers an area which is slightly smaller than the whole extent of the Crab nebula in this photograph.

Chapter 1

Introduction

1.1 About this Thesis

The contents of this thesis not only describe the work undertaken at Glasgow University between October 1987 and October 1989, but also describe the theoretical background which is necessary for an understanding of this work.

In this chapter, chapter 1, a brief review of the history and properties of the Crab nebula is given. We see what makes the Crab nebula a unique astrophysical object, why it has attracted so much attention from both theoretical and observational astronomers in the past and that there still remains much to be done before we can claim to understand the Crab nebula fully. Section 1.4 is a review of theoretical works on aspects of the nebula which are relevant to this thesis. The problems discussed here are by no means the only ones with which the Crab nebula presents us but the whole body of theoretical and observational work on the nebula is far greater than can be covered in this review and much of it has no bearing on this project.

Chapter 2 covers the basic theory of polarization and discusses the use of Stokes intensities and Stokes parameters with relevance to this thesis. The theory of polarization as related to the Crab nebula is taken further in chapter 3. Once we have outlined the theory of the processes of synchrotron radiation, which is the radiation mechanism of the Crab nebula, we go on to consider the polarization of such radiation. It is the polarization of synchrotron radiation which is recorded by the data of Woltjer [1] and McLean, Aspin and Reitsema [2] which are analysed in chapter 5.

In this thesis we also discuss the study of the Crab nebula as a plasma (chapter 4), the analysis of observational polarization data from the nebula (chapter 5) and the

development of a computer generated model of magnetic field structures similar to that of the nebula (chapter 6). Chapter 4 is mainly a review of plasma theory as it relates to the Crab nebula and chapters 5 and 6 comprise the body of original work in this thesis. Chapter 7 presents the conclusions drawn from this work.

The main motivation of this project was to study Woltjer [1] and McLean, Aspin and Reitsema's [2] data sets with the aim of finding out more about the structure of the magnetic field of the Crab nebula. The tests and manipulations performed on the data are discussed in chapter 5. The computer model was developed with the intent to compare the model with the observational data once the model was a sufficiently realistic representation of the nebula to make this exercise worthwhile.

As a result of considering the addition of toroidal components of magnetic field to the computer model, the analysis of the frozen-in field equation in chapter 4, section 4.5 was made. Solution of this equation is in itself a major task and, although not within the scope of this project, it is a prerequisite for further progress in the development of a realistic computer generated model of the Crab nebula magnetic field structure.

1.2 The Crab Nebula

The Crab nebula is the remnant of a supernova explosion which was observed and recorded by Chinese astronomers in 1054 AD. The nebula itself is a turbulent, expanding mass of diffuse cool gas and relativistic plasma. The gaseous composition of the nebula is mainly hydrogen and helium with some carbon, oxygen, nitrogen and small amounts of heavier elements [3]. The plasma, which consists of electrons and positrons [4], is the source of the nebula's radiation output from X-ray to radio wavelengths and it is the interaction of this plasma with the nebular magnetic field which is of most interest in this thesis. Within the nebula lies the Crab pulsar NP0532 +21. This highly magnetised, rotating neutron star provides

both the magnetic field and plasma particles which make up the nebula. Thus the pulsar is also of much interest in this work.

The Crab nebula lies approximately 2kpc from Earth in the direction of the constellation Taurus. The nebula itself is roughly elliptical in shape with a major axis, when observed at visual wavelengths, of 4pc and a minor axis of 3pc. The major axis lies in the north-west to south-east direction which is approximately parallel to the galactic equator. The three dimensional shape of the nebula is thought to be that of a prolate spheroid [5,6] so the axis along our line of sight is approximately 3pc. The size of the nebula at X-ray wavelengths is only a quarter that at optical wavelengths but the radio nebula is slightly larger than the optical nebula [7].

The measured expansion speed of the filaments of the nebula is approximately 2000 kms^{-1} [5]. The filaments within the nebula move with speeds close to the expansion speed but some features may move much faster than this. Particles ejected from the pulsar, which emit the synchrotron radiation that is observed in the nebula, move at relativistic speeds. The pulsar itself is moving towards the north-west with a large proper motion, which corresponds to a motion of 110 kms^{-1} in the plane of the sky, which was first measured by van Maanen in 1928 [8]. This motion is thought to explain certain asymmetries in brightness and structure in the north-west region of the nebula (see section 1.4). An extrapolation of the pulsar's position backwards in time to the supernova event does not coincide with the calculated expansion centre of the nebula [5]. No plausible explanation for this discrepancy has been proposed. Also, the geometrical expansion centre of the nebula does not coincide with the centre of mass estimated from the distribution of matter in the filaments of the nebula; obviously, the expansion of the Crab nebula is not symmetrical in terms of mass. This is not a surprising result considering the uneven distribution of mass within the nebula which can be seen in photographs of the nebula which show its

filamentary structure, e.g. figure 1.1[9]; studies of optical emission lines [3] show that the filaments are made up mainly of hydrogen and helium in higher concentrations than the rest of the nebula.

The magnetic field at the surface of the pulsar is $3x10^{12}$ G [10]. The average nebular magnetic field is approximately 10^{-3} - 10^{-4} G [11]. The exact structure of the nebular field is not known; neither is the mechanism by which it is produced. The aim of this thesis is to improve our understanding of these problems. The density of the electrons within the nebula is not very well known but has been measured as between 400 - 4000 cm^{-3} from [OII] and [SII] line ratios [3]. Osterbrock [12] calculated the electron density to be $1000cm^{-3}$. The chemical composition of the nebula is reasonably well known. Helium is overabundant with respect to hydrogen compared to solar abundances and accounts for 75% by mass of the composition of the filaments [3]. Other elements are present in the ratios found in the Sun but progenitor models for the pre-supernova star predict that more nitrogen should be present than is actually observed [3].

The Crab nebula is a strong X-ray and radio source and has a well measured spectrum at most wavelengths. The discovery that the Crab nebula emission was due to the synchrotron process (see section 1.3) was a major step forward in understanding the processes which govern the Crab nebula. However, the spectral index of the synchrotron radiation spectrum, which is discussed in chapter 3, varies with wavelength. The spectrum can be represented as a power law in either the visual, X-ray or radio region but has a different spectral index in each region. This variation of the spectral index with wavelength has been a major problem in the construction of models of the nebula but was most successfully overcome by Kennel and Coroniti [13].

1.3 The History of the Crab Nebula

From its birth in 1054 AD until the late 1960s the Crab nebula was a unique astrophysical object. In 1970 the Crab nebula was the sole topic of an I.A.U. Symposium [14] and it is indicative of the continuing importance of the Crab nebula that an entire workshop was devoted to it in 1984 [15]. Until February 1987 the Crab pulsar was the only pulsar whose birth date was known to the year but even SN1987A cannot displace the Crab nebula from its special place in astrophysics. The Crab nebula is the youngest supernova remnant in our Galaxy and is one of the most extensively studied astrophysical objects and certainly the most extensively studied supernova remnant. The Crab nebula provides an opportunity to study an evolved supernova remnant in all regions of the electromagnetic spectrum as it is a strong emitter of radiation in the X-ray, optical and radio regions. The Crab is also one of the few members of the subclass of supernova remnants known as plerions, or centre filled remnants, of which it was also the first known member. The Crab pulsar had the fastest observed spin rate (33 milliseconds) until the discovery of the first millisecond pulsar in the early 1980s.

Although the supernova explosion which created the nebula was observed by the Chinese in 1054, the Crab nebula was only "discovered" in the West in 1731 by John Bevis. It was catalogued in 1758 as number one in Messier's catalogue of objects which were a nuisance to observers of comets. Despite this, the Crab nebula became an object of much interest to astronomers at the time. Lord Rosse described the nebula as having the shape of a crab's claw and, although it may stretch the imagination to see this resemblance in figure 1.1, the name "Crab nebula" fell into common usage. By the end of the nineteenth century it was known that the nebula was an area of diffuse emission and not a group of unresolved stars, but how was the emitted radiation produced?

In the 1920s the nebula was conclusively identified as the remnant of the 1054

event [16]. The structural changes in the nebula due to its rapid expansion were observed and its expansion speed measured for the first time [17,18]. Spectra of the nebula were obtained by Slipher [19] allowing the study of the chemical composition and velocities within the nebula. The proper motion of the South Preceding Star was measured by van Maanen but this star had not yet been identified as the remnant of the supernova explosion. This identification was made by Baade[20] and Minkowski [21] in the early 1940s.

From 1949-1970 it was the nonthermal aspects of the Crab nebula which made it famous. In 1952 Shklovskii [22] proposed that the radiation emitted by the nebula was synchrotron radiation and thus should be linearly polarized (for details of the polarization of synchrotron radiation see chapter 3). This proposal can be considered to be the birth of high energy astrophysics. Dombrowsky [23] and Vashakidze [24] observed linear polarization of the nebula's optical wavelength radiation only two years after Shklovskii's prediction. Following this several studies of polarization of the nebula were made by Oort and Walraven [9], Walraven [23] and Baade [24]. These studies were performed partly to confirm Dombrowsky and Vashakidze's results and partly to make more detailed observations and thus improve our knowledge of the Crab nebula. The main conclusions of these studies were that the average direction of the polarization vector was north-west to south-east i.e. along the major axis of the nebula. The polarization data taken by Baade in 1954 and surface brightness distribution measurements by Walraven were published simultaneously in 1957 [25,1] and are used in this study. Details of this data set and of the other data set used (taken by McLean, Aspin and Reitsema in 1981 [2]) can be found in chapter 5.

During the 1950s and 60s popular and basic level texts on astronomy mainly discussed the X-ray and radio observations of the Crab nebula. However, the Crab is an excellent example of the role that visual wavelength observations play in

astrophysics. The distance to the nebula and the expansion speed of the nebula were determined from photographic plates [7,26,27]. The chemical composition, mass and kinetic energy of the expanding gas were calculated using optical wavelength spectra [3]; the only exception to this was the use of infrared observations to calculate the density of dust in the nebula [3]. The peak of the nebula's energy output is in the ultra-violet region of the spectrum and is very difficult to observe. We can estimate the position and intensity of this peak however from the study of the spectrum in the visual region. Another indication of the importance of optical wavelength observations is that the pulsar was originally timed optically although it can now be timed accurately from its radio pulses [10]. The visual and ultra-violet continua of the nebula are highly polarized [2,28]. There have been many studies of polarization of nebular emission at radio frequencies which was first observed in 1957 by Mayer, McCullough and Sloanaker [29]. Some of the most interesting radio surveys were made by Matveenko and Kostenko [30], Wilson [31,32,33], Swinbank [34], Swinbank and Pooley [35] and Velusamy [36]. It is interesting to note that features which appear in the optical polarization maps of the nebula are not always present in radio polarization maps. This may be due to the fact that Faraday rotation [37] affects the radio emission but does not have any measurable effect on the optical wavelength emission of the Crab nebula but it may eventually tell us something about the energy distribution of particles within the nebula. In this thesis we will concentrate on the polarization of the optical wavelength emissions.

In the 1960s several other plerions were discovered. Studies of these objects, e.g. 3C58, Milne 56, CTB 87 and G148+1, have been made but the Crab is still the most studied object of this class [3]. Apart from the Crab nebula, G148+1 is the only centre filled supernova remnant in which a pulsar has been observed.

The Crab nebula pulsar was discovered in 1968 [38], just one year after Bell and Hewish discovered the first pulsar. The following year the South Preceding Star

was identified as the pulsar [39]. As pulsar theory developed it became clear that the pulsar must in some way provide the magnetic field and energetic particles in the nebula. It is now accepted that the pulsar is the powerhouse of the nebula as the amount of energy transferred from the pulsar to the nebula as the pulsar's spin rate decreases is commensurate with the energy output of the nebula [4]. The mechanism of production of relativistic particles in pairs near the pulsar's magnetic polar caps was first proposed by Sturrock [40] and the subsequent outflow of these particles along open magnetic field lines was a feature of models even before the production mechanism was fully understood. Exactly where in the pulsar magnetosphere these pairs are produced and how many pairs are created depend on the magnetosphere model used. Nevertheless, electron-positron pairs created on open magnetic field lines form a plasma which streams out along these fields lines and is dense enough to be treated using the ideal magnetohydrodynamic equations (see chapter 4, section 4.2). If the electron density of the nebula is 10^3 cm^{-3} [12] then the electron-positron pairs have a lifetime of at least 2 years before they are annihilated by collisions. Therefore, electron-positron pairs must be created in other regions of the nebula as well as in the pulsar magnetosphere. We already know particles must be supplied throughout the nebula as the synchrotron lifetimes of relativistic particles are less than the expansion lifetime of the nebula. As we shall see in the next section, the production of magnetic field has been much studied since 1955 but is still a matter for further study. We will now examine the development of theoretical models of the structure and dynamics of the Crab nebula over the last three decades.

1.4 The Search for a Theoretical Model which Correctly Describes the Features of the Crab Nebula

Although the Crab nebula has been extensively studied there still remain many puzzles about its structure and dynamics which are unresolved. We are sure that the

nebular luminosity is due to synchrotron radiation but there is no consensus about how the magnetic field which causes this radiation is produced. Synchrotron lifetimes are small compared to the lifetime of the nebula and, as mentioned above, the electron-positron pairs produced in the pulsar magnetosphere eventually annihilate each other, so the energetic particles producing this radiation must be continuously supplied and accelerated throughout the nebula due to the action of the pulsar. Apart from this we do not really know how the pulsar interacts with the surrounding nebula. Many observational and theoretical studies have been undertaken in the last twenty years with a view to constructing a model which explains all the observed features of the Crab nebula; some progress has been made.

Once observations of polarization of visual wavelength radiation from the Crab nebula had been made [23,24], confirming that the nebular luminosity was produced by synchrotron radiation, the question which arose was "What is the origin of the magnetic field within the nebula?". Observations showed that the nebular magnetic field was too strong to be a "frozen-in" field left over from the pre-supernova star [41]. Adiabatic losses would have transformed almost all of the pre-supernova magnetic field energy into expansion energy during the lifetime of the nebula. Obviously, there is a mechanism within the nebula which produces the observed magnetic field. Piddington [42] was the first to suggest, in 1957, that the nebular magnetic field might be generated by a central magnetic star which was rotating. The theory of rotating stars with magnetic fields was not new [43], but it had not previously been considered in relation to the Crab nebula. Piddington also proposed that the energy required by the nebula to achieve the observed radiation output would be supplied by fast particles ejected from the star and that after the supernova event lines of magnetic force would link the central star and the remnant; differential rotation would cause toroidal magnetic fields to be formed in the nebula. The theory of neutron stars was quite well developed at this time but it was 10 years before the

first pulsar was observed. It was therefore a bold step for Piddington to make an estimate of 5 minutes for the rotation period of the central star required to create the observed field. In the light of current knowledge we find that several assumptions made in the calculation of this estimate are not valid but at the time a rotation period of 5 minutes was considered extreme and nobody would have considered a rotation period of 33 milliseconds as anything other than pure fiction.

By the 1960s the emphasis had switched from optical wavelength observations to theoretical studies and radio and X-ray observations of the Crab nebula. Korchakov and Syrovatskii [44] proposed that as the net polarization of the Crab was in the north-west to south-east direction the net magnetic field should be perpendicular to this. The difficulty with this simple model is that the particles would flow preferentially along the net magnetic field direction and the nebula should therefore be larger in this direction; the net magnetic field in this model is parallel to the minor axis of the nebula. According to Korchakov and Syrovatskii the shape of the magnetic field present in the nebula depends on the direction of rotation of the nebula. These authors claim that if the nebula is an elongated ellipsoid of rotation the magnetic field would be toroidal with its axis along the direction of elongation and that if the nebula is a flattened ellipsoid of rotation the magnetic field would be a dipole field with its axis of symmetry along the minor axis of the nebula. Although Korchakov and Syrovatskii do not explain clearly why this should be the case, it was later discovered that the pulsar spin axis is aligned in the north-west to south-east direction [45]. It seems reasonable to assume that the nebular rotation has the same axis as the pulsar rotation since they are closely linked; hence the nebula is an elongated ellipsoid of rotation and from Korchakov and Syrovatskii's theory we expect to find a toroidal field with its axis along the major axis of the nebula. However, since the pulsar is an oblique rotator (the magnetic axis of the pulsar is almost perpendicular to the rotational axis), the axis of the pulsar's dipole magnetic

field will be roughly aligned with to the minor axis of the nebula so that we have a combination of features from both of Korchakov and Syrovatskii's models. Other theories at the time predicted a twisting effect in the magnetic field, although a definitive mechanism for the formation of a toroidal field had not been found. Kardashev [46] suggested that the twisting could be due to the outflow of matter in the pulsar's rotational equatorial region during the stellar collapse.

By 1971 the rotating neutron star model for pulsars was generally accepted. If the magnetic and rotational axes of the pulsar are not aligned, energy is lost from the pulsar. Gunn and Ostriker [47] proposed that the Crab pulsar should produce a wave within the nebula which would have a frequency of approximately 30Hz (the same as the pulsar's rotation frequency). Such a wave could accelerate particles and provide a magnetic field in which these particles would emit synchrotron radiation. This theory was developed further in direct relation to the Crab nebula by Rees and Gunn [41]. They, however, suggested that the power emitted by the pulsar emerged partly as a 30Hz wave and partly as a relativistic wind which contained a toroidal magnetic field. Rees and Gunn argue that the part of the pulsar's magnetic field which is perpendicular to the rotation axis would produce a 30Hz wave and oscillatory magnetic field. The component of the magnetic field aligned to the rotation axis would provide open field lines along which the relativistic particles would escape and a toroidal magnetic field due to 'winding up' of field lines as suggested by Piddington [42]. Rees and Gunn also associated the wisps seen near the pulsar with the shock front which would be produced by the 30Hz wave. The test of this model was that if the 30Hz wave propagated into the nebula we would expect to see circular polarization at optical and radio wavelengths. Circular polarization has not even been detected in the Crab nebula at the 0.1% level [48,49] so the 30Hz wave definitely does not propagate into the nebula. Although Rees and Gunn were aware of the non-detection of circular polarization they still included the

wave in their model but only allowed it to exist as far as the shock front where the 30Hz wave would be completely absorbed. At the shock front the relativistic outflow pressure is balanced by the internal nebular pressure and the wave energy would be transferred into kinetic energy of relativistic electrons. This model remained the best explanation of the observed features of the Crab nebula until 1984 when Kennel and Coroniti [4,13] found that the plasma density of the pulsar magnetosphere was too low to support a wave of this type as the wave frequency is below the plasma frequency.

Another model of the Crab nebula considered the field structure to be a torus centred on the pulsar which is viewed almost side on and has its axis in the north-west to south-east direction. This theory, developed by Aschenbach and Brinkmann [45], agreed with the theory of Korchakov and Syrovatskii [44]. Aschenbach and Brinkmann's model assumed that the Crab pulsar was an oblique rotator. Accelerated particles in this model move out along open field lines as a relativistic wind which is mainly confined to the rotational equatorial plane of the pulsar. A similar structure was postulated by Benford, Bodo and Ferrari [50] who found that in their model the relativistic wind moving away from the pulsar was almost spherically symmetric but had a tendency to form a disc in the rotational equatorial plane. Benford, Bodo and Ferrari proposed that the relativistic wind was produced by electrons and ions which were accelerated by a large amplitude wave at the edge of the pulsar light cylinder. The edge of the light cylinder defines the distance from the pulsar where the co-rotating magnetosphere's angular velocity is equal to the speed of light. The radius of the light cylinder is given simply by the ratio of the speed of light to the pulsar's rotational frequency. Benford, Bodo and Ferrari thought that the wisps were caused by plasma instabilities occurring in rings about the pulsar. This effect was also a feature of Aschenbach and Brinkmann's model [45]. Both these sets of authors found that new work in allied fields would

have important effects on their models. Benford, Bodo and Ferrari realised that adjustments would need to be made to their model to take account of a recently introduced theory at that time which put forward a mechanism for the generation of a relativistic wind by the production of electron-positron pairs at the magnetic poles of the pulsar [40,51]. Aschenbach and Brinkmann found from observational studies that the optical continuum of the nebula did not show geometrical symmetry about the pulsar but in fact had a region of enhanced brightness to the north-west of the pulsar. The centroid of X-ray emission also lies in this region. Aschenbach and Brinkmann concluded that this asymmetry could be due to the motion of the pulsar which is in this direction.

In 1984 Kennel and Coroniti produced two papers dealing with the Crab nebula and the relativistic wind in terms of magnetohydrodynamics [4,13]. Since the 30Hz wave [4] could not exist at plasma densities which were consistent with the pair production model the relativistic particles produced at the poles must be transported through the nebula in some other way; magnetohydrodynamic processes were the obvious choice. The first paper [4] dealt with the confinement of the pulsar's relativistic wind by the supernova remnant. In this model the relativistic wind from the pulsar is spherically symmetric. The wind terminates at a magnetohydrodynamic shock approximately 0.1pc from the pulsar. The wind is also magnetised and Kennel and Coroniti found that a toroidal magnetic field is a characteristic feature of such a wind emanating from a rotating central object. In the second paper [13] Kennel and Coroniti calculated the properties of the synchrotron spectrum expected from the model developed in the first paper. They found from comparison with observations of the spectrum of the Crab nebula that the spectral index of the synchrotron power law spectrum which best fit the observations at visual wavelengths was p=0.6. This corresponds to an energy spectral index of α=2.2 which tallies well with observational measurements of this parameter e.g. Greve and

van Genderen [52] found the energy spectral index to be α=2.32 (for a more detailed discussion of the power law spectrum and energy spectrum see chapter 3). In the region outside the magnetohydrodynamic shock the transport of particles is non-relativistic and the particles move at speeds close to the expansion speed of the nebula. Kennel and Coroniti calculated that approximately 10-20% of the spin down luminosity of the pulsar is converted into nebular radiation. This model accounts for the underluminous region which surrounds the pulsar and could coincide with the region inside the magnetohydrodynamic shock. The model also accounts for many other features of the nebula but its main failing is that it does not provide radio emission.

However, Kennel and Coroniti's model did not explain exactly how the magnetic field structure of the nebula is generated. A model for the structure of the magnetic field inside the light cylinder was developed by Barnard [53]. Barnard used a long neglected solution for the magnetic field surrounding a rotating conducting sphere in vacuo which was found by Deutsch in 1955 [43]. When considering a pulsar the plasma surrounding the pulsar may cause problems with this solution as the plasma leads to reconnection in parallel magnetic force lines. Even so, Deutsch's model is a good approximation and gives expressions for the magnetic field components in spherical polar coordinates. The orientation of the pulsar given by Kristian et al [54] is an angle between the line of sight and the rotational axis of 83° and an inclination of the dipole to rotational axis of 90°. Using these angles with Barnard's theory indicates that a wind regime must dominate the nebula outside the light cylinder and that inside the light cylinder the magnetic field can be approximated by a dipole field. Barnard did not extend his work to consider the polarization pattern of the nebula as a whole but concentrated on polarization position angle swings of the pulse component, which are directly related to the pulsar rotation.

Deutsch's solution actually permits the possibility of two of more independent magnetic fields around a rotating star; each of these fields must be symmetrical about its own axis but they need not have the same axis of symmetry. This implies that a pulsar can not only have its own dipole field but also a toroidal field, as is suggested in many of the theoretical models mentioned in this chapter. Deutsch's starting point for his model is the frozen-in field equation

$$\frac{\partial \underline{\mathbf{B}}}{\partial t} = \underline{\nabla} \wedge (\underline{\mathbf{v}} \wedge \underline{\mathbf{B}})$$

The same equation is utilised by the most recently published theoretical model for the Crab nebula magnetic field structure by Tsikarishvili et al [55]. Here the authors consider the pulsar magnetic field inside the light cylinder to be a dipole field. Since the pulsar is an oblique rotator, open fields lines near the magnetic poles of the pulsar cross the light cylinder. Such field lines become distorted as the pulsar magnetosphere co-rotates with the pulsar but the plasma outside the light cylinder does not and the field is "frozen" into this plasma. As the angle between the rotational axis and magnetic axis is not exactly 90° two discs of toroidal magnetic field are formed around the rotational equator. The generation of this field takes place only near the light cylinder and further out in the nebula this field is transported by the expanding electron-positron plasma. This paper also explains the observed enhancement of radiation around the nebular filaments as being due to a build up of field around the filaments a the field is carried out through the nebula. This idea was originally suggested by Wilson [33]. Tsikarishvili et al also attempted to find a mathematical expression for the toroidal field component by solving the frozen-in field equation. Unfortunately, Tsikarishvili et al's solution does not agree with Deutsch's solution and their method of solution is not adequate. Further discussion of this paper is undertaken in chapter 4.

The basic state of current theory about the magnetic field structure of the Crab nebula is as follows. The pulsar has a dipole field and in some way the rotation of the pulsar produces the observed nebular magnetic field. The fast particles which emit synchrotron radiation within this field are produced at the poles of the pulsar and flow out along open field lines into the nebula. The exact structure of the magnetic field outside the light cylinder is unknown and no adequate theory for the field production mechanism has yet been developed.

Chapter 2

Polarization and the Stokes Parameters

2.1 Introduction

In this chapter we will initially deal with a special case of polarization found when dealing with monochromatic waves of the same phase. Having derived the Stokes intensity parameters for this special case in section 2.2, we will see in section 2.3 how the parameters can be adjusted to deal with waves of random phases but the same wavelength. Section 2.4 deals with the relationship between Stokes intensity parameters and Stokes parameters and their relation to this thesis. Sections 2.2 and 2.3 follow closely the derivation of Stokes intensity parameters given in Rybicki and Lightman [56]. Section 2.4 follows simply from the definition of the Stokes parameters for linear polarization, equation (2.16).

2.2 Polarization of Monochromatic Waves

Electromagnetic radiation can be described in terms of waves propagating through space. Such a description follows directly from solutions of Maxwell's equations. If we consider the case for radiation of a single wavelength we find that the electric and magnetic fields can be expressed as

$$\underline{\mathbf{E}} = \hat{\underline{\mathbf{a}}}_1 \, E_0 \, e^{\,i\,(\underline{\mathbf{k}}\cdot\underline{\mathbf{r}} - \omega t)} \tag{2.1a}$$

$$\underline{\mathbf{B}} = \hat{\underline{\mathbf{a}}}_2 \, B_0 \, e^{\,i\,(\underline{\mathbf{k}}\cdot\underline{\mathbf{r}} - \omega t)} \tag{2.1b}$$

where $\hat{\underline{\mathbf{a}}}_1$ and $\hat{\underline{\mathbf{a}}}_2$ are unit vectors, E_0 and B_0 are complex constant amplitudes, and $\underline{\mathbf{k}}=k\underline{\mathbf{n}}$ and ω are the wave vector and frequency of the wave respectively. Equations (2.1) represent waves travelling along $\underline{\mathbf{n}}$ where $\hat{\underline{\mathbf{a}}}_1$ and $\hat{\underline{\mathbf{a}}}_2$ are perpendicular to $\underline{\mathbf{n}}$ and

to each other. The wave described by equation (2.1a) is 100% *linearly polarized,* which simply means that the electric vector oscillates in a unique direction $\hat{\mathbf{a}}_1$. This direction, together with the direction of propagation, defines the *plane of polarization.*

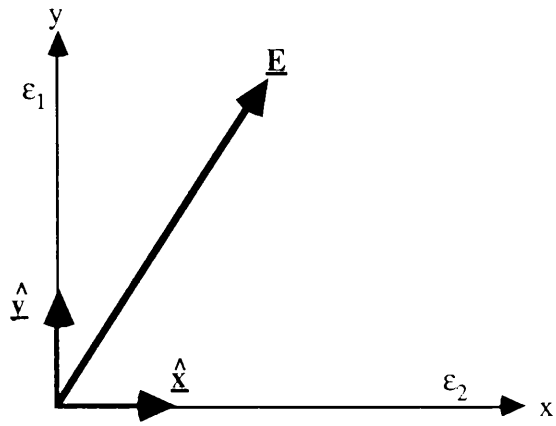

Figure 2.1: Coordinate system for the electric vector $\underline{\mathbf{E}}$.

To consider the simplest state of polarization for a wave of given wave vector and frequency we superpose two such waves which oscillate in directions perpendicular to each other. We will consider only the electric vector because the magnetic vector is always perpendicular to and has the same magnitude as the electric vector. If we now take an electric vector at an arbitrary point and choose axes as shown in figure 2.1, with the wave propagating out of the page, then the electric vector is

$$\underline{\mathbf{E}} = (\hat{\mathbf{x}}\, E_1 + \hat{\mathbf{y}}\, E_2)\, e^{-i\omega t} \equiv \underline{\mathbf{E}}_0\, e^{-i\omega t} \qquad (2.2)$$

where E_1 and E_2 are complex amplitudes;

$$E_1 = \varepsilon_1 e^{i\phi_1} \qquad E_2 = \varepsilon_2 e^{i\phi_2}$$

In order to obtain equations which describe the position of the tip of the electric field vector in the (x,y) plane, i.e. the physical components of the electric field in the x and y unit vector directions, we take the real part of $\underline{\mathbf{E}}$;

$$E_x = \varepsilon_1 \cos(\omega t - \phi_1) \tag{2.3a}$$

$$E_y = \varepsilon_2 \cos(\omega t - \phi_2) \tag{2.3b}$$

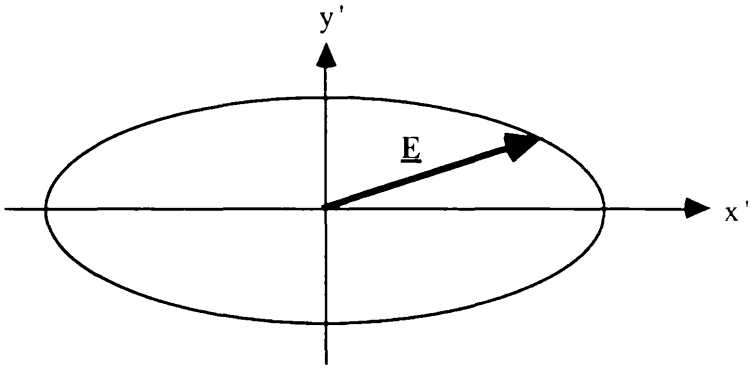

Figure 2.2 : The ellipse described by the tip of the electric vector $\underline{\mathbf{E}}$.

We now consider figure 2.2. The equations for a general ellipse relative to its principal axes x' and y' are;

$$E_{x'} = \varepsilon_0 \cos\beta \cos\omega t \tag{2.4a}$$

$$E_{y'} = -\varepsilon_0 \sin\beta \sin\omega t \tag{2.4b}$$

where $-\pi/2 \leq \beta \leq \pi/2$. The magnitudes of the major and minor axes are $\varepsilon_0 |\cos\beta|$ and $\varepsilon_0 |\sin\beta|$ as

$$\left(\frac{E_{x'}}{\varepsilon_0 \cos\beta}\right)^2 + \left(\frac{E_{y'}}{\varepsilon_0 \sin\beta}\right)^2 = 1$$

For $0 < \beta < \pi/2$ the ellipse is traced out in a clockwise direction as viewed by the observer towards whom the wave is propagating. This is generally known as *right-handed* elliptical polarization. For $-\pi/2 < \beta < 0$ the same observer would see the ellipse being traced out in an anti-clockwise direction. This is *left-handed* elliptical polarization. Special cases of polarization exist when $\beta = \pm \pi/4$, the ellipse becomes a circle, and when $\beta = 0$ or $\pm \pi/2$, the ellipse becomes a straight line. In the former case we have *circular polarization* and in the latter case, *linear polarization.* A linearly polarized wave is neither left nor right-handed.

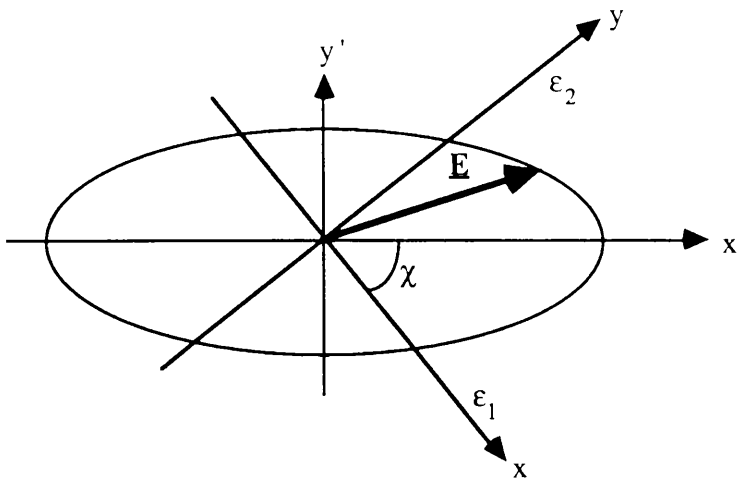

Figure 2.3 : System of axes for the rotation of the components of $\underline{E}$ in x and y through the angle χ so that they coincide with the principal axes of the polarization ellipse, x' and y'.

We want to establish relationships between the quantities in equations (2.3) and those in equations (2.4). To do so we must look at figure 2.3 and transform the field components of equations (2.4) to an (x,y) axis system by rotating through the angle χ. By this procedure we obtain;

$$E_x = \varepsilon_0 (\cos\beta \cos\chi \cos\omega t + \sin\beta \sin\chi \sin\omega t) \qquad (2.5a)$$

$$E_y = \varepsilon_0 (\cos\beta \sin\chi \cos\omega t - \sin\beta \cos\chi \sin\omega t) \qquad (2.5b)$$

To make equations (2.5) and (2.3) equivalent we must take;

$$\varepsilon_1 \cos\phi_1 = \varepsilon_0 \cos\beta \cos\chi \tag{2.6a}$$

$$\varepsilon_1 \sin\phi_1 = \varepsilon_0 \sin\beta \sin\chi \tag{2.6b}$$

$$\varepsilon_2 \cos\phi_2 = \varepsilon_0 \cos\beta \sin\chi \tag{2.6c}$$

$$\varepsilon_2 \sin\phi_2 = -\varepsilon_0 \sin\beta \cos\chi \tag{2.6d}$$

Equations (2.6) can be solved for ε_0, β and χ if ε_1, ε_2, ϕ_1 and ϕ_2 are known. The usual method of solving these equations is by defining the *Stokes intensity parameters* for monochromatic waves as follows;

$$I \equiv \varepsilon_1^2 + \varepsilon_2^2 = \varepsilon_0^2 \tag{2.7a}$$

$$I_Q \equiv \varepsilon_1^2 - \varepsilon_2^2 = \varepsilon_0^2 \cos2\beta \cos2\chi \tag{2.7b}$$

$$I_U \equiv 2\varepsilon_1\varepsilon_2 \cos(\phi_1 - \phi_2) = \varepsilon_0^2 \cos2\beta \sin2\chi \tag{2.7c}$$

$$I_V \equiv 2\varepsilon_1\varepsilon_2 \sin(\phi_1 - \phi_2) = \varepsilon_0^2 \sin2\beta \tag{2.7d}$$

Notice that we could also write

$$\sin2\beta = \frac{I_V}{I} \tag{2.8}$$

$$\tan2\chi = \frac{I_U}{I_Q} \tag{2.9}$$

Since elliptical polarization is defined purely by ε_0,β and χ we expect a relationship

to exist between the four Stokes intensity parameters. The relationship we find is

$$I^2 = I_Q^2 + I_U^2 + I_V^2 \tag{2.10}$$

The Stokes parameters have the following meanings. I is always positive and proportional to the total energy flux, i.e. the intensity, of the wave. It is common practice to introduce a proportionality constant into the definition of the Stokes parameters (equations (2.7)) so that I is exactly equal to the intensity. I_V is a circularity parameter. It is a measure of the ratio of the principal axes of the ellipse. If I_V is positive the wave is a right-handed polarized wave, if I_V is negative the wave is a left-handed polarized wave and if I_V equals zero the wave is 100% linearly polarized. I_Q and I_U are mutually dependent parameters (see equation (2.9)) and measure the orientation of the ellipse relative to the x-axis (see figure 2.3). The angle of this orientation χ is known as the *angle of polarization*. If $I_Q=I_U=0$ the wave is 100% circularly polarized.

2.3 Degree of Polarization and Depolarization

In practice we never see a single monochromatic wave but always a wave which we can consider as a superposition of several monochromatic components each with its own polarization and of random phase. In order to calculate the net polarization of this "quasi-monochromatic" wave we utilise the fact that the Stokes intensity parameters are linearly additive. The total Stokes intensities are simply given by;

$$I_{Qtot} = \sum_{\text{all waves}} I_{Qm} \tag{2.11a}$$

$$I_{Utot} = \sum_{\text{all waves}} I_{Um} \tag{2.11b}$$

$$I_{Vtot} = \sum_{\text{all waves}} I_{Vm} \qquad (2.11c)$$

where I_{Qm}, I_{Um}, I_{Vm} are the parameters of each monochromatic component wave. We can define a quantity, known as the *degree of polarization*, which is the ratio between the intensity of the polarized part of a wave to the total intensity of the wave,

$$\Pi = \frac{I_{pol}}{I} = \frac{(I_Q^2 + I_U^2 + I_V^2)^{\frac{1}{2}}}{I} \qquad (2.12)$$

A monochromatic wave is completely polarized, $I_{pol}=I$ or $\Pi=100\%$.

If we now consider two linearly polarized waves, a and b, which are polarized in opposing directions, we find that $I_V=0$ for both waves and that since the electric vectors are antiparallel

$$I_{Qa} = -I_{Qb} \quad \text{and} \quad I_{Ua} = -I_{Ub}$$

Therefore the total Stokes intensities for the superposed waves are

$$I_{Qtot} = I_{Qa} + I_{Qb} = 0$$

$$I_{Utot} = I_{Ua} + I_{Ub} = 0$$

Thus, the net polarization is zero. This effect is known as *depolarization*. For a quasi-monochromatic wave the effect of depolarization is to reduce the degree of polarization from the 100% which each component wave possesses. The total intensity is a simple linear sum of the intensity of each component but the polarized intensity is given by equation (2.10). So, $I_{pol} < I_{tot}$ and $\Pi < 100\%$.

It is useful in this work to consider the special case where $I_V=0$ and the light is partially linearly polarized. Analysis of the light using a linear polarizing filter can be made. The maximum intensity passed by the filter, I_{max}, will be detected when the filter is aligned with the plane of polarization (x'-axis in figure 2.3). The minimum intensity, I_{min}, will be detected when the filter is aligned perpendicular to the plane of polarization (y'-axis in figure 2.3). The total unpolarized intensity is distributed equally between these two directions so

$$I_{max} = \frac{1}{2} I_{unpol} + I_{pol} \tag{2.13}$$

$$I_{min} = \frac{1}{2} I_{unpol} \tag{2.14}$$

The polarized intensity is

$$I_{pol} = (I_Q^2 + I_U^2)^{\frac{1}{2}}$$

and the unpolarized intensity is

$$I_{unpol} = I - (I_Q^2 + I_U^2)^{\frac{1}{2}}$$

If we substitute for the maximum and minimum intensities in equation (2.12) we find that the degree of polarization can be expressed, in this case, as

$$\Pi = \frac{I_{max} - I_{min}}{I_{max} + I_{min}} \tag{2.15}$$

2.4 Stokes Parameters, Stokes Intensities and Their Use in this Thesis

Equations (2.7) define the Stokes intensities for polarized light and we have the definition of degree of polarization, equation (2.12). Using these equations and equation (2.9) we can define the *normalised Stokes intensities* or *Stokes parameters* for a linearly polarized wave as

$$Q = \frac{I_Q}{I} \quad , \quad U = \frac{I_U}{I} \tag{2.16}$$

then

$$\Pi = (Q^2 + U^2)^{\frac{1}{2}} \tag{2.17}$$

$$\tan 2\chi = \frac{U}{Q} \tag{2.18}$$

From equations (2.7) and (2.12) we see that

$$\Pi = \frac{(I_Q^2 + I_U^2)^{\frac{1}{2}}}{I} = \frac{[(\varepsilon_0^2 \cos 2\beta \cos 2\chi)^2 + (\varepsilon_0^2 \cos 2\beta \sin 2\chi)^2]^{\frac{1}{2}}}{I}$$

$$\Pi = \frac{\varepsilon_0^2 \cos 2\beta}{I} \tag{2.19}$$

So we can write the Stokes intensity parameters as;

$$I_Q = I\Pi \cos 2\chi \tag{2.20a}$$

$$I_U = I\Pi \sin 2\chi \tag{2.20b}$$

Alternatively, the Stokes parameters are;

$$Q = \Pi \cos 2\chi \tag{2.21a}$$

$$U = \Pi \sin 2\chi \tag{2.21b}$$

The above equations are the most useful definitions of the Stokes parameters for use in this thesis. The data published in Woltjer's paper [1] are given as intensity I, degree of polarization Π and the position angle of the maximum of the electric vector measured anti-clockwise from the north direction, in other words the polarization angle χ. Therefore, we can calculate the Stokes parameters directly from this data using equations (2.21) above. McLean et al's data [2], which is also used in this thesis, is presented directly in the form of Stokes parameters and total intensity.

Chapter 3

The Theory of Synchrotron Radiation

3.1 Introduction

Particles which are accelerated by a magnetic field will emit electromagnetic radiation. If such particles are moving at relativistic speeds the radiation emitted is known as *synchrotron radiation* and has a complex frequency spectrum. Such radiation is the source of the luminosity of the Crab nebula. The theory of synchrotron radiation was developed in the 1950s and it was Shklovskii [20] who suggested that the Crab nebula's emission may be caused by the synchrotron mechanism. The analysis in sections 3.2, 3.3 and 3.4 follows that given in Rybicki and Lightman [56]. Section 3.5 develops the theory of polarization of synchrotron radiation with respect to the Crab nebula. The basic outline of the theory in the latter section can be found in Brown, Craig and Melrose [57].

3.2 The Power of the Emitted Radiation

The motion of any relativistic particle of rest mass m and charge q moving with velocity $\underline{\mathbf{v}}$ in a magnetic field $\underline{\mathbf{B}}$ is described by two equations, the equation for the acceleration of the particle

$$\frac{d}{dt}(\gamma m \underline{\mathbf{v}}) = q\,(\underline{\mathbf{v}} \wedge \underline{\mathbf{B}}) \tag{3.1}$$

and the equation for conservation of energy

$$\frac{d}{dt}(\gamma m c^2) = q\,(\underline{\mathbf{v}} \cdot \underline{\mathbf{E}}_m) = 0 \tag{3.2}$$

where $\underline{\mathbf{E}}_m$ is the macroscopic electric field in the plasma and is equal to zero and γ is

the Lorentz factor $(1- v^2/c^2)^{-1/2}$. The terms $(\gamma m\underline{\mathbf{v}})$ and (γmc^2) represent the total relativistic momentum and the total relativistic energy of the particle. Equation (3.2) implies that γ, and thus $|\underline{\mathbf{v}}|$, is constant and so

$$m\gamma \frac{d\underline{\mathbf{v}}}{dt} = q\,(\underline{\mathbf{v}} \wedge \underline{\mathbf{B}}) \tag{3.3}$$

If we separate the velocity field into components parallel and perpendicular to the magnetic field we obtain the following:

$$\frac{d\underline{\mathbf{v}}_{\parallel}}{dt} = 0 \tag{3.4}$$

$$\frac{d\underline{\mathbf{v}}_{\perp}}{dt} = \frac{q}{\gamma m}(\underline{\mathbf{v}}_{\perp} \wedge \underline{\mathbf{B}}) \tag{3.5}$$

Equation (3.4) follows directly from the fact that the vector cross product of parallel vectors is identically zero. Obviously, the parallel component of the velocity is constant and, as $|\underline{\mathbf{v}}|$ is constant, the perpendicular component of the velocity is constant. For motion in a plane perpendicular to the magnetic field we can write

$$\frac{d\underline{\mathbf{v}}_{\perp}}{dt} = -\,\underline{\mathbf{v}}_{\perp} \wedge \underline{\omega}_B \tag{3.6}$$

where

$$\underline{\omega}_B = \frac{-q\underline{\mathbf{B}}}{\gamma m} \tag{3.7}$$

So this vector points along $\underline{\mathbf{B}}$ for negatively charged particles and in the opposite direction to $\underline{\mathbf{B}}$ for positively charged particles.

All the factors on the right hand side of equation (3.6) are constant so the

acceleration is constant in magnitude and is perpendicular to the velocity and the magnetic field. We also have

$$\underline{v}_{\perp} = \underline{\omega}_B \wedge \underline{r}_c \tag{3.8}$$

where $\underline{r}_c$ is the particle position with respect to the centre of gyration. Again, since the other factors in the equation are constants $\underline{r}_c$ is a constant and thus the solution of the equation of motion is uniform circular motion in a plane perpendicular to the magnetic field. When combined with the uniform motion along the magnetic field the circular motion gives rise to helical motion with a frequency of gyration ω_B. For an electron the frequency of gyration is

$$\omega_B = \frac{e\underline{B}}{\gamma m_e} \tag{3.9}$$

The total power of emitted radiation for a non-relativistic particle is

$$P = \frac{dW}{dt} \tag{3.10}$$

where dW is the total amount of energy emitted in the time interval dt. This is neglected in the energy conservation equation above, equation (3.2), since $\gamma mc^2/P$ is much greater than the orbital period. For a relativistic particle the total energy emitted in a frame K moving relative to the particle with velocity $-\underline{v}$ is

$$dW = \gamma dW' \tag{3.11}$$

where dW′ represents the total energy emitted in a frame of reference K′ which is instananeously at rest relative to the particle. This relation follows directly from the transformation properties of the four-momentum (for details see Rybicki and

Lightman [56], pg 136). The time interval in K is clearly related to dt′, the time interval in K′, by

$$dt = \gamma dt' \tag{3.12}$$

Therefore the total emitted power in K′ is

$$P' = \frac{dW'}{dt'} \tag{3.13}$$

The total emitted power is clearly a Lorentz invariant parameter.

We now use the Larmor formula for the total emitted power

$$P = \frac{2q^2}{3}(\underline{a}' \cdot \underline{a}') = \frac{2q^2}{3}(a_{\parallel}'^2 + a_{\perp}'^2) \tag{3.14}$$

where $\underline{a}'$ is the particle acceleration in the instantaneous rest frame K′. In terms of the frame K the acceleration components are:

$$a_{\parallel}' = \gamma^3 a_{\parallel} \tag{3.15}$$

$$a_{\perp}' = \gamma^2 a_{\perp} \tag{3.16}$$

Rewriting equation (3.14) we obtain an expression for the power in terms of the acceleration in K,

$$P = \frac{2q^2\gamma^4}{3}(a_{\perp}^2 + \gamma^2 a_{\parallel}^2) \tag{3.17}$$

For the case which we are considering here, that of helical motion, there is no acceleration parallel to the magnetic field and the perpendicular component of the

acceleration is given by equation (3.6). Simplifying equation (3.6) and using this result in equation (3.17) gives

$$P = \frac{2\,q^2\gamma^4}{3}\left(\frac{q^2B^2\underline{v}_\perp^2}{\gamma^2m^2}\right) = \frac{2q^4\gamma^2B^2\underline{v}_\perp^2}{3m^2} \tag{3.18}$$

3.3 The Spectral Index of Synchrotron Radiation

The spectrum of synchrotron radiation is related to the variation of the electric field which is seen by the observer. Beaming effects cause the radiation to appear concentrated in a narrow set of directions about the particle's trajectory. The observer sees a radiation pulse which is confined to an interval less than the gyration period of the particle. The spectrum is therefore spread over a broader region than one of the order of $\omega_B/2\pi$. This is a primary feature of synchrotron radiation.

If the angular width of the cone of emission $1/\gamma$ at a point along the particle trajectory includes the observer's direction then the observer will see the pulse of radiation emitted from that point (see figure 3.1). The distance along the trajectory Δs is then simply

$$\Delta s = a\Delta\phi \tag{3.19}$$

where a is the radius of curvature of the trajectory. Geometric relations show that

$$\Delta\phi = 2\left(\frac{1}{\gamma}\right) = \frac{2}{\gamma} \tag{3.20}$$

Therefore

$$\Delta s = \frac{2a}{\gamma} \tag{3.21}$$

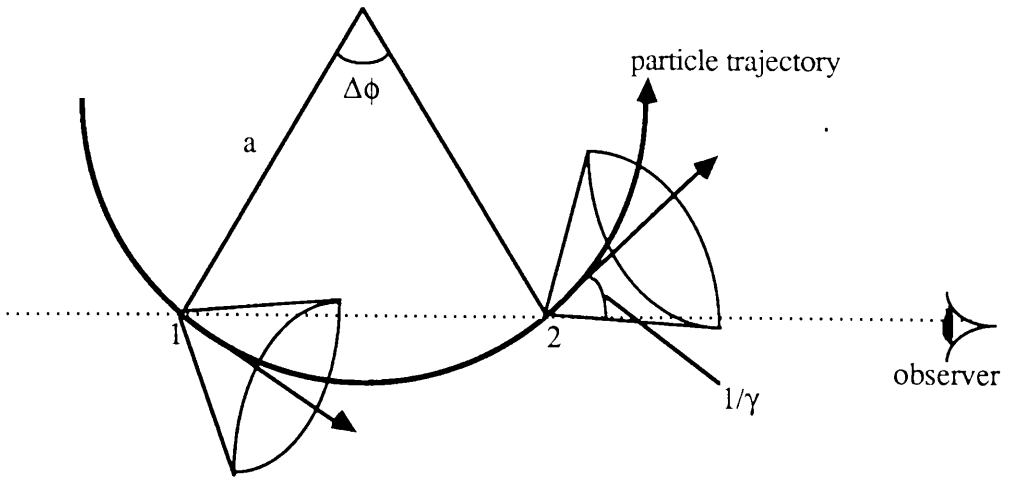

Figure 3.1 : Emission cones at points along a particle trajectory 1 and 2 where the observer's line of sight lies within the angular width of the emission cone.

We can find an expression for the radius of curvature from the equation of motion

$$\gamma m \frac{\Delta \underline{v}}{\Delta t} = q(\underline{v} \wedge \underline{B}) \tag{3.22}$$

$|\Delta \underline{v}| = v\Delta\phi$ and $\Delta s = v\Delta t$ so we rewrite equation (3.22) as

$$\frac{\Delta\phi}{\Delta s} = \frac{q\underline{B}\sin\theta}{\gamma m \underline{v}} \tag{3.23}$$

where θ is the angle between the magnetic field $\underline{B}$ and the velocity $\underline{v}$. Thus, substituting for $\underline{\omega}_B$ from equation (3.9)

$$a = \frac{\Delta s}{\Delta\phi} = \frac{\underline{v}}{\underline{\omega}_B \sin\theta} \tag{3.24}$$

So Δs is defined by the expression

$$\Delta s = \frac{2\underline{v}}{\gamma \underline{\omega}_B \sin\theta} \tag{3.25}$$

However, it is clear that the distance travelled along the trajectory can be expressed as the product of the particle velocity and the time interval taken for the particle to travel between points 1 and 2

$$\Delta s = v\,(t_2 - t_1) \tag{3.26}$$

where t_1 and t_2 are the times when the particle passes points 1 and 2 respectively. Combining equations (3.25) and (3.26) we obtain

$$(t_2 - t_1) = \frac{2}{\gamma \underline{\omega}_B \sin\theta} \tag{3.27}$$

If t_1^A, t_2^A are the times of arrival of radiation at the observer's position then $(t_2^A - t_1^A)$ is less than $(t_2 - t_1)$ by an amount which is equal to the time for radiation to travel along the distance Δs, $\Delta s/c$. The time interval between pulses as seen by the observer is then

$$(t_2^A - t_1^A) = \Delta t^A = \frac{2}{\gamma \underline{\omega}_B \sin\theta}\left(1 - \frac{\underline{v}}{c}\right) \tag{3.28}$$

We are considering particles with relativistic velocities so $\gamma >> 1$ and we can use the approximation

$$1 - \frac{v}{c} \cong \frac{1}{2\gamma^2} \tag{3.29}$$

Using this approximation equation (3.28) becomes

$$\Delta t^A = \frac{1}{\gamma^3 \omega_B \sin\theta} \tag{3.30}$$

This shows clearly that the width of the observed pulses is smaller than the gyration period by a factor of γ^3. We can define a critical frequency

$$\omega_c = \frac{3}{2}\gamma^3 \omega_B \sin\theta \tag{3.31}$$

or

$$\nu_c = \frac{3}{4\pi}\gamma^3 \omega_B \sin\theta \tag{3.32}$$

We expect the spectrum of the radiation pulse to be of the order of ω_c in width.

The electric field is a function of only the polar angle about the direction of motion ϕ due to the beaming effect. Therefore we can write the electric field as

$$E(t) \propto F(\gamma\phi) \tag{3.33}$$

where t is time measured in the observer's frame of reference. When the pulse is centred on the observer we set t=0 and the path length to s and we find that

$$\phi \cong s/a \tag{3.34}$$

and

$$t \cong \frac{s}{v}\left(1 - \frac{v}{c}\right) \tag{3.35}$$

The relationship between ϕ and t is

$$\gamma\phi \cong 2\gamma(\gamma^2\omega_B \sin\theta)t \tag{3.36}$$

$$\gamma\phi \propto \omega_c t \tag{3.37}$$

So we rewrite equation (3.33) with the electric field as a function of the critical frequency and time

$$E(t) \propto g(\omega_c t) \tag{3.38}$$

Taking the Fourier transform of the electric field and changing the variable of integration to $\xi=\omega_c t$ we have

$$\hat{E}(\omega) \propto \int_{-\infty}^{\infty} g(\xi) \exp\left(\frac{i\omega\xi}{\omega_c}\right)\, d\xi \tag{3.39}$$

The power emitted per unit frequency per unit solid angle is proportional to the square of the electric field. We can integrate over the solid angle and divide by the orbital period (both of which are independent of frequency) to find an expression for the time averaged power per unit frequency

$$\frac{dW}{dt\, d\omega} = \frac{1}{T}\frac{dW}{d\omega} \equiv P(\omega) = C_1 f\left(\frac{\omega}{\omega_c}\right) \tag{3.40}$$

f is a dimensionless function and C_1 a constant of proportionality. Compare the total power evaluated by the integral over angular frequency with equation (3.18):

$$P = \int_0^{\infty} P(\omega)\, d\omega = C_1 \int_0^{\infty} f\left(\frac{\omega}{\omega_c}\right) d\omega = \omega_c\, C_1 \int_0^{\infty} f(x)\, dx \tag{3.41}$$

where $x=\omega/\omega_c$. We can evaluate C_1 and find that the power for a given frequency is

$$P(\omega) = \frac{\sqrt{3}\, q^3 B\, \sin\theta}{2\pi m} f\left(\frac{\omega}{\omega_c}\right) \tag{3.42}$$

Here we have set $C_1=\sqrt{3}/2\pi$ as this is the value it takes for the most commonly used normalization of f. This is a very useful result as we can approximate the synchrotron spectrum as a power law over a certain frequency range and define a spectral index p which is a constant in the expression

$$P(\omega) \propto \omega^{-p} \tag{3.43}$$

We must also consider the particle distribution of relativistic electrons in a similar fashion. The number density of particles with energy between γ and $\gamma+d\gamma$ can be approximated by a power law

$$n(\gamma)\, d\gamma = C\gamma^{-\alpha}\, d\gamma \qquad \gamma_1 < \gamma < \gamma_2 \tag{3.44}$$

The total power radiated per unit volume per unit frequency by this type of particle distribution is given by the integral of $n(\gamma)d\gamma$ multiplied by the single particle radiation formula over all energies:

$$P_{total}(\omega) = C\int_{\gamma_1}^{\gamma_2} P(\omega)\,\gamma^{-\alpha} d\gamma \propto \int_{\gamma_1}^{\gamma_2} f\left(\frac{\omega}{\omega_c}\right)\gamma^{-\alpha}\, d\gamma \tag{3.45}$$

Changing the variable to $x=\omega/\omega_c$ again and remembering that $\omega_c \propto \gamma^2$ we have

$$P_{total}(\omega) \propto \omega^{\frac{-(\alpha-1)}{2}} \int_{x_1}^{x_2} f(x)\, x^{\frac{(\alpha-3)}{2}}\, dx \tag{3.46}$$

If γ_1 and γ_2 are sufficiently widely separated x_1 and x_2 can be approximated to zero and infinity respectively. The expression for the power then becomes

$$P_{total}(\omega) \propto \omega^{\frac{-(\alpha-1)}{2}} \tag{3.47}$$

Thus the spectral index p is related to the particle distribution index α by the equality

$$p = \frac{\alpha - 1}{2} \tag{3.48}$$

3.4 The Spectrum and Polarization of Synchrotron Radiation

Consider figure 3.2 below. The coordinates have been chosen such that the particle has velocity $\underline{v}$ along the x-axis at a time t′=0. The unit vectors in the orbital plane are shown and

$$\underline{\varepsilon}_{\parallel} = \underline{n} \wedge \underline{\varepsilon}_{\perp} \tag{3.49}$$

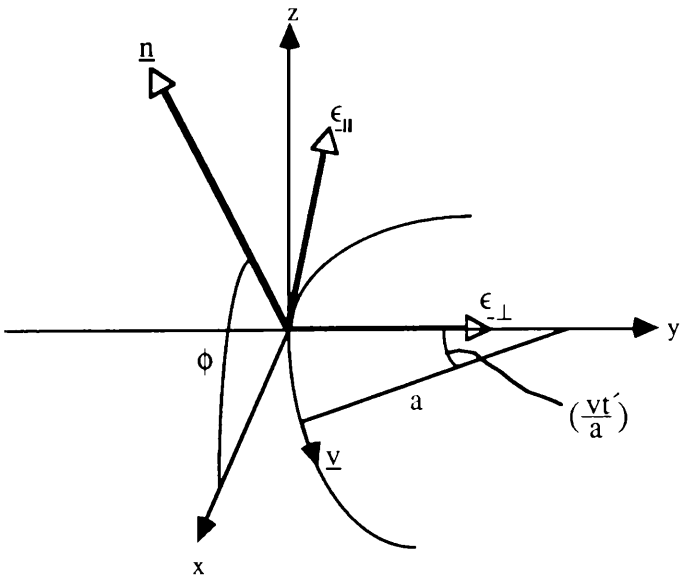

Figure 3.2: Coordinate system for the polarization of synchrotron radiation. The particle trajectory is in the x-y plane and at t′=0 the velocity is along the x-axis. The origin of the coordinates coincides with the location of the particle at t′=0. a is the radius of curvature of the particle trajectory.

We see from figure 3.2 that

$$\underline{n} \wedge (\underline{n} \wedge \underline{\beta}) = -\underline{\varepsilon}_{\perp} \sin\left(\frac{vt'}{a}\right) + \underline{\varepsilon}_{\parallel} \cos\left(\frac{vt'}{a}\right) \sin\phi \tag{3.50}$$

where $\underline{\beta} = \underline{v}/c$, $\underline{v}$ is the particle velocity, and $|\underline{\beta}| = 1$. The energy per unit frquency per unit solid angle of a radiation field for a single particle is

$$\frac{dW}{d\omega\, d\Omega} = \left(\frac{q^2\omega^2}{4\pi}\right) \left| \int \underline{n} \wedge (\underline{n} \wedge \underline{\beta}) \exp\left(i\omega[t' - \underline{n} \cdot \underline{r}_0(t')]\right) dt' \right|^2 \tag{3.51}$$

For details of the derivation of this equation see Rybicki and Lightman pg 82 [56].

Equation (3.50) gives us the first factor in equation (3.51). The second factor can be expressed as follows:

$$t' - \underline{n} \cdot \underline{r}_0(t') = t' - a\cos\phi \sin\left(\frac{vt'}{a}\right)$$

$$\cong (2\gamma^{-1}) \left[(1+\gamma^2\phi^2)t' + \frac{\gamma^2 t'^3}{3a^2}\right] \tag{3.52}$$

The sine and cosine functions have been expanded and the approximation stated in equation (3.29) used again. Elsewhere in the expression we have set v=c.

We are now in a position to consider the polarization of the radiation emitted by a relativistic particle. Expand the sine and cosine functions in equation (3.50). We know that

$$\frac{dW}{d\omega\, d\Omega} = \frac{dW_{\parallel}}{d\omega\, d\Omega} + \frac{dW_{\perp}}{d\omega\, d\Omega} \tag{3.53}$$

From the equations (3.51) and (3.52) above we find that

$$\frac{dW_{\parallel}}{d\omega\, d\Omega} = \frac{q^2\omega^2\phi^2}{4\pi}\left| \int \exp\left[\frac{i\omega}{2\gamma^2}\left(\phi_\gamma^2 t' + \frac{c^2\gamma^2 t'^3}{3a^2}\right)\right] dt' \right|^2 \tag{3.54}$$

$$\frac{dW_{\perp}}{d\omega\, d\Omega} = \frac{q^2\omega^2}{4\pi}\left| \int \frac{ct'}{a} \exp\left[\frac{i\omega}{2\gamma^2}\left(\phi_\gamma^2 t' + \frac{c^2\gamma^2 t'^3}{3a^2}\right)\right] dt' \right|^2 \tag{3.55}$$

where $\phi_\gamma^2 = 1+\gamma^2\phi^2$. Performing the following change of variables equations (3.54) and (3.55) can be rewritten.

$$\zeta = \frac{\gamma ct'}{a\phi_\gamma} \quad ; \quad \eta = \frac{\omega\, a\, \phi_\gamma^3}{3\gamma^3} \tag{3.56}$$

$$\frac{dW_{\parallel}}{d\omega\, d\Omega} = \frac{q^2\omega^2\phi^2}{4\pi^2}\left(\frac{a\phi_\gamma}{\gamma}\right)^2 \left| \int_{-\infty}^{\infty} \exp\left[\frac{3}{2} i\eta \left(\zeta + \frac{1}{3}\zeta^3\right)\right] d\zeta \right|^2 \tag{3.57}$$

$$\frac{dW_{\perp}}{d\omega\, d\Omega} = \frac{q^2\omega^2}{4\pi^2}\left(\frac{a\phi_\gamma^2}{\gamma^2}\right)^2 \left| \int_{-\infty}^{\infty} \zeta \exp\left[\frac{3}{2} i\eta \left(\zeta + \frac{1}{3}\zeta^3\right)\right] d\zeta \right|^2 \tag{3.58}$$

The integrals are functions only of η and since most of the radiation occurs at angles of $\phi \equiv 0$ we rewrite

$$\eta = \eta(\phi=0) = \frac{\omega}{2\omega_c} \tag{3.59}$$

using equations (3.24) and (3.31).

The integrals in equations (3.57) and (3.58) can be expressed in terms of modified Bessel functions of orders 1/3 and 2/3:

$$\frac{dW_{\perp}}{d\omega\, d\Omega} = \frac{q^2\omega^2}{3\pi^2}\left(\frac{a\phi_\gamma^2}{\gamma^2}\right) K_{\frac{2}{3}}^2(\eta) \tag{3.60}$$

$$\frac{dW_{\parallel}}{d\omega\, d\Omega} = \frac{q^2\omega^2\phi^2}{3\pi^2}\left(\frac{a\phi_\gamma}{\gamma}\right)^2 K^2_{\frac{1}{3}}(\eta) \tag{3.61}$$

where definitons of $K_{1/3}$ and $K_{2/3}$ are given in Abramowitz and Stegun, formulas 10.4.26,10.4.31,10.4.32 [58]. Integration of equations (3.60) and (3.61) over unit solid angle gives the energy per frequency range radiated by the particle per complete orbit in the projected normal plane. The element solid angle is taken as $d\Omega=2\pi\sin\theta d\phi$ so

$$\frac{dW_{\perp}}{d\omega} = \frac{2q^2\omega^2a^2\sin\theta}{3\pi\gamma^4}\int_{-\infty}^{\infty}\phi_\gamma^4\, K^2_{\frac{2}{3}}(\eta)\, d\phi \tag{3.62}$$

$$\frac{dW_{\parallel}}{d\omega} = \frac{2q^2\omega^2a^2\sin\theta}{3\pi\gamma^2}\int_{-\infty}^{\infty}\phi_\gamma^2\phi^2\, K^2_{\frac{1}{3}}(\eta)\, d\phi \tag{3.63}$$

We can integrate over all space because the integrand is concentrated to small values of $\Delta\phi$ about θ; of the order of $1/\gamma$. The integrals in equations (3.62) and (3.63) can be reduced further [Westfold] so that the components of emitted power become

$$\frac{dW_{\perp}}{d\omega} = \frac{\sqrt{3}\, q^2\gamma\sin\theta}{2}\Big[F(x) + G(x)\Big] \tag{3.64}$$

$$\frac{dW_{\parallel}}{d\omega} = \frac{\sqrt{3}\, q^2\gamma\sin\theta}{2}\Big[F(x) - G(x)\Big] \tag{3.65}$$

where $x=\omega/\omega_c$ and F(x), G(x) are

$$F(x) = x\int_{x}^{\infty} K_{\frac{5}{3}}(\zeta)\, d\zeta \tag{3.66}$$

$$G(x) = x\, K_{\frac{2}{3}}(x) \tag{3.67}$$

Division by the orbital period $T=2\pi/\omega_B$ will convert the above equations to emitted power per unit frequency

$$P_{\perp}(\omega) = \frac{\sqrt{3}\, q^3 B \sin\theta}{4\pi m} \left[F(x) + G(x) \right] \tag{3.68}$$

$$P_{\parallel}(\omega) = \frac{\sqrt{3}\, q^3 B \sin\theta}{4\pi m} \left[F(x) - G(x) \right] \tag{3.69}$$

Thus the total emitted power per frequency is simply the sum of the parallel and perpendicular components

$$P(\omega) = \frac{\sqrt{3}\, q^3 B \sin\theta}{4\pi m} F(x) \tag{3.70}$$

which we can compare with equation (3.42). The power in terms of frequency ν is simply

$$P(\nu) = 2\pi P(\omega) = \frac{\sqrt{3}\, q^3 B \sin\theta}{2m} F(x) \tag{3.71}$$

For any distribution of particles which varies smoothly with the pitch angle θ, emission cones from both sides of the line of sight will contribute equally to the total radiation seen. In such a case the elliptically polarized components which arise from each particle will cancel out leaving the radiation linearly polarized. This polarization can be described simply by using the powers per unit frquency parallel and perpendicular to the projection of the magnetic field on the plane of the sky. Since the polarization is linear we can use the expression for the degree of linear polarization for particles of a single energy given by equation (2.15),

$$\Pi = \frac{I_{max} - I_{min}}{I_{max} + I_{min}} \tag{2.15}$$

We know that the parallel component of the emitted power is equivalent to the minimum intensity passed by a polarizing filter and that the perpendicular component is equivalent to the maximum intensity so we can write

$$\Pi = \frac{P_{\perp}(\omega) - P_{\parallel}(\omega)}{P_{\perp}(\omega) + P_{\parallel}(\omega)} \tag{3.72}$$

Using equations (3.68) and (3.69) we find that equation (3.72) reduces to

$$\Pi = \frac{G(x)}{F(x)} \tag{3.73}$$

For particles which have a power law distribution the degree of polarization can be shown to be

$$\Pi = \frac{\alpha + 1}{\alpha + \frac{7}{3}} \tag{3.74}$$

3.5 The Theory of Polarization of Synchrotron Radiation

Polarization of radiation emitted by the Crab nebula is solely due to the fact that the radiation is caused by electrons spiralling around the magnetic field lines of the nebula. This is electron synchrotron radiation which is always highly polarized if the magnetic field is non-random and the medium is optically thin. The spectral distribution is commonly represented by a power law spectrum in photon frequency. In this case the electron spectrum is also a power law,

$$n(\gamma, \underline{r}) = n_0(\underline{r})\,\gamma^{-\alpha(\underline{r})} \tag{3.75}$$

where $n(\gamma,\underline{r})$ is the distribution of electron energy, γ is the Lorentz factor, $(1-v^2/c^2)^{-1/2}$, $\alpha(\underline{r})$ is the spectral index and $n_0(\underline{r})$ is the electron density function.

The power of synchrotron emission per steradian per unit frequency range is then given by equation (3.45). We can convert equation (3.45) to frequency ν quite simply (see equation (3.71)) and insert the relevant constant to obtain

$$P(\nu) = \frac{e^2 \nu_0(\underline{r})}{\sqrt{3}} \int_0^\infty n(\gamma, \underline{r}) F\left(\frac{\nu}{\gamma^2 \nu_0(\underline{r})} \right) d\gamma \qquad (3.76)$$

where

$$\nu_0 = \frac{3eB\sin\theta}{4\pi m_e} \qquad (3.77)$$

and θ is the angle between $\underline{\mathbf{B}}$ and the line of sight. m_e is the electron mass and e the electronic charge. $B = |\underline{\mathbf{B}}|$ The function F is related to the modified Bessel function $K_{5/3}$ as shown in equation (3.66). From equation (3.75) a substitution can be made for $n(\gamma, \underline{r})$ in equation (3.76) giving

$$P(\nu) = \frac{e^2 \nu_0(\underline{r}) n_0(\underline{r})}{\sqrt{3}} \int_0^\infty \gamma^{-\alpha(\underline{r})} F\left(\frac{\nu}{\gamma^2 \nu_0(\underline{r})} \right) d\gamma \qquad (3.78)$$

Replace $\nu / \gamma^2 \nu_0(\underline{r})$ with x:

$$P(\nu) = \frac{e^2 \nu_0(\underline{r}) n_0(\underline{r})}{2\sqrt{3}} \left(\frac{\nu}{\nu_0} \right)^{\frac{1-\alpha(\underline{r})}{2}} \int_0^\infty x^{\frac{\alpha(\underline{r})-3}{2}} F(x)\, dx \qquad (3.79)$$

Hence, we can write an expression for the power of synchrotron emission per unit frequency for the whole volume,

$$P(\nu) = \frac{e^2}{2\sqrt{3}} \int_V \nu_0(\underline{r}) \left(\frac{\nu}{\nu_0}\right)^{\frac{1-\alpha(\underline{r})}{2}} n_0(\underline{r})\, F(\alpha(\underline{r}))\, dV \qquad (3.80)$$

where

$$F(\alpha(\underline{r})) = \int_0^\infty x^{\frac{\alpha(\underline{r})-1}{2}} \int_x^\infty K_{\frac{5}{3}}(x')\, dx'\, dx \qquad (3.81)$$

$F(\alpha(\underline{r}))$ is a constant if $\alpha(\underline{r})$, the spectral index, is a constant with wavelength, which is assumption 5 in chapter 6, section 6.1, so we will consider only the case where this holds. If we know the value of the spectral index it is relatively simple to calculate $F(\alpha)$ numerically in terms of gamma functions. We shall discuss the evalution of the functions F and G in terms of gamma functions further in chapter 6. Once evaluated $F(\alpha)$ or $G(\alpha)$ can be removed from the integrand and becomes simply a scale factor in equations (3.85), (3.86) and (3.87).

The powers per unit volume per unit frequency which are related to the Stokes intensities are represented by equations which are similar to equation (3.80):

$$P_Q(\nu) = \frac{e^2}{2\sqrt{3}} \int_V n_0(\underline{r})\, \nu_0(\underline{r}) \left(\frac{\nu}{\nu_0}\right)^{\frac{1-\alpha(\underline{r})}{2}} \cos 2\chi(\underline{r})\, G(\alpha(\underline{r}))\, dV \qquad (3.82)$$

$$P_U(\nu) = \frac{e^2}{2\sqrt{3}} \int_V n_0(\underline{r})\, \nu_0(\underline{r}) \left(\frac{\nu}{\nu_0}\right)^{\frac{1-\alpha(\underline{r})}{2}} \sin 2\chi(\underline{r})\, G(\alpha(\underline{r}))\, dV \qquad (3.83)$$

where $\chi(\underline{r})$ is the angle of polarization and

$$G(\alpha(\underline{r})) = \int_0^\infty x^{\frac{\alpha(\underline{r})-1}{2}} \int_x^\infty K_{\frac{2}{3}}(x')\, dx'\, dx \qquad (3.84)$$

$G(\alpha(\underline{r}))$ is a constant if $\alpha(\underline{r})$ is a constant and can be evaluated numerically in a similar way to $F(\alpha(\underline{r}))$.

Since ν_0 is related to the component of the magnetic field which is perpendicular to the line of sight, $B_\perp$, we can use equation (3.77) to replace ν_0 in equations (3.80), (3.82) and (3.83). Also, we can change the integral over volume to an integral per unit area over the line of sight. This gives us a set of equations which tell us what we would see in terms of Stokes intensities if we observed the magnetic field $B_\perp$ along a line of sight s. These operations yield the following three equations:

$$I(\nu) = \kappa F(\alpha) \int_{-\infty}^{\infty} n_0(\underline{r}) (B_\perp)^{\frac{1+\alpha}{2}} \, ds \tag{3.85}$$

$$I_Q(\nu) = \kappa G(\alpha) \int_{-\infty}^{\infty} n_0(\underline{r}) (B_\perp)^{\frac{1+\alpha}{2}} \cos 2\chi \, ds \tag{3.86}$$

$$I_U(\nu) = \kappa G(\alpha) \int_{-\infty}^{\infty} n_0(\underline{r}) (B_\perp)^{\frac{1+\alpha}{2}} \sin 2\chi \, ds \tag{3.87}$$

where $F(\alpha)$, $G(\alpha)$ and χ are treated as constant with respect to $\underline{r}$ and κ is a constant for a given frequency,

$$\kappa = \frac{e^2 \nu^{\frac{1-\alpha}{2}}}{2\sqrt{3}}$$

Equations (3.85), (3.86) and (3.87) are used in the models described in chapter 6 to generate values of the Stokes intensities for given magnetic field structures.

Chapter 4

Plasma Theory

4.1 Introduction

In this chapter we deal with the basic plasma physics needed to study the Crab nebula. The theory presented in section 4.2 follows that given in Bittencourt [59] and leads us to the concept of "frozen-in" magnetic fields. In section 4.3 we discuss briefly the plasma aspects of the Crab nebula. Section 4.4 elaborates on the previous discussion with reference to recent work in this field. In particular, section 4.4 includes a discussion of the paper by Tsikarishvili et al [55] which prompted the work on the frozen-in field equation which is presented in section 4.5.

4.2 Macroscopic Magnetohydrodynamic Equations

A plasma can be treated as a conducting fluid and there is no need to specify the species of particles present in the plasma. Transport equations can be derived which describe the behaviour of the plasma as a whole. As well as these hydrodynamic transport equations we require a set of electrodynamic equations to fully describe the properties of the plasma. Dealing with a plasma in this way we can make several simplifying assumptions which result in a set of equations that completely describe the plasma behaviour. These equations, generally known as simplified magnetohydrodynamic (MHD) equations, are as follows:

1) the equation of continuity for the plasma

$$\frac{\partial \rho_m}{\partial t} + \underline{\nabla} \cdot (\rho_m \underline{v}) = 0 \qquad (4.1)$$

2) the equation of motion

$$\rho_m \left(\frac{D\underline{\mathbf{v}}}{Dt}\right) = (\underline{\mathbf{J}} \wedge \underline{\mathbf{B}}) - \underline{\nabla}\, p \tag{4.2}$$

3) the adiabatic equation for conservation of energy

$$\underline{\nabla}\, p = v_s^2\, \underline{\nabla}\, \rho_m \tag{4.3}$$

4) the Maxwell curl equation for the electric field

$$\underline{\nabla} \wedge \underline{\mathbf{E}} = -\frac{\partial \underline{\mathbf{B}}}{\partial t} \tag{4.4}$$

5) the Maxwell curl equation for the magnetic field

$$\underline{\nabla} \wedge \underline{\mathbf{B}} = \mu_0 \underline{\mathbf{J}} \tag{4.5}$$

Note that we neglect the displacement current term in this Maxwell curl equation when dealing with a plasma;

6) a generalised form of Ohm's law in which the Hall effect term is neglected leaving

$$\underline{\mathbf{J}} = \sigma_0 \left(\underline{\mathbf{E}} + \underline{\mathbf{v}} \wedge \underline{\mathbf{B}} \right) \tag{4.6}$$

In equations (4.1) to (4.6) viscosity and thermal conductivity are neglected. ρ_m is the total mass density, $\underline{\mathbf{v}}$ the average fluid velocity, $\underline{\mathbf{J}}$ the electric current density, $\underline{\mathbf{B}}$ magnetic flux density, σ_0 is the electrical conductivity of the fluid, $\underline{\mathbf{E}}$ the electric field, μ_0 the magnetic permeability of free space, p the total scalar pressure and v_s the adiabatic speed of sound

$$v_s = \left(\frac{\gamma p}{\rho_m}\right)^{\frac{1}{2}} \tag{4.7}$$

We also assume here that charge neutrality is maintained to a high degree on a macroscopic scale and that the time derivatives and pressure gradients are negligible in equation (4.6).

The generalised form of Ohm's law can be used to obtain a simple expression for the magnetic flux density $\underline{\mathbf{B}}$. Taking the curl of equation (4.6) we obtain

$$\underline{\nabla} \wedge \underline{\mathbf{J}} = \sigma_0 \left[(\underline{\nabla} \wedge \underline{\mathbf{E}}) + \underline{\nabla} \wedge (\underline{\mathbf{v}} \wedge \underline{\mathbf{B}}) \right] \tag{4.8}$$

Using equations (4.4) and (4.5) to replace the current density and the curl of the electric field modifies equation (4.8) to

$$\underline{\nabla} \wedge (\underline{\nabla} \wedge \underline{\mathbf{B}}) = \mu_0 \sigma_0 \left[-\frac{\partial \underline{\mathbf{B}}}{\partial t} + \underline{\nabla} \wedge (\underline{\mathbf{v}} \wedge \underline{\mathbf{B}}) \right] \tag{4.9}$$

A well known vector identity shows that

$$\underline{\nabla} \wedge (\underline{\nabla} \wedge \underline{\mathbf{B}}) = \underline{\nabla}(\underline{\nabla} . \underline{\mathbf{B}}) - \nabla^2 \underline{\mathbf{B}} \tag{4.10}$$

Here we make use of Maxwell's equation for the divergence of the magnetic flux density,

$$\underline{\nabla} . \underline{\mathbf{B}} = 0 \tag{4.11}$$

in conjunction with equation (4.10) so that equation (4.9) reduces to

$$\frac{\partial \underline{\mathbf{B}}}{\partial t} = \underline{\nabla} \wedge (\underline{\mathbf{v}} \wedge \underline{\mathbf{B}}) + n_m \nabla^2 \underline{\mathbf{B}} \tag{4.12}$$

n_m is called the *magnetic viscosity* and is given by the expression

$$n_m = \frac{1}{\mu_0 \sigma_0}$$

The first term of the right hand side of equation (4.12) is the *flow term* and the second is the *diffusion term.* It is often useful to consider the relative importance of these terms. To do this a ratio between the flow and diffusion terms is taken and called the magnetic Reynolds number,

$$R_m = \frac{vL}{n_m} \tag{4.13}$$

where L denotes the characteristic length of variation of the parameters. If R_m is much less than unity diffusion dominates the plasma behaviour. In this case equation (4.12) can be simplified to

$$\frac{\partial \underline{\mathbf{B}}}{\partial t} = n_m \nabla^2 \underline{\mathbf{B}} \qquad (R_m << 1) \tag{4.14}$$

As a result of diffusion the magnetic field will decay and L is related to the decay time. The time of decay depends strongly on the size of the conductor; the larger the conductor, the longer the decay time.

In the case where the magnetic Reynolds number is much greater than unity the flow term dominates equation (4.12) which becomes

$$\frac{\partial \underline{\mathbf{B}}}{\partial t} = \underline{\nabla} \wedge (\underline{\mathbf{v}} \wedge \underline{\mathbf{B}}) \qquad (R_m >> 1) \tag{4.15}$$

In this case the above equation implies that, instead of the magnetic field diffusing away, the magnetic field lines move along with the fluid (or vice versa). This type of behaviour is usually referred to as a "frozen-in" field. The fluid is free to move independently along the magnetic field lines but independent motion perpendicular to the magnetic field lines is severely restricted. Any motion of the fluid in such a

direction causes an equivalent motion in the magnetic field and vice versa. An alternative illustration of this effect, with particular reference to pulsars, was given by Barnard [53]; "A frozen-in field implies that a field line that is anchored at a point on a surface that is co-rotating with the neutron star at a radius equal to the radius of the light cylinder will pass through the locus of all points at which there is plasma which has passed through that particular point.".

4.3 The Crab Nebula as a Plasma

The Crab nebula is an electron-positron plasma with an average electron density of approximately $n_e=10^3\ cm^{-3}$ [12]. The plasma particles are produced by pair production around the pulsar's magnetic polar caps [40,51] and ejected along the open field lines, in the form of a relativistic MHD wind [4,13] into the main part of the nebula. The pulsar magnetosphere has two components [4,13,53,55], a closed region where the plasma and the pulsar co-rotate and an open region where the relativistic electron-positron wind dominates. The closed region exists within the pulsar's light cylinder, while outside the light cylinder particles spiral around the magnetic field lines causing the observed electron synchrotron radiation which gives the Crab nebula many of its unique characteristics (see figure 4.1).

Theory of the magnetic field structure in the closed region of the pulsar magnetosphere is quite well understood and states that the field should have a dipole structure [43,53]. For this reason, and because the closed region is far too small to be observed at the resolution of the data used in this work (see chapter 5), we have concentrated on the region outside the light cylinder. Here the magnetic field is "frozen-in" to the plasma and we can use the set of macroscopic MHD equations defined in section 4.1 to describe the plasma behaviour of the open region of the Crab nebula.

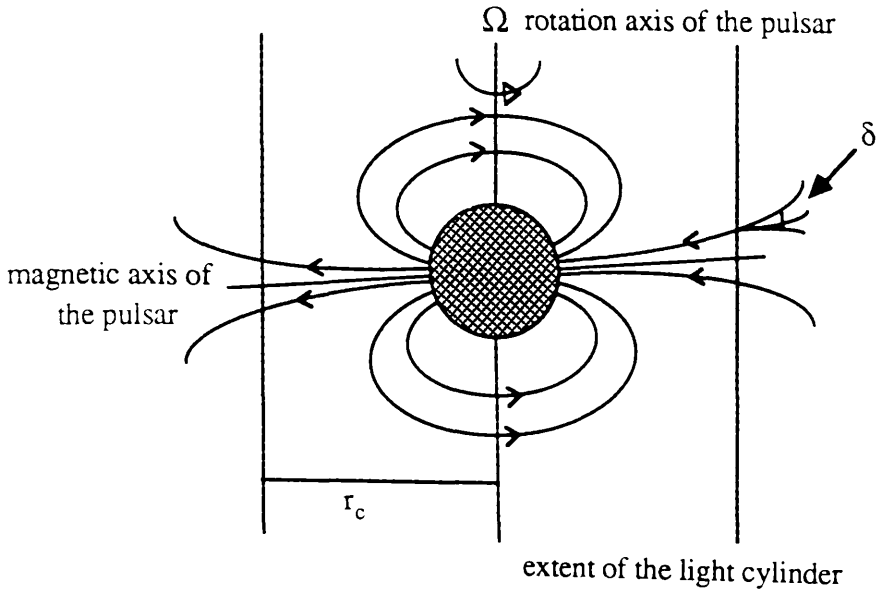

Figure 4.1: The Crab nebula pulsar is an oblique rotator, i.e. the magnetic axis is at an angle to the rotational axis. The angle between the magnetic axis and the rotational axis of the Crab pulsar is almost 90°. r_c is the radius of the light cylinder and δ is the angle of divergence of the plasma as it leaves the light cylinder. (After Tsikarishvili et al [55].)

4.4 Recent Work on Plasma Aspects of the Crab Nebula

Treatment of the Crab nebula as a plasma is not a new idea [42]. Deutsch [43] solved the frozen-in field equation (equation 4.15) to find the magnetic field structure surrounding a rotating magnetic star in a vacuum. Although Deutsch's solution did not allow for the effects of a plasma surrounding the star his model holds quite well in the closed region of the pulsar magnetosphere and the frozen-in field equation is still valid within a plasma that can be treated using the ideal MHD equations. A more recent attempt to find a solution of the frozen-in field equation in the open region of the Crab nebula was made by Tsikarishvili et al [55]. These authors used the frozen-in field equation to describe the structure of the magnetic field outside the light cylinder. The main difference between the treatment given by Tsikarishvili et al to that of earlier papers is that previously [41,42] the build up of a toroidal field was thought to take place during the whole lifetime of the nebula whereas Tsikarishvili et al postulate that the toroidal field component is generated continuously, and almost instantaneously, in the neighbourhood of the light cylinder

and then transferred to the rest of the nebula by the outflow of relativistic particles. The time for this transfer to occur is of the order of months compared to transfer times of hundreds of years suggested by previous models. Thus the field structure is only changed by nebula expansion and movement of the pulsar and the authors present a "quasi-stationary" picture of the nebula where the necessary outlet for magnetic energy is provided by reconnection around the filaments and consequent annihilation of directionally opposed fields.

The qualitative picture of magnetic field development presented in this paper is similar to previous models of the magnetic field structure but differs mainly in that a double layer disc of toroidal magnetic field is expected to form around the pulsar's rotational equator rather than a single disc of toroidal field [44,45,50]. The disc is expected to be approximately 20 arcseconds in radius; this size corresponds to 4 pixels at the resolution used by Woltjer [1] and 13 pixels at the resolution of McLean, Aspin and Reitsema's data [2] and so should be detectable (for further details see chapter 5).

Consider figure 4.1. The angle between the pulsar rotation axis and its magnetic axis is not exactly 90°. The electron-positron plasma flows out along the open field lines across the light cylinder boundary with a small divergence δ. The plasma leaves the light cylinder almost tangentially as the rotational energy of the magnetosphere is transferred to kinetic energy of the relativistic particles and carries the magnetic field with it. The magnetic field is frozen-in to the plasma outside the light cylinder and rotates more slowly than the pulsar; the rotation velocity of the Crab nebula can be considered to be zero in the observer's frame. Thus the open field lines are dragged out into a spiral or torus. If the pulsar's magnetic axis were at exactly 90° to its rotational axis the open field lines for each of the two magnetic poles would form two interlocked spirals which would move outwards. As these spirals moved outwards they would meet and reconnect. This would destroy the toroidal field components as the magnetic fields in the spirals are oppositely directed. Since the angle between the axes is not 90° the two spirals of frozen-in magnetic

field form separately, one above and one below the rotational equator (see figure 4.2).

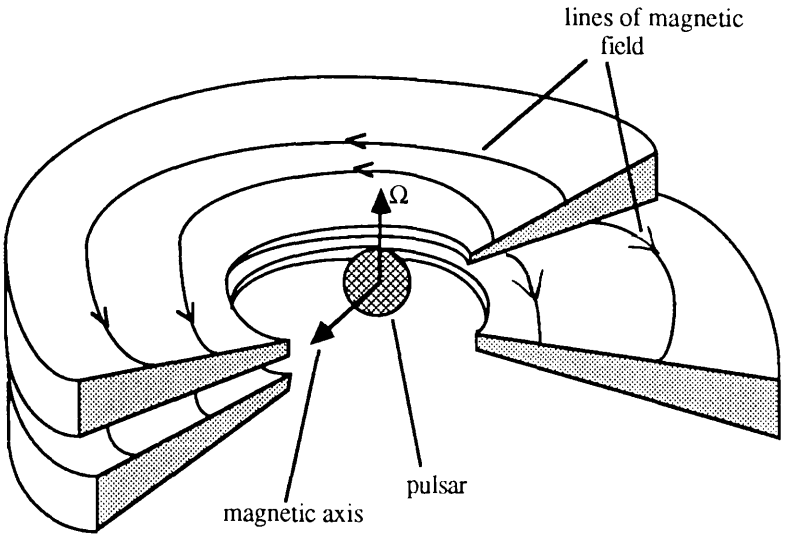

Figure 4.2: The two discs of magnetic field produced as the pulsar rotates. The field direction in the top disc is opposite in sense to that in the lower disc. The inner boundary of the discs coincides with the outer boundary of the light cylinder. (After Tsikarishvili et al [55].)

Tsikarishvili et al predict that the toroidal magnetic field generated in this way will be transported radially outwards by the plasma. This field would decrease as the inverse of the distance from the pulsar. Thus the synchrotron radiation intensity would decrease towards the edges of the nebula as observed. The toroidal character of the magnetic field is lost as it moves out through the nebula because the field cannot pass through the filaments as easily as the plasma can. Tsikarishvili et al use a theory, proposed in 1972 by Wilson [33], which allows the field to pass by the filaments by reconnection but also accounts for the enhanced radiation seen from the filaments by a build up of magnetic field around them. The magnetic field wraps around the filament and eventually reconnects on the downstream side, leaving a ring of magnetic field around the filament (see figure 4.3). Such rings of magnetic field would cause currents to run through the filaments as originally proposed by

Woltjer [60]. Such enhancement could also account for the high degrees of polarization seen in the eastern and western bays of the nebula (chapter 5, figures 5.1 and 5.3) where the polarization pattern indicates a ring of field around a region of conducting gas.

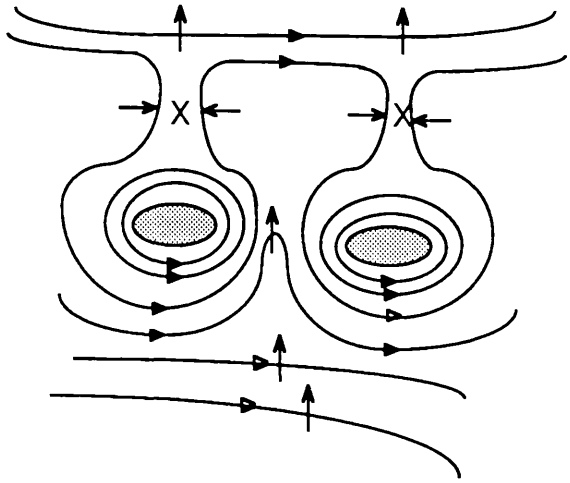

Figure 4.3: As the plasma flows outwards past the filaments (shaded regions) the magnetic field is distorted around them. Areas of reconnection (X) occur on the downstream side of the filaments and rings of magnetic field form about the filaments which may explain the enhanced emission seen here and the presence of currents which are thought to run through the filaments. Filaments do not obstruct the outflow of magnetic field but contribute to the degradation of its toroidal character. (After Wilson [33].)

Qualitatively, this model describes the features of the Crab nebula well but the quantitative analysis undertaken by Tsikarishvili et al [55] is not adequate. Choosing the rotation axis of the pulsar to be the z-axis the authors expanded equation (4.15) in cylindrical polar coordinates and attempted to find a solution which would give an expression for the magnetic field component in the ϕ direction; this would correspond to the toroidal component of the field. Deutsch's solution of the frozen-in field equation [43] gives the field components in the open region of the nebula in spherical polar coordinates as wave functions but Tsikarishvili et al have

tried to solve the equation for a non-wave field by setting all time derivatives of the magnetic field equal to zero. The main problem with their analysis is that they neglected terms from the expansion of equation (4.15) which are in fact not negligible and were inconsistent in their treatment of the radial component of the magnetic field. In equation (8) of Tsikarishvili et al's paper the radial component is considered to be independent of the distance from the pulsar but in equation (10) is given as a function of the distance

$$B_r = B_{rc} \left(\frac{r_c}{r}\right)^k$$

where B_{rc} is the radial component of the magnetic field at the perimeter of the light cylinder, r_c is the radius of the light cylinder, r is the distance from the pulsar and k is a constant which the authors set equal to 2 outside the light cylinder. This expression is similar to expressions used in Barnard [53]. The method of solution of the partial differential equation for B_ϕ used in Tsikarishvili et al's paper is incorrect due to the neglect of terms which do not have a negligible effect on the solution and the fact that the solution is obtained by setting each term equal to zero in turn, solving the equation thus obtained and superposing the solutions of each of these equations. The solution obtained in this way is not comparable to a static case of Deutsch's wave solution although it satisfies the criteria outlined by Tsikarishvili et al in their qualitative discussion.

4.5 Treatment of the Frozen-in Field Equation

We will now consider equation (4.15)

$$\frac{\partial \underline{\mathbf{B}}}{\partial t} = \underline{\nabla} \wedge (\underline{\mathbf{v}} \wedge \underline{\mathbf{B}})$$

in relation to the static solution ($\partial \underline{\mathbf{B}}/\partial t=0$) for the Crab nebula in more detail. The

curl of a vector $\underline{u}$ in cylindrical polar coordinates is

$$\underline{\nabla} \wedge \underline{\mathbf{u}} = \hat{\mathbf{r}} \left[\frac{1}{r}\frac{\partial u_z}{\partial \phi} - \frac{\partial u_\phi}{\partial z} \right] + \hat{\phi} \left[\frac{\partial u_r}{\partial z} - \frac{\partial u_z}{\partial r} \right] + \hat{\mathbf{z}} \left[\frac{1}{r}\frac{\partial}{\partial r}(r u_\phi) - \frac{1}{r}\frac{\partial u_r}{\partial \phi} \right] \quad (4.16)$$

The cross product of the vectors $\underline{\mathbf{v}}$, the velocity of the plasma, and $\underline{\mathbf{B}}$, the magnetic flux intensity, in cylindrical polar coordinates is

$$\underline{\mathbf{v}} \wedge \underline{\mathbf{B}} = \hat{\mathbf{r}} (v_\phi B_z - v_z B_\phi) + \hat{\phi} (v_z B_r - v_r B_z) + \hat{\mathbf{z}} (v_r B_\phi - v_\phi B_r) \quad (4.17)$$

combining equations (4.16) and (4.17) we find that we have three equations involving the components of the magnetic field:

$$\frac{\partial B_r}{\partial t} = \frac{1}{r}\frac{\partial}{\partial \phi}(v_r B_\phi - v_\phi B_r) - \frac{\partial}{\partial z}(v_z B_r - v_r B_z) \quad (4.18)$$

$$\frac{\partial B_\phi}{\partial t} = \frac{\partial}{\partial z}(v_\phi B_z - v_z B_\phi) - \frac{\partial}{\partial r}(v_r B_\phi - v_\phi B_r) \quad (4.19)$$

$$\frac{\partial B_z}{\partial t} = \frac{1}{r}\frac{\partial}{\partial r}(r (v_z B_r - v_r B_z)) - \frac{1}{r}\frac{\partial}{\partial \phi}(v_\phi B_z - v_z B_\phi) \quad (4.20)$$

For a static solution the time derivatives in equations (4.18), (4.19) and (4.20) should equal zero. These three partial differential equations cannot be solved unless we know the form of the velocity components with relation to the magnetic field, or vice versa.

In the solution attempted by Tsikarishvili et al all dependencies on ϕ were neglected so that all derivatives with respect to ϕ were equal to zero. If the field generated is a spiral field as suggested and is generated simply by winding up the open magnetic field lines then it is reasonable to assume that the magnetic flux density does not vary with ϕ i.e. the field is rotationally symmetric and will look the same no matter from which value of ϕ it is viewed. Making this assumption

simplifies equations (4.18), (4.19) and (4.20) as follows:

$$\frac{\partial B_r}{\partial t} = 0 = -\frac{\partial}{\partial z}(v_z B_r - v_r B_z) \tag{4.21}$$

$$\frac{\partial B_\phi}{\partial t} = 0 = \frac{\partial}{\partial z}(v_\phi B_z - v_z B_\phi) - \frac{\partial}{\partial r}(v_r B_\phi - v_\phi B_r) \tag{4.22}$$

$$\frac{\partial B_z}{\partial t} = 0 = \frac{1}{r}\frac{\partial}{\partial r}(r\,(v_z B_r - v_r B_z) \tag{4.23}$$

From equation (4.11), Maxwell's equation for the divergence of the magnetic flux density, we see that

$$\underline{\nabla} \cdot \underline{\mathbf{B}} = 0 = \frac{1}{r}\frac{\partial}{\partial r}(rB_r) + \frac{1}{r}\frac{\partial B_\phi}{\partial \phi} + \frac{\partial B_z}{\partial z} \tag{4.24}$$

Neglecting the ϕ derivative term we have

$$\frac{1}{r}\frac{\partial}{\partial r}(rB_r) + \frac{\partial B_z}{\partial z} = 0 \tag{4.25}$$

We must assume that B_z is a function of z, especially if the toroidal component is confined to two discs in the rotational equatorial region of the pulsar. Therefore, rB_r must be a function of r and z and not a constant as is assumed in equation (8) of Tsikarishvili et al's paper.

We now have a set of four partial differential equations, (4.21), (4.22), (4.23) and (4.25). In order to solve these equations for the magnetic field structure we still need to know the form of the velocity field. No further analysis of these equations will be made in this thesis. The original intention behind the study of the paper by Tsikarishvili et al [55] was to obtain an expression for B_ϕ which could be employed in the theoretical model which had been developed (see chapter 6), not to derive an

exact analytical solution of this set of equations. Solution of equations (4.21), (4.22), (4.23) and (4.25) would be extremely time consuming and is not within the scope of this thesis, but it would be interesting if a solution were found as it could then be incorporated into the theoretical model.

Chapter 5

Analysis of the Data Sets of Woltjer and McLean, Aspin and Reitsema

5.1 Introduction

In this chapter we present the data analysis performed as part of this project. We discuss the tests and manipulations which were performed on the two data sets and the results of these tests. The observations which produced the two data sets used in this work are separated by a period of 26 years.

Photoelectric observations of the surface brightness and linear polarization of the Crab nebula were made by Baade[1] and Walraven[25] in 1954-55. This data was published in a paper by Woltjer[1]. The resolution of the data is 5.25" over an area of 5x4 arcminutes; this covers all of the optically visible nebula. In all, Woltjer's data set contains values of the angle of polarization χ, the degree of polarization Π and the intensity of emitted radiation from the nebula I for 1044 pixels. 57 other pixels within the area observed had no measured data values and so values were interpolated from surrounding data points (see section 5.2) making a total number of 1101 pixels. This data set is quite small, was typed into the Acorn Cambridge Workstation directly from the paper and is easily handled by the computer programs used whereas the second data set used in this work is much larger. This second data set come from CCD observations of the polarization parameters of the Crab nebula made by McLean, Aspin and Reitsema in 1981 [2]. These observations cover a slightly smaller area of the nebula than Woltjer's data but the observations were made using a resolution of 1.5" instead of 5.25". McLean, Aspin and Reitsema's data set covers the observed area with a 357x264 pixel scan. For each pixel there is a measurement of the intensity I, the Stokes parameter Q and the Stokes parameter U. This data was obtained by Cawthorne and Brown on the Royal Observatory

Edinburgh's STARLINK Vax. Stars were removed from the field and the data then stored on a magnetic tape in Vax Fortran format. In order for it to be used in this project the data was read from the tape onto the Glasgow University Local Area VAX Cluster (LAVc), which is a system comprising one VAX 8250 and two MicroVAX 3600 processors. Initially all the work on Woltjer's data set was performed using an Acorn Cambridge Workstation but was repeated using the LAVc mainframe computers.

Listings of all the computer programs mentioned in this chapter can be found in appendix A. These programs are written in Fortran.

5.2 Initial Analysis of Woltjer's Data

Interpolations of data values for the 57 pixels with no recorded data were obtained by simply summing the surrounding data values for the required parameter and dividing this sum by the number of data values used. Most interpolations used 8 data values, but some had as few as 3 existing measurements for the calculation. This method yielded interpolated data values which did not vary greatly from neighbouring measurements and, in fact, gave a smooth variation on the small scale which was comparable with areas of the nebula where no interpolations were made.

In its original format the data comprised two files, one containing values of polarization angle, degree of polarization and intensity and another defining the length of each row of data relative to the greatest extent of either side of the nebula (i.e. how wide the nebula is at that height of the ordinate axis). This measurement of the width of the nebula was necessary because the measurements were made by scanning from one edge of the nebula to the other at a given height and not by scanning a rectangular area covering the nebula and some of the surrounding sky. Simply plotting each row of data from these files, starting at the far left hand side of the plotting area would not give the plot shown in figure 5.1 but would give a picture of the nebula with a straight vertical edge on the left and an uneven outline on

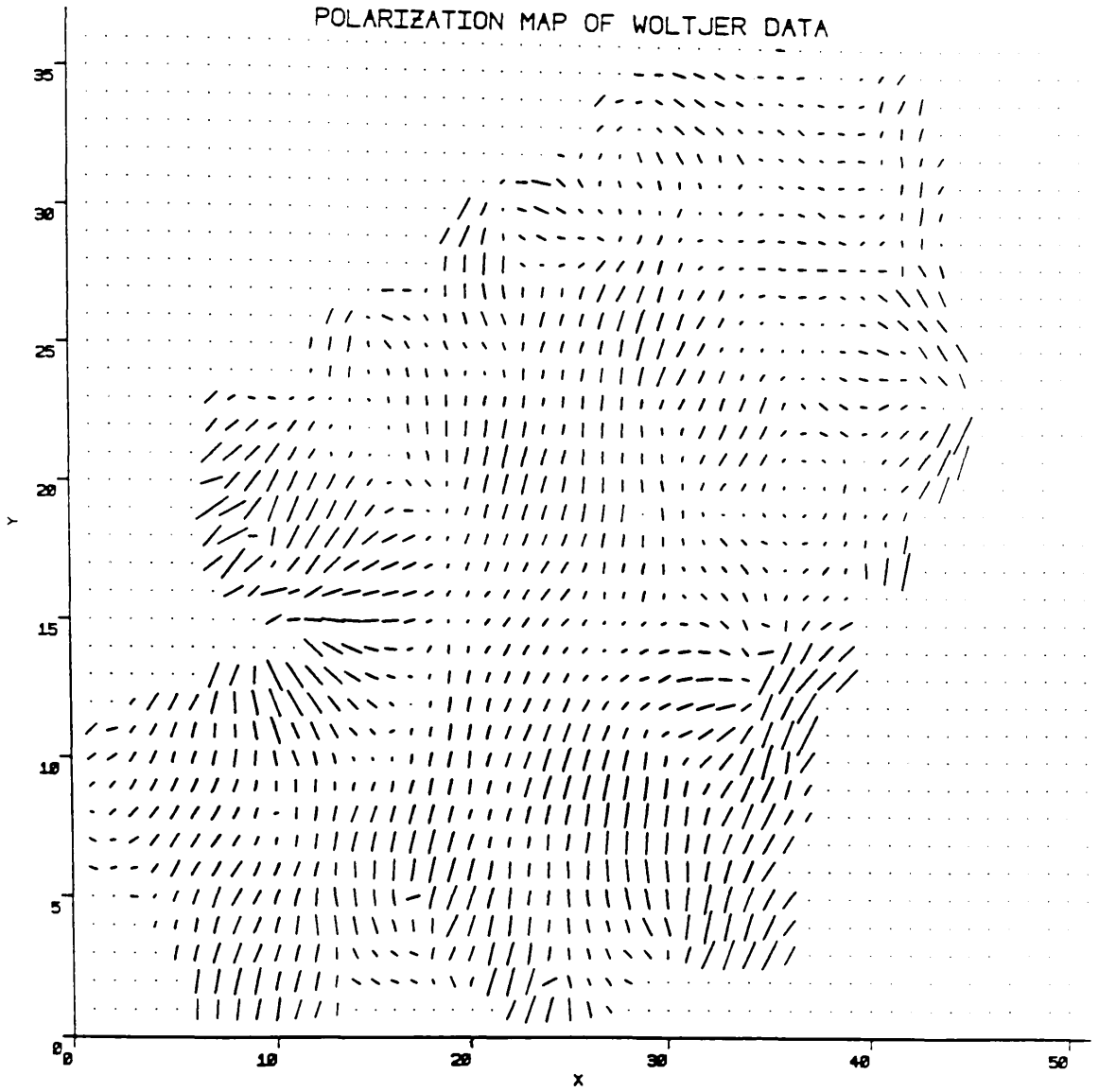

Figure 5.1: A polarization vector plot produced from Woltjer's data set. North is vertically upwards and east is to the right. Notice the areas of strong polarization with a sweeping pattern, the eastern and western bays, which are in the centre of either edge of the nebula. The angle of polarization is represented as an angle rotated anti-clockwise from the vertical and the degree of polarization is represented as the length of the line. As with other polarization plots in this thesis the maximum degree of polarization here is approximately 70%.

the right. Using the values for the ends of each line of data relative to the ordinate axis a polarization map could be plotted (see figure 5.1). Filling the region not covered by the observations with null data values produced a set of data which occupied a 51x37 pixel box and facilitated further manipulation of the data. This process was performed by program FILLCRAB.FOR. In the filled data set the pulsar is positioned at the coordinates (30,15).

The next step in analysis of Woltjer's data was the conversion of the original data from angle, degree of polarization and intensity to intensity and Stokes parameters (Q and U). This was achieved by use of the relations given in chapter 2, equations (2.21):

$$Q = \Pi \cos(2\chi) \tag{5.1}$$

$$U = \Pi \sin(2\chi) \tag{5.2}$$

The program IQUPROG.FOR performs the calculations necessary for the conversion which was necessary to enable direct comparisons to be made between Woltjer's data and McLean, Aspin and Reitsema's data [2].

A polarization vector plot as shown in figure 5.1 can be produced from Woltjer's original data set or the filled data set quite straightforwardly. The polarization angle can be plotted as a rotation anti-clockwise from the vertical direction (this corresponds to the north direction on the sky) and the degree of polarization can be represented as the length of the line drawn. Program CRABPLOT.FOR produces such a vector plot. To produce the same diagram from the Stokes parameters we must first recalculate the angle and degree of polarization using the relations given by equations (2.17) and (2.18) in chapter 2:

$$\Pi = (U^2 + Q^2)^{\frac{1}{2}} \tag{5.3}$$

$$\tan 2\chi = \frac{U}{Q} \qquad (5.4)$$

The vectors can then be drawn. Program FULLPLOT.FOR draws such a polarization vector plot, which is identical to figure 5.1, using the converted data set.

5.3 Initial Analysis of McLean, Aspin and Reitsema's Data

Since McLean, Aspin and Reitsema's (hereafter referred to as MAR) data set contains values of three parameters for almost 10^5 pixels it is not useful to plot the polarization vectors for the whole area covered by this data in one map; in order for each polarization vector to be discernibly separate and indicative of the degree of polarization such a map would have to be *at least* $1.5m^2$. Because of the sheer volume of data in this set the main data file was separated into a number of smaller data files. This was a relatively simple process but is repetitive and consumes large amounts of CPU time.

The program HIGHRES.FOR sorts the data into 56 files each covering an area of 51x33 pixels. Any of these files can then be selected and a polarization plot made using program HRPLOT.FOR, which employs the same plotting method as FULLPLOT.FOR. Program HIGHRES2.FOR sorts the main data file into 204 files, each covering a 21x22 pixel area. Any of these areas can be plotted by HR2PLOT.FOR. The final program in this series is HIGHRES3.FOR. This program sorts the main data set first into 21x24 pixel areas and then into 1683 7x8 pixel areas. This two stage process was employed simply because it is more efficient in terms of program length and running time and because it is not sensible to open 1683 Fortran logical units simultaneously as this is wasteful of filespace and running time.

The point of this process was twofold. First, we can use HR3PLOT.FOR to plot the polarization vector map for any 7x8 pixel area of the nebula we wish and can investigate this area at high resolution. By plotting the vector maps for several areas

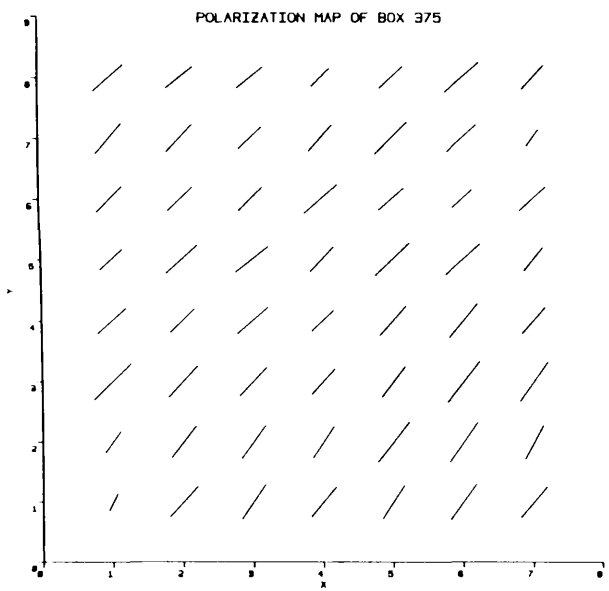

(a)

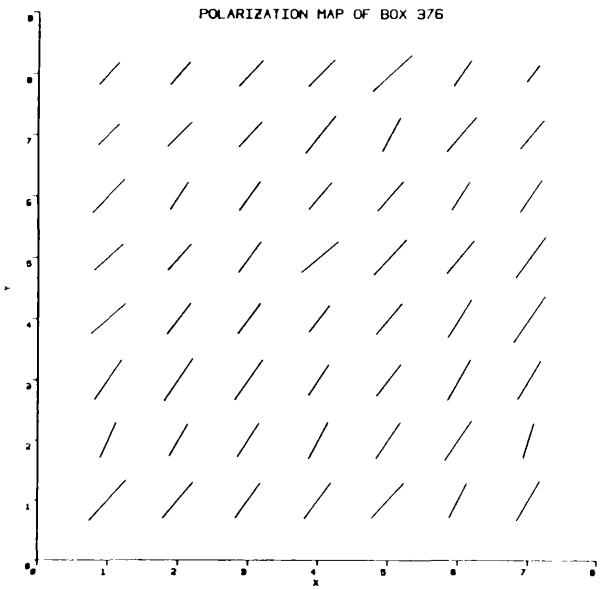

(b)

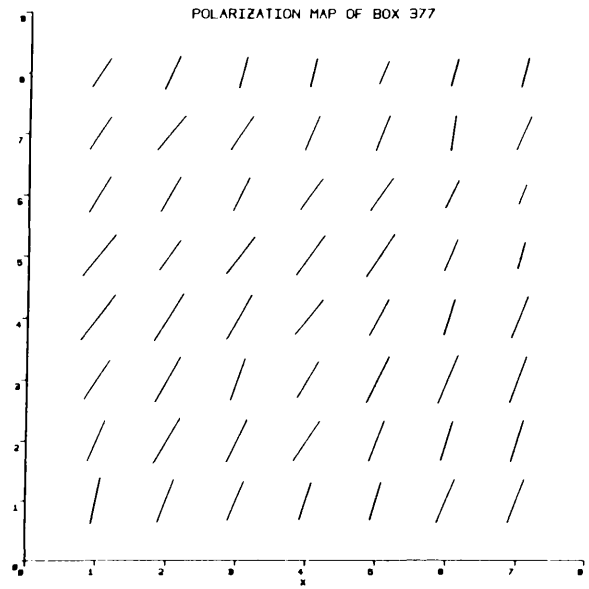

(c)

Figure 5.2: (e) The area, box 427, contains the pulsar position. Notice the rapid and multiple swings in polarization angle here as compared to the surrounding areas (a)-(d) and (f)-(i).

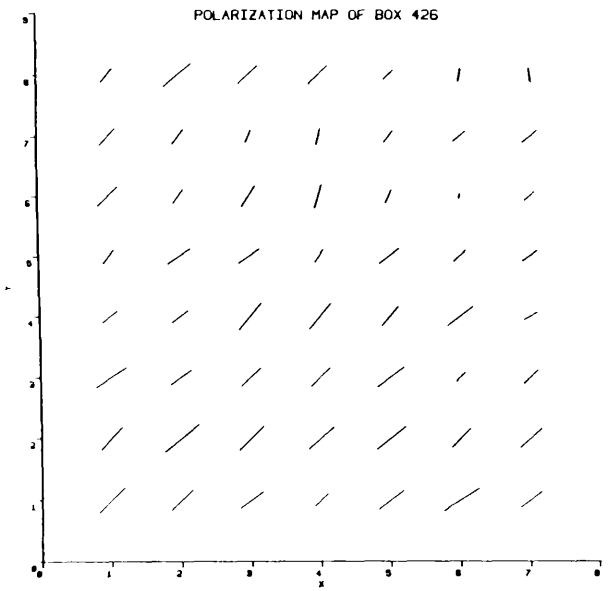
POLARIZATION MAP OF BOX 426
Y
X

(d)

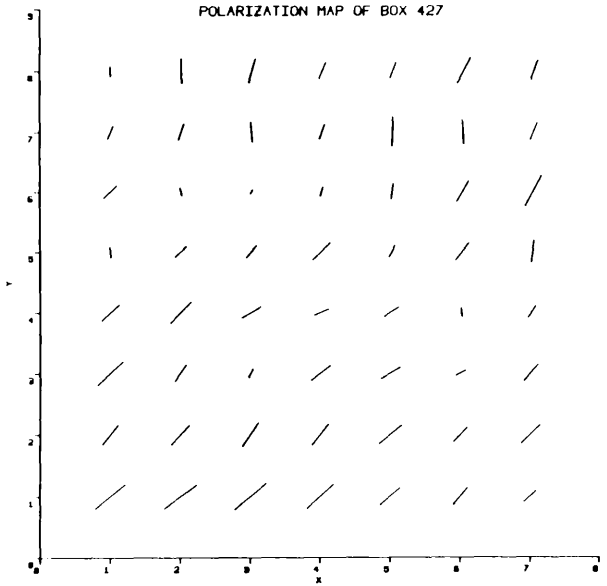
POLARIZATION MAP OF BOX 427
Y
X

(e)

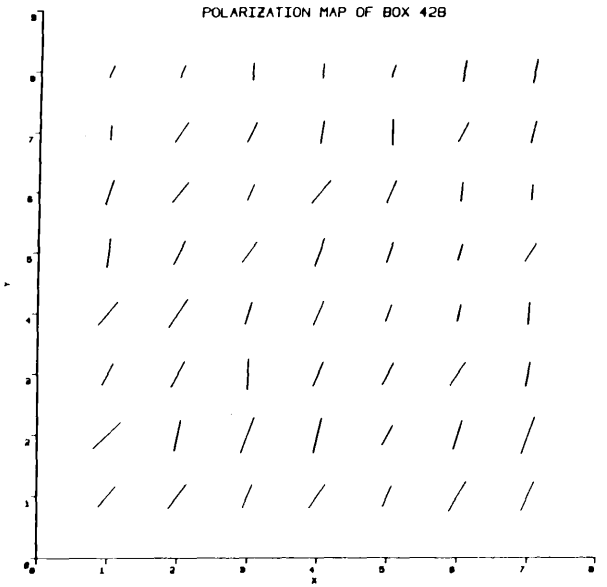
POLARIZATION MAP OF BOX 428
Y
X

(f)

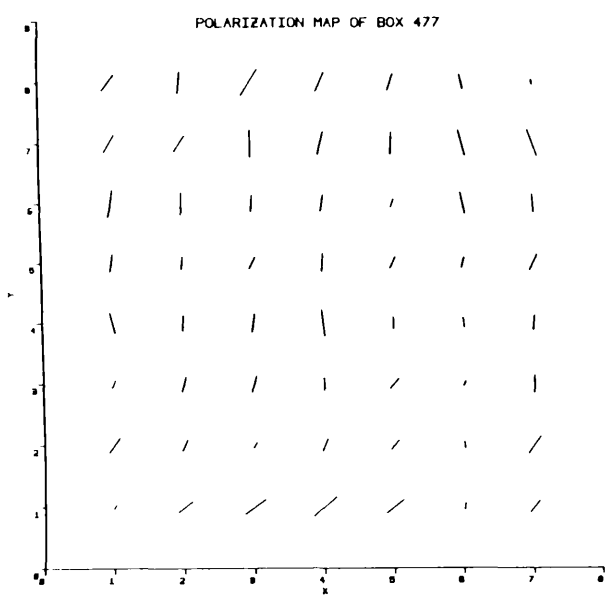
POLARIZATION MAP OF BOX 477
Y
X

(g)

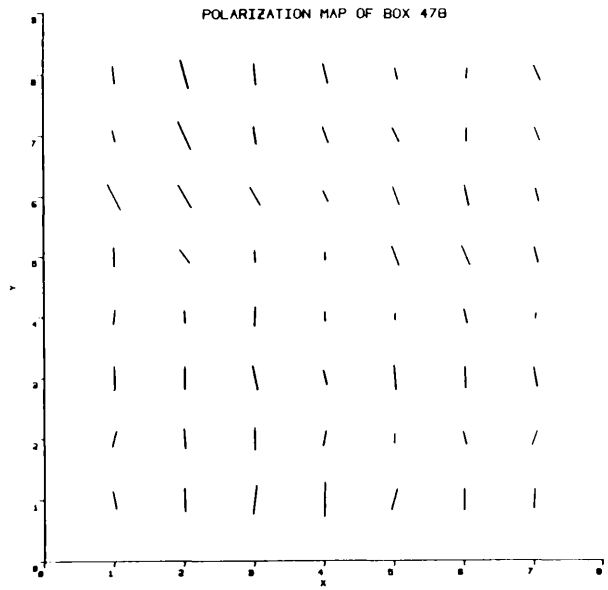
POLARIZATION MAP OF BOX 478
Y
X

(h)

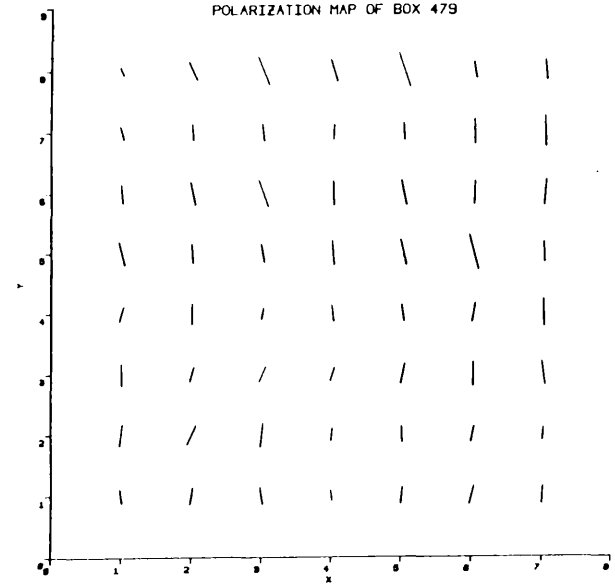
POLARIZATION MAP OF BOX 479
Y
X

(i)

it was possible to determine that the pulsar was situated at a position in the nebula which was covered by the 427th output file created by HIGHRES3.FOR. The angle of polarization changed quite rapidly in this area several times whereas the variation in the surrounding areas was smooth and in only one direction (see figure 5.2). The second and main reason for producing the 7x8 pixel files was to reduce the resolution of MAR's data to a resolution similar to that of Woltjer's data. The main data set had to be divided into 7x8 pixel blocks because these numbers (like 51 and 33, 21 and 22 and 21 and 24) are factors of 357 and 264 and this meant that the computer program for sorting the data could be relatively simple. Fortunately, this division of the data leads to a decrease in resolution which is such that MAR's data is comparable to Woltjer's. For each 7x8 block of pixels and average was taken for each of the three parameters measured. The average was obtained by adding all the non-zero values for each parameter within the block and dividing by the number of such values (see program LOWRES.FOR). This allows us to find the average value of a parameter at the edge of the nebula without including null data points which indicate the region covered by the observations which are not part of the nebula. Inclusion of these points would result in a lower average value of the parameter than we would expect. As a result of this reduction in resolution we obtained a data set which represented a 51x33 pixel box covering a region of the nebula slightly smaller than that covered by Woltjer's data. This data set was filled with zeros so that not only did it represent 51x37 pixels (the same as Woltjer's filled data set), but so that the pulsar appears in the same pixel in both data sets; x=30, y=15. It is obviously much easier to compare the two data sets when they have been processed in this fashion. A polarization vector plot of this data set, produced by LOWRESPLOT.FOR, is shown in figure 5.3.

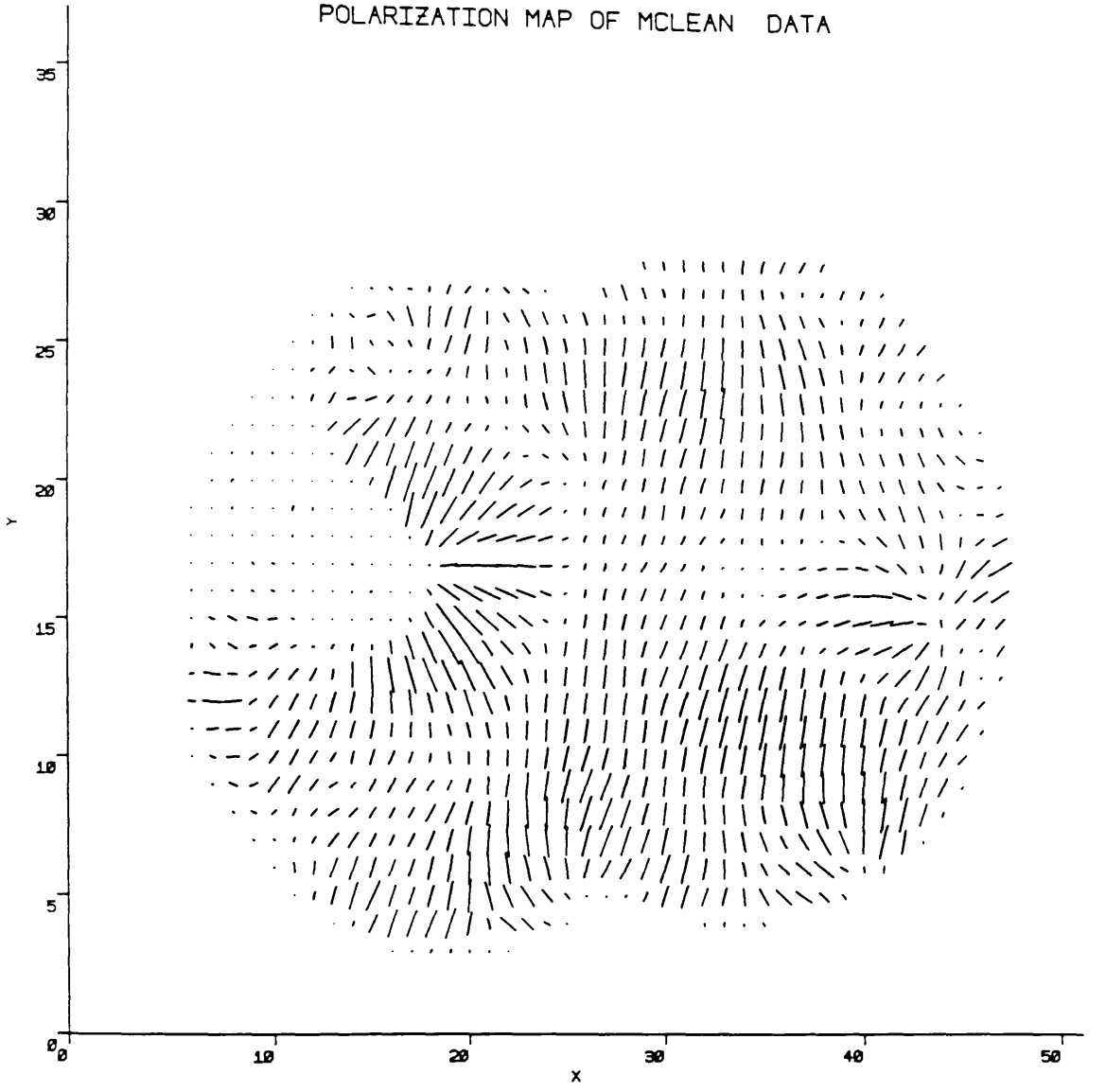

Figure 5.3: A polarization vector plot produced from MAR's reduced resolution data set. North is vertically upwards and east is to the right. Notice again the areas of strong polarization with a sweeping pattern, the eastern and western bays, which are in the centre of either edge of the nebula. The angle of polarization is represented as an angle rotated anti-clockwise from the vertical and the degree of polarization is represented as the length of the line.

5.4 Test for an Average or Preferred Angle of Polarization

Two methods were used to investigate the behaviour of the angle of polarization χ. Each method was applied to Woltjer's data and to the reduced resolution set of MAR's data.

The first method of investigation was a binning method. The polarization angle data was sorted into 5° bins by BINS.FOR and BINS1.FOR and the resulting plots of number in each bin versus angle for each data set are shown in figure 5.4. The graph shows that the most common angle of polarization lies between 150° and 170°. The spread in the peaks of the histogram is quite large (full width at half maximum ~25°). Therefore an exact value of the most common angle of polarization can not be given but we can say that the most common angle lies within the 150°-170° range. This result was used later to check that the second testing method gave results in the correct range. The large peak at 0° in the plot for MAR's binned data is due to the large number of null data points in this data set.

The second method of investigation of polarization angle utilises a type of chi-squared test to find the preferred angle of polarization. The preferred angle test assumes that the nebula has a uniform angle of polarization χ_0 and then tests how well this hypothesis compares with the observational data. The difference between the assumed χ_0 and measured angle is found for each data point. In ANGLE1.FOR and ANGLE2.FOR the sum is taken of all the differences for each data point and this is repeated for values of χ_0 from 0° to 180° at 5° intervals. ANGLE1.FOR deals with Woltjer's data and ANGLE2.FOR with MAR's data. Programs ANGLE1S.FOR and ANGLE2S.FOR deal with Woltjer's and MAR's data respectively. These programs take a sum of the squares of the differences over the same range of values of χ_0 as ANGLE1.FOR and ANGLE2.FOR. The results of these four tests are shown in figures 5.5 and 5.6. The linear sum test was performed to check that the shape of the squared sum curve was not an artifact of the test method. Clearly, the minimum value of the sum of the squared differences should be

related to the most common angle of polarization.

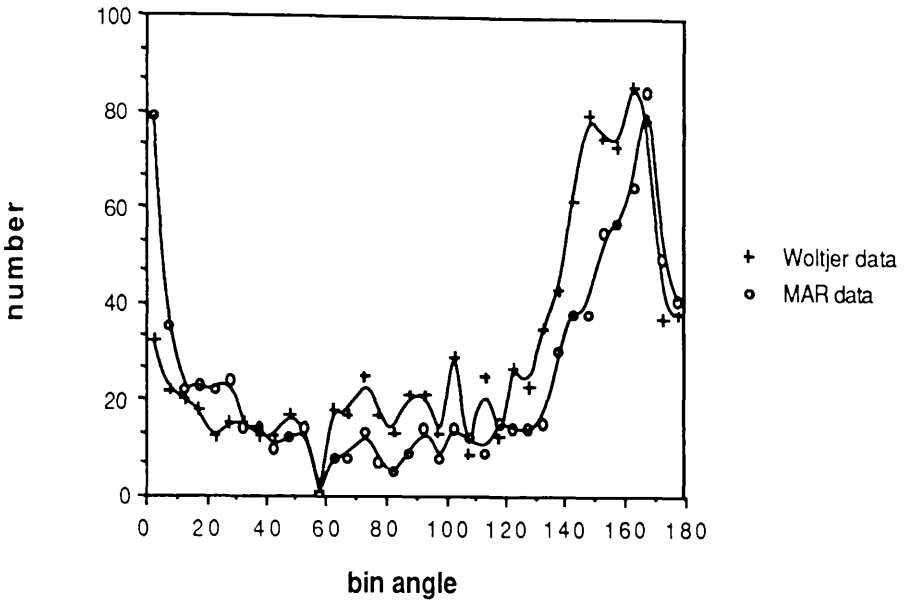

Figure 5.4: A histogram of the number of occurances of a polarization angle in the Crab nebula. The size of the bins is 5°. The large peak at 0° for MAR's data is caused by the number of null data points in this data set. There are less null data points in Woltjer's data. The figure shows that the most commonly occuring angle in Woltjer's data is 155° and in MAR's data it is 165°.

This test indicates that the preferred angle of polarization for Woltjer's data set is ~150°, which compares favourably with the result obtained by binning the data. For MAR's data the preferred test indicates a preferred angle of polarization of ~165°, which is again within the range of the binned data results. As can be seen in figures 5.5 and 5.6 the minimum of the curve is quite shallow and can therefore only give an approximate value of the preferred angle but as this is a test over the whole nebula we would not expect the curve to have a very sharp minimum.

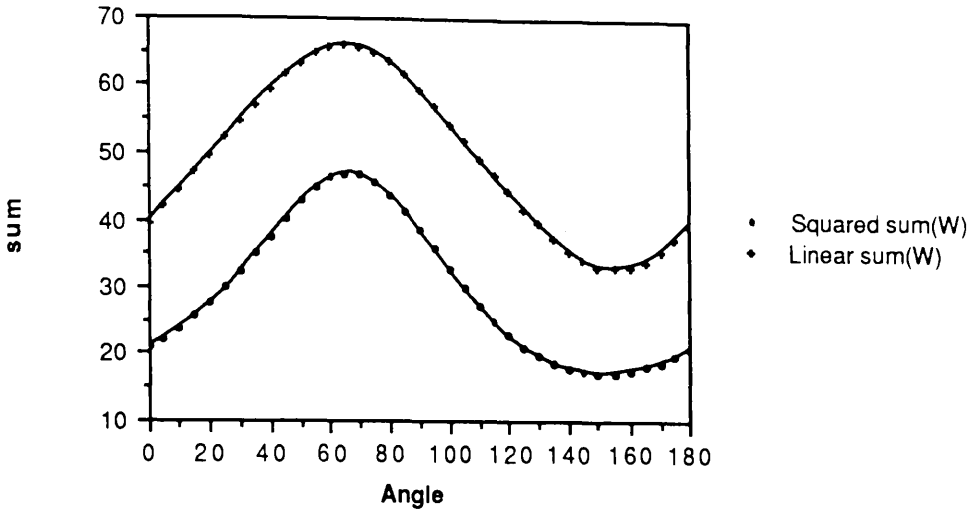

Figure 5.5: Results of the linear sum and squared sum preferred angle tests for Woltjer's data. The linear sum was taken to test whether the shape of the squared sum curve was a product of the squaring or a feature of the data. As we can see above the shape of the curve is a feature of the data. The preferred angle of polarization indicated by these curves is ~155°.

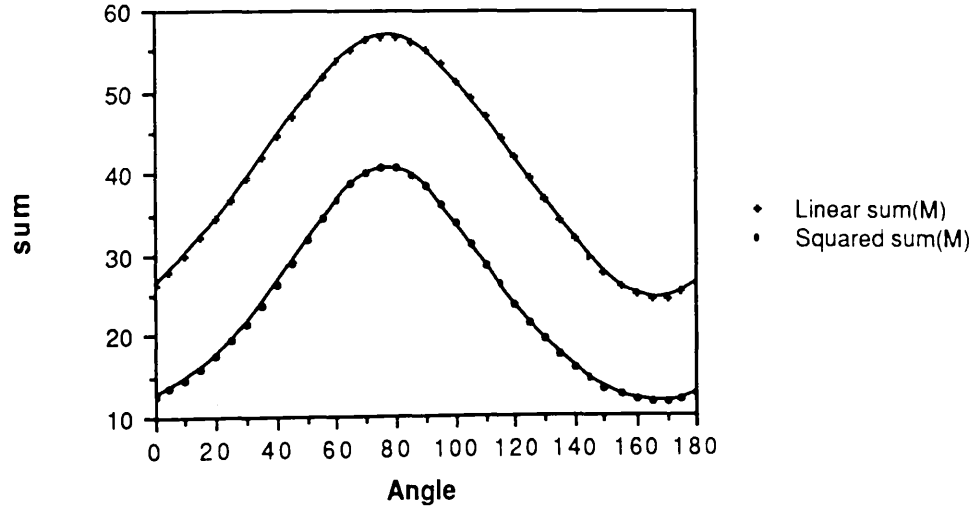

Figure 5.6: Results of the linear sum and squared sum preferred angle tests for MAR's data. The preferred angle of polarization indicated by these curves is ~165°.

The most common direction of polarization in the Crab nebula is then in the north-west to south east direction. This result agrees with those of Rees and Gunn [41], Scargle [61] and others who have made studies of the overall polarization of the Crab nebula.

Having established that this test of preferred angle of polarization was adequate an examination was made of the preferred angle of polarization in various areas of the nebula. In order to separate the nebula into various areas of interest both sets of data (Woltjer's filled set and MAR's reduced resolution set) were converted from Cartesian coordinates to polar coordinates. Since the position of the pulsar relative to both data sets was known (see sections 5.2 and 5.3) the pulsar position was used as the origin of the polar coordinate system. The coordinate conversions were performed by programs COTRAN.FOR and COTRAN1.FOR. Here we assume that the pulsar is in some way located at the centre of the nebula. This may not be true, as a backward extrapolation of the pulsar's proper motion does not bring it to a position which coincides with the extrapolated centre of the expansion of the filaments in 1054 AD [5]. However, the proper motion of the pulsar is small enough that it is below the resolution of either of the data sets used in this project. Therefore, we can use the pulsar position as a reference point for comparison of the two data sets.

Two programs, SECTOR.FOR and SECTOR1.FOR, were developed in order to investigate the distribution of polarization angles in the Crab nebula in more detail. These programs use the same statistical test as ANGLE1S.FOR and ANGLE2S.FOR but test at 1° intervals of χ_0 rather than 5° intervals and deal with Woltjer's and MAR's data in their polar coordinate forms respectively. Examples of the results from these programs are shown in figure 5.7. These graphs show the results plotted at 5° intervals (this gives the same curve as plotting all the data, but the data points are not so crowded) for the preferred angle test for a sector of each data set which has a radius of 10 pixels from the pulsar and covers an angle of 90°. The minima of the curves shown in figure 5.7 are narrower than those in figures 5.5

a) Results from the preferred angle test on a sector of radius 10 pixels, 0° to 90°.

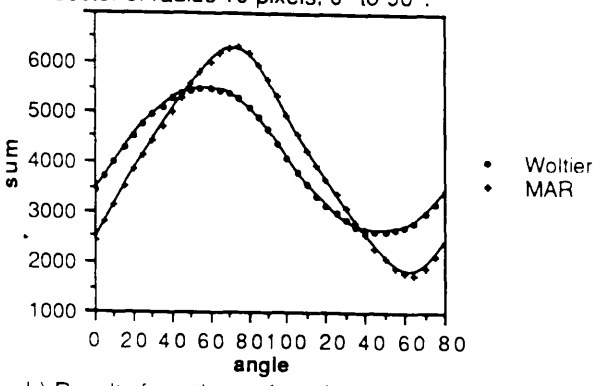

b) Results from the preferred angle test on a sector of radius 10 pixels, 90° to 180°

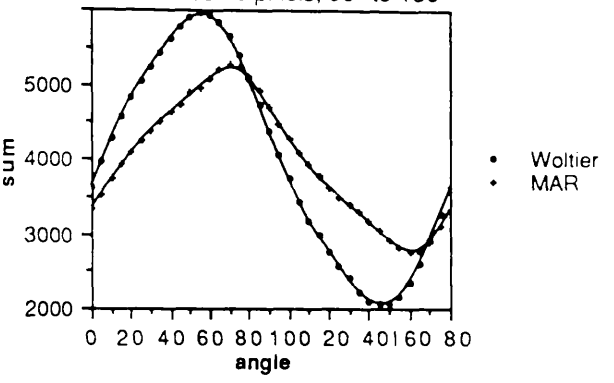

c) Results from the preferred angle test on a sector of radius 10 pixels, 180° to 270°.

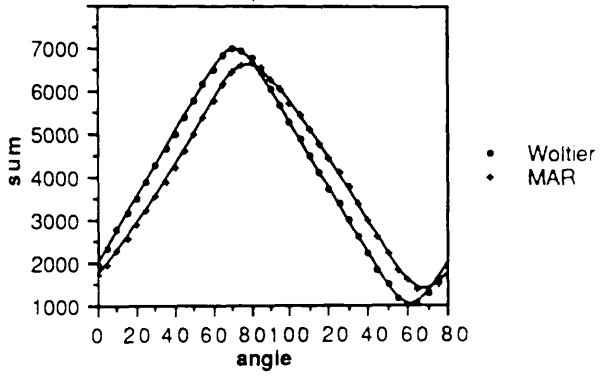

d) Results from the preferred angle test on a sector of radius 10 pixels, 270° to 360°.

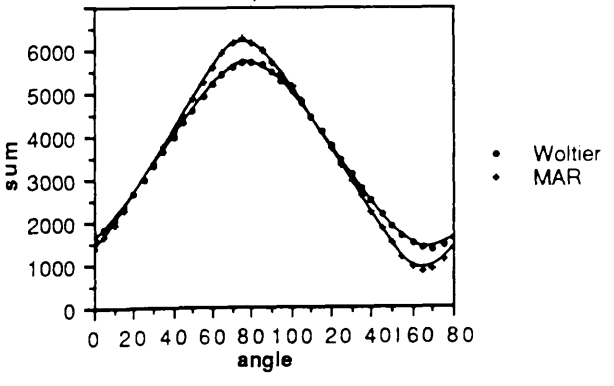

Figure 5.7: Results of the preferred angle tests for various sectors of the nebula.

and 5.6 which indicates that there is less variation of polarization angle in these regions than in the nebula as a whole. Also the preferred angle of polarization indicated by the minimum of the graphs varies from one sector to another.

Radius of annulus (pixels)		Preferred angle of pol'n		Difference
Inner	Outer	Woltjer	MAR	(MAR - W)
0	5	148°±12°	159°±2°	11°
5	10	157°± 6°	168°±7°	11°
10	15	170°± 6°	3°±7°	13°
15	20	138°± 6°	147°±8°	9°
20	25	95°± 7°	180°±12°	85°
25	30	137°± 7°	no data	-

Table 5.1: Results from SECTOR.FOR and SECTOR1.FOR for annuli centred on the pulsar. The preferred angle of polarization and the range of plausible values, derived from the standard deviation of the data, are given for both data sets. The results for the outer annuli are not reliable due to the lack of data values in these regions. 1 pixel ~5 arcseconds.

Tables 5.1 and 5.2 show the results from the programs SECTOR.FOR and SECTOR1.FOR. Table 5.1 presents the preferred angle for Woltjer's data, McLean's data and the difference between these values for concentric annuli of 5 pixels width. The two outer annuli lack enough non-zero data values to give meaningful results as they mainly cover the region outside the edges of the nebula. The 20-25 pixel and 25-30 pixel annuli for Woltjer's data do not contain enough data points to provide reliable results. Hence the difference of 85° shown for the 20-25 pixel annulus is discarded. Table 5.2 shows the preferred angle for each data set in the same annuli as table 5.1 but the annuli have been divided into four sectors, 0°-90°, 90°-180°, 180°-270° and 270°-360°. In both table 5.1 and 5.2, the figure given after each preferred angle of polarization is the plausible range of values of the angle derived from the standard deviation of the squared sum data by

$$\text{range} = \pm 2\sqrt{\frac{\sigma^2}{n}}$$

In the above expression n is the number of data values in the area which is under test and σ the standard deviation of the data. Although this figure is not actually an error on the preferred angle, which is in fact related to the mode of the data, the range of plausible values gives us an indication of how widely the observed polarization angles in a region of the nebula vary from our model of a uniform polarization angle throughout the nebula. We would not expect this model to be a good fit to the Crab nebula but we need to know how good the model is before we can interpret the meaning (if any) of the difference between the preferred angles of polarization for the two data sets. The test used thoughout this section has a related confidence level of 95%. The range of plausible values for most annuli of sectors is large compared to the differences given in the fifth columns of tables 5.1 and 5.2. This does not, however, mean that the difference is purely a product of the non-uniform nature of the data. A visual inspection of figures 5.1 and 5.3 shows that, at least in the central region of the nebula, there is a small difference in polarization angles between the two data sets.

We can also perform a simple test of the difference between the data sets over the whole nebula by calculating the difference between the average polarization angles of the two sets of data

$$\bar{\chi}_W - \bar{\chi}_M \pm 2\sqrt{\sigma_W\sigma_M\left(\frac{1}{n_W} - \frac{1}{n_W}\right)}$$

where σ_W and σ_M are the standard deviations and n_W and n_M the number of measured polarization angles for Woltjer and MAR's data respectively. This test gives us a result of $11° \pm 5°$, at a confidence level of 95%, which shows that there has been some significant and measurable change in the polarization pattern of the

nebula in the time between observations. This is the difference between average angles of polarization rather than between the preferred angles of polarization but confirms the result, from table 5.1, that the net change in preferred angle over the whole nebula is 11°.

Inner and outer radii of annulus	Sector	Preferred angle		Difference (MAR - W)
		Woltjer	MAR	
0 - 5	0°-90°	134°± 17°	153°± 5°	19°
0 - 5	90°-180°	146°± 28°	160°± 3°	14°
0 - 5	180°-270°	158°± 7°	169°± 3°	11°
0 - 5	270°-360°	159°± 11°	156°± 2°	-3°
5 - 10	0°-90°	153°± 12°	167°± 14°	14°
5 - 10	90°-180°	131°± 12°	165°± 12°	34°
5 - 10	180°-270°	171°± 10°	170°± 15°	-1°
5 - 10	270°-360°	171°± 10°	169°± 16°	-2°
10 - 15	0°-90°	164°± 9°	12°± 13°	28°
10 - 15	90°-180°	170°± 11°	180°± 13°	10°
10 - 15	180°-270°	7°± 12°	5°± 15°	-2°
10 - 15	270°-360°	161°± 21°	168°± 15°	7°
15 - 20	0°-90°	127°± 16°	130°± 11°	3°
15 - 20	90°-180°	134°± 10°	180°± 15°	46°
15 - 20	180°-270°	156°± 13°	151°± 10°	-5°
15 - 20	270°-360°	143°± 12°	137°± 5°	-6°

Table 5.2: Results for the preferred angle test in sections of the nebula defined by an inner and outer radius and limiting angles. Radii of the annuli are in pixels. 1 pixel ~5 arcseconds.

It is interesting that in table 5.2 we see that there seems to have been a large change in the polarization angle in the northern half of the nebula, where an anti-clockwise rotation of ~20° has occurred, but in the southern half of the nebula the rotation of the polarization angle appears to be small (~5°) and in the clockwise direction. The pattern which is repeated in the data points to the existance of a real effect, even though the errors on each difference are quite large. These results are discussed further in section 5.5.

5.5 Comparison of the Two Data Sets

The Crab nebula lies approximately 2 kpc away from the Earth. The change in angular position of any moving part of the nebula over a period of time can be calculated using the expression

$$\text{angular displacement in arcseconds} = \frac{(\text{velocity of movement})\text{x}(\text{time period})\text{x}(2\text{x}10^5)}{(\text{distance to the nebula})}$$

where the factor of $2\text{x}10^5$ converts the angle from radians to arcseconds.

It has been postulated that some features within the nebula may move at close to or at the speed of light [4,13]. If this were the case the change in angular position of such features over a 26 year period would be $780''$ ($13'$!). If we can detect movements on the scale of Woltjer's resolution then we should be able to detect movements which occur with velocities of more than 2000 kms^{-1}. Since quoted expansion velocities for the filaments are of the order of 2000 kms^{-1} [5,26] we might expect to see differences between the two data sets, although there may only have been movements of the scale of one pixel. A pixel for pixel comparison of the data sets was attempted but did not yield any meaningful or useful results. This may be because the intensity ranges of the data sets are different and difficult to calibrate with respect to each other or due to the difference in the quality of the data (see section 5.6), but is probably mainly due to the fact that a given pixel does not correspond to exactly the same part of the nebula in both data sets. The reduction in resolution of MAR's data is such that it is close to but not exactly the same as Woltjer's resolution. We have manipulated the data so that the pulsar appears in pixel (30,15) in both data sets but as we move radially outwards from the pulsar the mismatch between the area of the nebula covered by a given pixel of each data set increases. In order for significant pixel to pixel comparisons to be made between Woltjer and MAR's data the resolution of MAR's data must be made commensurate with Woltjer's resolution so that we would be studying the same area of the nebula

separated by a time span of 26 years. When we are considering annuli or sectors of the nebula this mismatch effect is not significant as the difference in coverage is small compared to the size of the whole area covered.

The results of the statistical tests above show that there has been some change in the direction of the angle of polarization, and thus in the direction of magnetic field, in the Crab nebula in the 26 year period between observations. The results in table 5.2 imply that the magnetic field has rotated anti-clockwise in the northern half of the nebula and clockwise in the southern half of the nebula. We can not state the exact angular extent of these rotations but the rotation in the northern half of the nebula is larger than that in the southern half. It is possible that the ~5° clockwise rotation of polarization angle in the southern half of the nebula is an effect of the non-uniformity of the data. The anti-clockwise rotation in the northern half of the nebula is large and likely to be a real effect. The cause of this effect is not known. If these effects were due solely to expansion of the nebular material we might expect to see changes of the same scale in all parts of the nebula. The cause of other asymmetries in the nebula is thought to be the motion of the pulsar, 110 kms^{-1} towards the west-north-west [3]. How the pulsar motion would affect the magnetic field is not currently known but this motion is in the direction of the area of the nebula where we see the greatest change in polarization angle with time. Before we can say exactly what causes the change in the nebular magnetic field with time we need to know how the magnetic field in the nebula is derived from the pulsar and how far into the nebula any toroidal field created by the pulsar extends. These questions can not be answered by current theories.

5.6 Finding a Centre of the Polarization Pattern of the Nebula

An investigation of the data sets was made to examine whether the nebula had a centre of symmetry in either polarization or intensity. The programs which

performed this test are NEWCEN.FOR, NEWCEN1.FOR, NEWICEN.FOR and NEWICEN1.FOR. The programs NEWCEN.FOR and NEWCEN1.FOR tested for a centre in the polarization pattern of Woltjer's and MAR's data respectively. NEWICEN.FOR and NEWICEN1.FOR tested for a centre in the intensity data for Woltjer's and MAR's data respectively.

The method used to search for a centre is basically the same for each program. First the program user enters the Cartesian coordinates of the centre which is to be examined. The appropriate data set is then read from a file. For the polarization centre test the Stokes parameters of each pixel are converted to Stokes intensities. Multiplying the Stokes parameter of a pixel by its intensity gives the Stokes intensity (see chapter 2, equations (2.16)). The program then runs through the data selecting pixels from an area which measures 32x20 pixels and is centred at the point which is being investigated. The search is restricted to this area to confine the test to the body of the nebula and so prevent null values being tested against actual values; this would lead to spurious results. The selected pixels are dealt with as pairs. Each pair of pixels comprises a pixel selected in turn along the scan of one row of data and the pixel which is diametrically opposite to this relative to the chosen centre. For each pair of pixels the difference between the measured parameters is calculated and a sum of the squares of these differences is computed.

The results obtained from the four centre testing programs were used to create the three dimensional plots shown in figures 5.8 and 5.9. The position of the pulsar is marked with a P in these diagrams and is at (30,15). Figure 5.8 shows the results of the tests on Woltjer's data. The three dimensional plots do not indicate that there is a definite centre either of the polarization pattern or intensity. The lowest point in the polarization test map is at (23,15) but does not coincide with the lowest point of the intensity test map, (22,20), which is not very well defined. It is probable that these poor results reflect the quality of the data rather than the lack of a centre of the polarization pattern. Figure 5.9 shows the results for MAR's data. Here we see that

there is an indication that point (32,18) may be a centre of symmetry of intensity and that (31,17) is a likely centre of polarization symmetry. The most likely centres for each set of results are in the same part of the nebula. Also these points are placed to the north-west of the pulsar's position. It is very interesting to note that the centroid of the X-ray emission of the Crab nebula is is the north-west region of the nebula [45] and that the pulsar's proper motion is in the direction of this region. MAR's data therefore seems to indicate that any symmetry in the nebula is likely to be centred to the north-west of the pulsar by 5-10 arcseconds (1 or 2 pixels at or resolution). It is unfortunate that we can not determine whether or not the centre of symmetry has moved in the time between the observations of Woltjer and MAR but this would be unlikely if the effect were due to the motion of the pulsar. As stated above, the estimated motion of the pulsar is 110 kms^{-1} [3] and would in fact be undetectable at the resolution of the data used here. In the vicinity of the light cylinder the estimated Alfven speed is much less than the velocity of the pulsar so we can not explain the observed asymmetry in terms of plasma waves caused by, but propagating ahead of, the pulsar motion (also the plasma is unlikely to support plasma waves [4,13]).

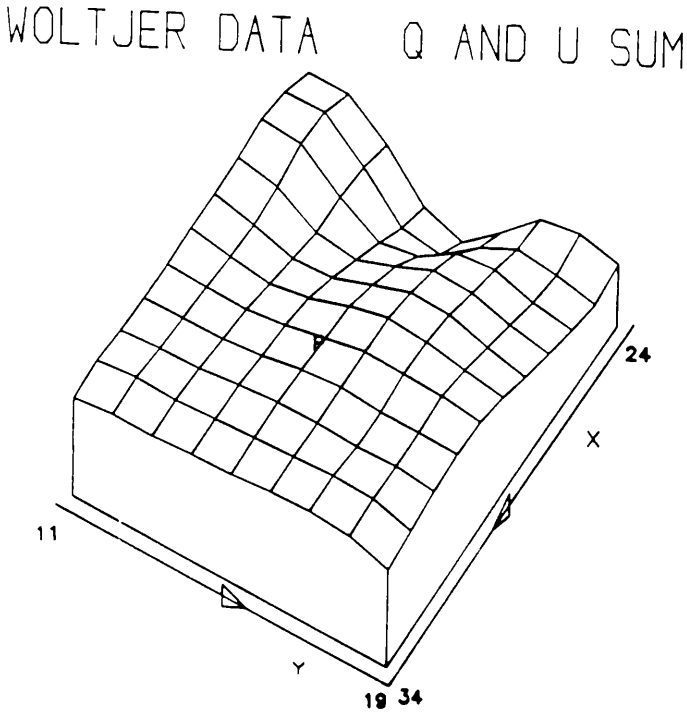

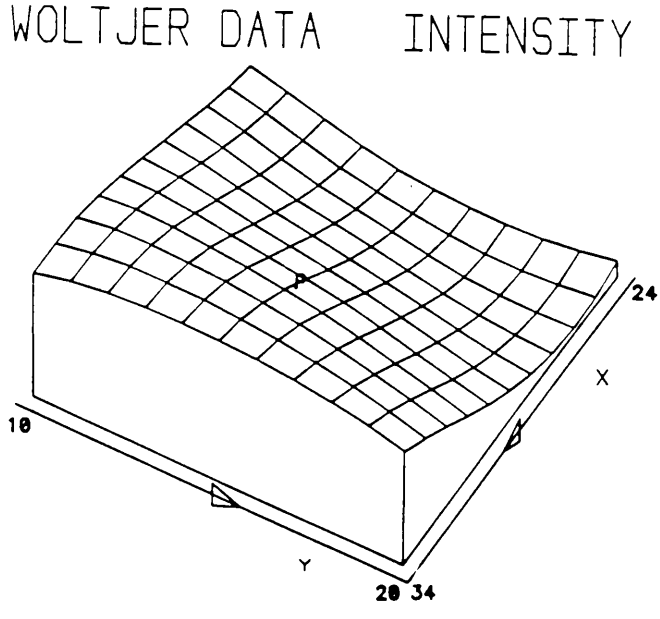

Figure 5.8: A three dimensional plot of the results from the centre testing programs NEWCEN.FOR and NEWICEN.FOR, which test Woltjer's data. In the diagram which shows the results of the test on the Stokes parameters Q and U the lowest point of the graph is at (23,15). For the results of the test of the intensity data the lowest point is at (22,20). In both diagrams the pulsar is at position (30,15).

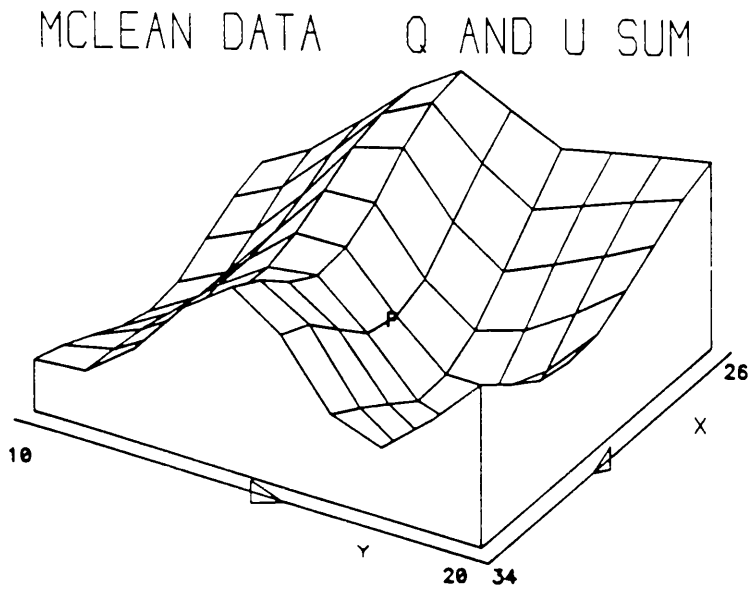

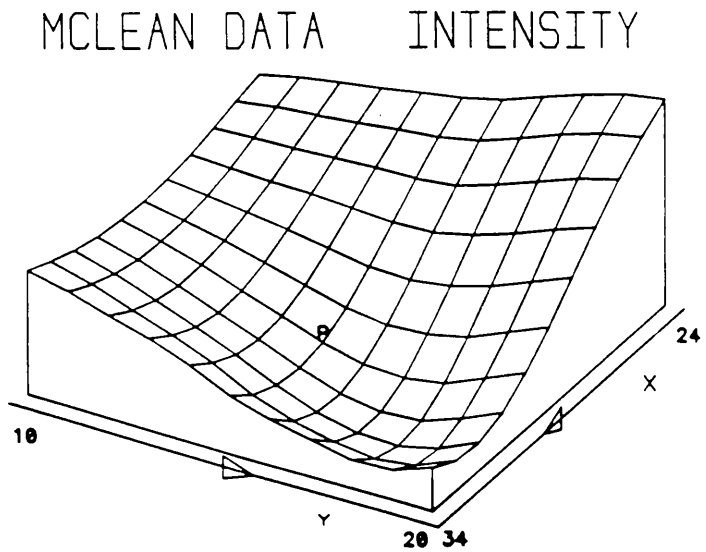

Figure 5.9: A three dimensional plot of the results from the centre testing programs NEWCEN1.FOR and NEWICEN1.FOR, which test MAR's data. In the diagram which shows the results of the test on the Stokes parameters Q and U the lowest point of the graph is at (31,17). For the results of the test of the intensity data the lowest point is at (32,18). In both diagrams the pulsar is at position (30,15).

Chapter 6

Constructing a Model for the Crab Nebula Magnetic Field Structure

6.1 Introduction

In this chapter we discuss the development of a computer model which will calculate the polarization parameters, intensity I, degree of polarization Π and angle of polarization χ, produced by synchrotron emission from electrons in a specified magnetic field. All the computer programs mentioned in this chapter can be found in appendix B. The programs are written in Fortran and were developed on the LAVc computers. The polarization maps in this chapter were produced using SIMPLEPLOT on the Glasgow University Physics and Astronomy Department IBM 4361 computer. All integrations in the programs were performed by a routine from the NAG Fortran library (D01AJF). NAG routine S14AAF was used to evaluate the modified Bessel functions found in equations (3.85), (3.86) and (3.87).

In order to construct a computer program which calculates the polarization parameters of a model of the Crab nebula's magnetic field structure it is best to begin by simplifying the problem as much as possible. We can then gradually add features which will make the model more realistic. The initial assumptions made for this model were:

1) that the magnetic field does not change with time, i.e. we did not allow for rotation of the pulsar or expansion of the nebular material. Rotation of the pulsar may cause winding effects in the nebular magnetic field and the generation of toroidal fields (see chapter 4, section 4.3). If the field is "frozen-in" (see chapter 4, section 4.3) to the nebula then expansion of the nebular material will cause expansion of the magnetic field. Obviously, both of these effects could play a key role in the formation of the actual structure of the Crab nebula magnetic field

but are too complicated to be incorporated into the initial model;

2) that only the electrons emit synchrotron radiation. This is not true as the positrons will also emit synchrotron radiation but the effect of the positrons will be to double the intensity of the observed radiation, as there must be an equal number of electrons and positrons in the plasma for charge neutrality to be maintained. The positrons spiral around the magnetic field lines in the opposite sense to the electrons. However, it is linear polarization which we see and we can not distinguish between the two species of particle as the linearly polarized light emitted by an electron is polarized at exactly 180° to that from a positron. The effect of the positrons on angle and degree of polarization is nil and since these are the very quantities we are studying we can neglect the effect of the positrons without adversely affecting our results;

3) that the electron density of the nebula is homogeneous. A glance at a photograph of the Crab nebula, e.g. figure 1.1, will show that this is clearly not the case in reality. The intensity of synchrotron radiation is proportional to the electron density (see equation (3.85)). The intensity of optical synchrotron radiation from the Crab nebula is far from uniform which indicates a non-uniform electron distribution. The effect of a decline in the electron density as r^{-1} would be to reduce the depolarization effect of varying magnetic field direction along the line of sight since most of the intensity will originate from areas where the electron density is greatest;

4) that the nebula magnetic field is cylindrically symmetric. Morphological studies of the nebula [5,6] show that it is roughly an ellipsoid with a major axis of 4 pc and both the minor axes of 3 pc so this assumption seems reasonable. Also, the magnetic field close to the pulsar is a dipole field which is by its nature cylindrically symmetric; this explains our decision to begin by constructing a model of a dipole magnetic field ;

5) that the electron distribution is isotropic with an energy spectrum of spectral

index (as defined in chapter 3, equation (3.48)) at electron energies corresponding to visible wavelength emission that is constant over that range of wavelength. We can see from figure 6.1 that this is a reasonable assumption for the visible region but we could not extend this work to other regions of the electromagnetic spectrum without allowing for some variation of the spectral index with wavelength. For the calculations in this thesis a spectral index $\alpha = 2.32$, as measured by Greve and van Genderen [52], was used. This is equivalent to Kennel and Coroniti's value derived from figure 6.1;

6) that the magnetic field of the nebula must be derived from the pulsar, as explained in chapter 1, section 1.4. The observed average magnetic field strength of the nebula is 10^{-3}-10^{-4}gauss [11]. This field is far too strong to be a frozen-in primordial field [4,13,41] and so must be created in situ. The only reasonable source of such a field is the pulsar so in our model we begin by using a dipole field structure as would be found within the pulsar's light cylinder. We would like to know by what mechanism the nebular magnetic field is derived from the pulsar.

The first model constructed was for a dipole magnetic field viewed either from the side or along the magnetic axis. It was easy to visualise exactly how the polarization pattern should look in these special cases and so check that the program generating the polarization parameters functioned correctly. The dipole model was then enhanced so that the polarization pattern for an observer at an arbitrary angle of inclination to the dipole magnetic axis could be calculated. It is important to have this facility within the model as we do not know the actual value of the inclination of the general nebular magnetic field relative to our line of sight during either period of observation. We do know that the pulsar's rotation axis lies north-west to south-east in the plane of the sky and that its magnetic axis is almost perpendicular to this [54,61] , but as the pulsar rotates the angle of inclination of the magnetic field to the

observer's line of sight changes. The integration times of the observational data used in this thesis are greater than the rotation period of the pulsar and so we see in effect a time averaged polarization vector from the magnetic field which co-rotates with the pulsar. The magnetic field in the rest of the nebula does not corotate with the pulsar (see chapter 4, section 4.2) and we do not know the alignment of this part of the field to our line of sight.

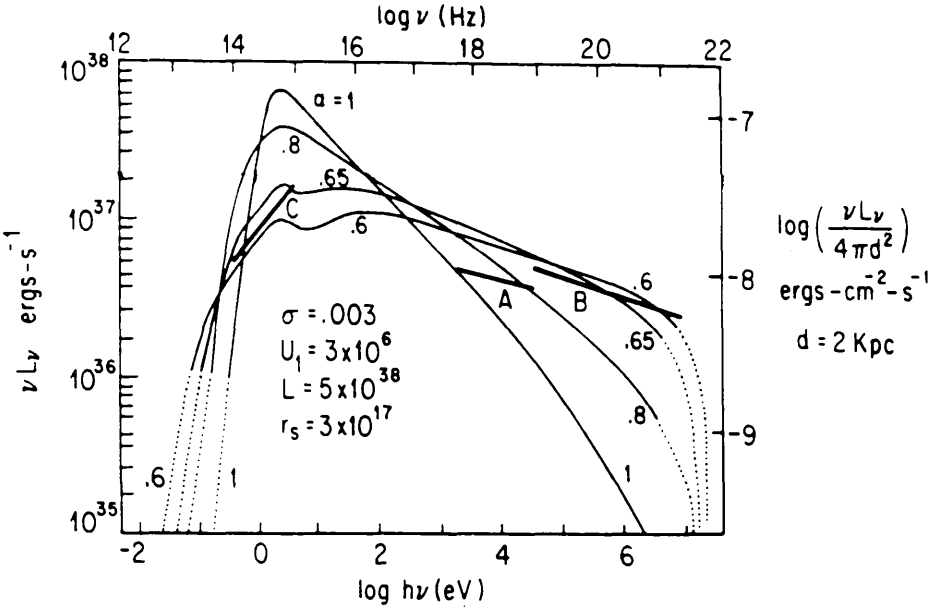

Figure 6.1: This diagram is from Kennel and Coroniti [13]. It shows the spectral luminosity of the Crab nebula calculated for the best fit flow solution of their model for spectral indices between 0.6 and 1. The dotted lines represent the extremes of the calculation where the results are uncertain. The solid lines **A** and **B** are the X-ray and γ-ray spectra observed by Pravdo and Serlemitsos [62] and Walraven et al [63]. **C** is the optical-UV spectrum from observations by Grasdalen [64] and Wu [65]. Here the quantity α is equivalent to p in our equation (3.48) and the best fit value of 0.6 is equivalent to a spectral index of 2.2. Notice that the best fit spectrum peaks in the UV, where the nebula spectrum is observed to reach a peak [3].

A computer model for the structure of the Crab nebula magnetic field should also include the toroidal field component which is thought to be generated by the rotation of the pulsar (chapter 4, section 4.3). Our initial models did not allow for this type of field. A first step towards inclusion of a toroidal field was made by simply adding a magnetic field component in the ϕ-direction of our coordinate system which was of a constant ratio to the other components of the magnetic field. This produced some interesting results but no further progress was made on the addition of a toroidal component as a quantitative expression for the field generated by the pulsar rotation could not be found (see chapter 4, sections 4.3 and 4.4). If a toroidal field component can be successfully modelled it would be interesting to compare the model with the observational data which were used in this thesis [1,2]. The model developed here is, however, still far too simplified to warrant comparison with the observational data.

To predict the values of the Stokes intensity parameters (see chapter 2, section 2.4 for definitions) for a given part of the magnetic field which we wish to study, we need to find the component of the magnetic field which is perpendicular to the observer's line of sight, $B_{\perp}$. Normally, we would also need to know the form of the electron density function $n_0(\underline{r})$ but here we treat this function as a constant (see assumption 3). Tests were made to see how sensitive the computer models were to the electron density function. Using $n_0(\underline{r})$ proportional to r^{-1} or r^{-2} did not alter the directions of the polarization vectors generated by the programs to any detectable extent but affected the degree of polarization slightly. Since it is mainly the direction of the polarization that we are concerned with, the electron density function was treated as a constant in all the programs developed. If we can evaluate $B_{\perp}$ for any magnetic field structure which we wish to consider, we can use equations (3.85), (3.86) and (3.87) to calculate the Stokes intensity parameters for that field.

The electron density function can be incorporated into the constant κ which greatly simplifies our computations. All terms in the equations, except for the

perpendicular component of the magnetic field and the terms involving the polarization angle χ, are constant and so can be removed from the integrand. As we want to calculate the degree of polarization from the Stokes intensities we find that the constant terms will cancel in equation (2.12), so we need only perform the integration and do not need to evaluate the constant term at all. Similarly, the tangent of twice the angle of polarization is the ratio of I_U to I_Q and so here the constant terms also cancel. For the purposes of our calculations we can say that,

$$I \equiv F(\alpha) \int_s (B_\perp)^{1.66} \, ds \tag{6.1}$$

$$I_Q \equiv G(\alpha) \int_s (B_\perp)^{1.66} \cos 2\chi \, ds \tag{6.2}$$

$$I_U \equiv G(\alpha) \int_s (B_\perp)^{1.66} \sin 2\chi \, ds \tag{6.3}$$

where s represents distance along the line of sight of the observer. $F(\alpha)$ and $G(\alpha)$ can be evaluated using gamma functions according to equation 11.4.22 of Abramovitz and Stegun [58];

$$\int_0^\infty t^\mu K_\nu(t) \, dt = 2^{\mu-1} \Gamma\left(\frac{\mu+\nu+1}{2}\right) \Gamma\left(\frac{\mu-\nu+1}{2}\right) \qquad \Re(\mu \pm \nu) > -1$$

In each program the relevant gamma functions are evaluated by NAG Fortran routine S14AAF.

All the model generating programs make calculations over a grid which is 25 units square. The units actually run from 1 to 26 as coordinate values of zero can not be used. Zero values of the coordinates cause divide by zero errors when used in equations such as equation (6.11) as the computer can not perform this calculation at

x=0. However, this is not a great setback. We will later see from polarization vector plots that the polarization patterns produced by the programs show smooth variations and thus behaviour at the origin and along the axes can be inferred from the rest of the map.

For a given line of sight each program calculates the required parameters at each point of the grid. Integration over the line of sight is performed by the NAG Fortran routine D10AJF. Having calculated the Stokes intensities, the angle and degree of polarization can be calculated. the main difference between the programs for different models is that the expressions defining $B_{\perp}$ and $\tan\chi$ differ.

The polarization vector plot for any model is produced by program MODELPLOT.FOR. In the remainder of this chapter we will consider each of the models developed for this thesis, beginning with the simplest case, a dipole magnetic field viewed along the axis of symmetry.

6.2 The Dipole Magnetic Field

To construct a model which will calculate the parameters required to produce a polarization map for a dipole magnetic field we must begin by converting the standard equations for the components of a dipole magnetic field from spherical polar coordinates to Cartesian coordinates. Lorrain and Corson [66] give the components of a dipole field in spherical polar coordinates as:

$$B_r = \frac{2\mu_0 m}{4\pi r^3} \cos\theta \tag{6.4}$$

$$B_\theta = \frac{\mu_0 m}{4\pi r^3} \sin\theta \tag{6.5}$$

$$B_\phi = 0 \tag{6.6}$$

where m is the dipole magnetic moment and μ_0 is the permeability of free space.

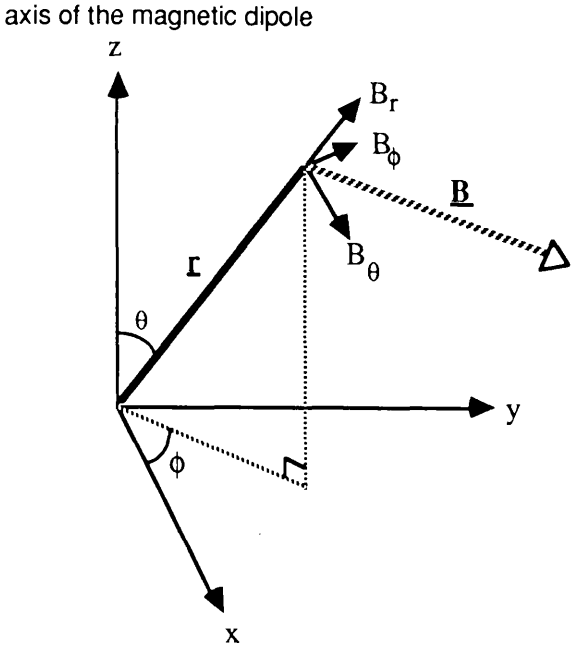

Transformations:

$x = r \sin\theta\cos\phi$

$y = r \sin\theta\sin\phi$

$z = r \cos\theta$

$r^2 = x^2 + y^2 + z^2$

$\sin\theta = (x^2+y^2)^{1/2} / r$

$\cos\theta = z / r$

Figure 6.2 : Axes for Cartesian and spherical polar coordinates showing the magnetic dipole axis z, the components of the magnetic dipole in spherical polar coordinates and the relevant transformation equations.

Using the transformations from figure 6.2 equations (6.4), (6.5) and (6.6) become:

$$B_x = \frac{3\mu_0 mxz}{4\pi r^5} \tag{6.7}$$

$$B_y = \frac{3\mu_0 mzy}{4\pi r^5} \tag{6.8}$$

$$B_z = \frac{\mu_0 m\,(2z^2 - x^2 - y^2)}{4\pi r^5} \tag{6.9}$$

6.3 Dipole Magnetic Field Model for an Observer Looking Along the Dipole Axis z

In the case where the observer's line of sight is along the z-axis, i.e. along the axis of the dipole, the perpendicular component of the magnetic field is found from simple geometry, as shown in figure 6.3, to be

$$B_{\perp} = (B_x^2 + B_y^2)^{\frac{1}{2}} = \frac{3\mu_0 mz}{4\pi r^5}(x^2 + y^2)^{\frac{1}{2}} \tag{6.10}$$

and the angle of polarization is given by the expression

$$\tan \chi = \frac{B_y}{B_x} = \frac{y}{x} \tag{6.11}$$

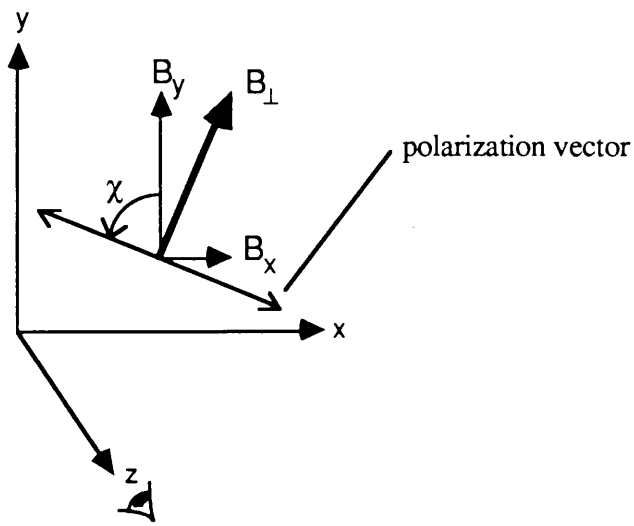

Figure 6.3: The geometry for an observer viewing along the z-axis.

Notice that in this case the angle of polarization does not depend on z; this greatly reduces the complexity of the calculation of the polarization parameters. Because the angle of polarization does not depend on z we do not need to make a calculation for each value of z and integrate. Program MODEL1.FOR, which deals with the end-on dipole case, calculates the integrated value of the perpendicular component of the

magnetic field along the line of sight z. Using equation (6.11) and the half angle formulae we find that

$$\cos 2\chi = \frac{1 - \tan^2\chi}{1 + \tan^2\chi} = \frac{x^2 - y^2}{x^2 + y^2} \tag{6.12}$$

$$\sin 2\chi = \frac{2\tan\chi}{1 + \tan^2\chi} = \frac{2xy}{x^2 + y^2} \tag{6.13}$$

Neither equation (6.12) nor (6.13) show a dependence on z so equations (6.2) and (6.3) become

$$I_Q = \frac{G(\alpha)}{F(\alpha)} I \cos 2\chi \tag{6.14}$$

$$I_U = \frac{G(\alpha)}{F(\alpha)} I \sin 2\chi \tag{6.15}$$

where I is given by equation (6.1).

The program MODEL1.FOR evaluates the integral for I and then, for each value of x and y in our grid, I_Q and I_U can be evaluated without integration. This allows us to calculate the degree of polarization as given by equation (2.12). The angle of polarization for each point (x,y) is calculated directly via equation (6.11).

The polarization map for this model is shown in figure 6.4.

6.4 Dipole Magnetic Field for an Observer Viewing the Dipole Side-on

Consider figure 6.2. If the observer were to look along either the x or y-axis in this coordinate system they would see exactly the same magnetic field structure because of the inherent rotational symmetry of the field about the dipole axis, z. Thus the same polarization pattern would be seen. The program MODEL.FOR

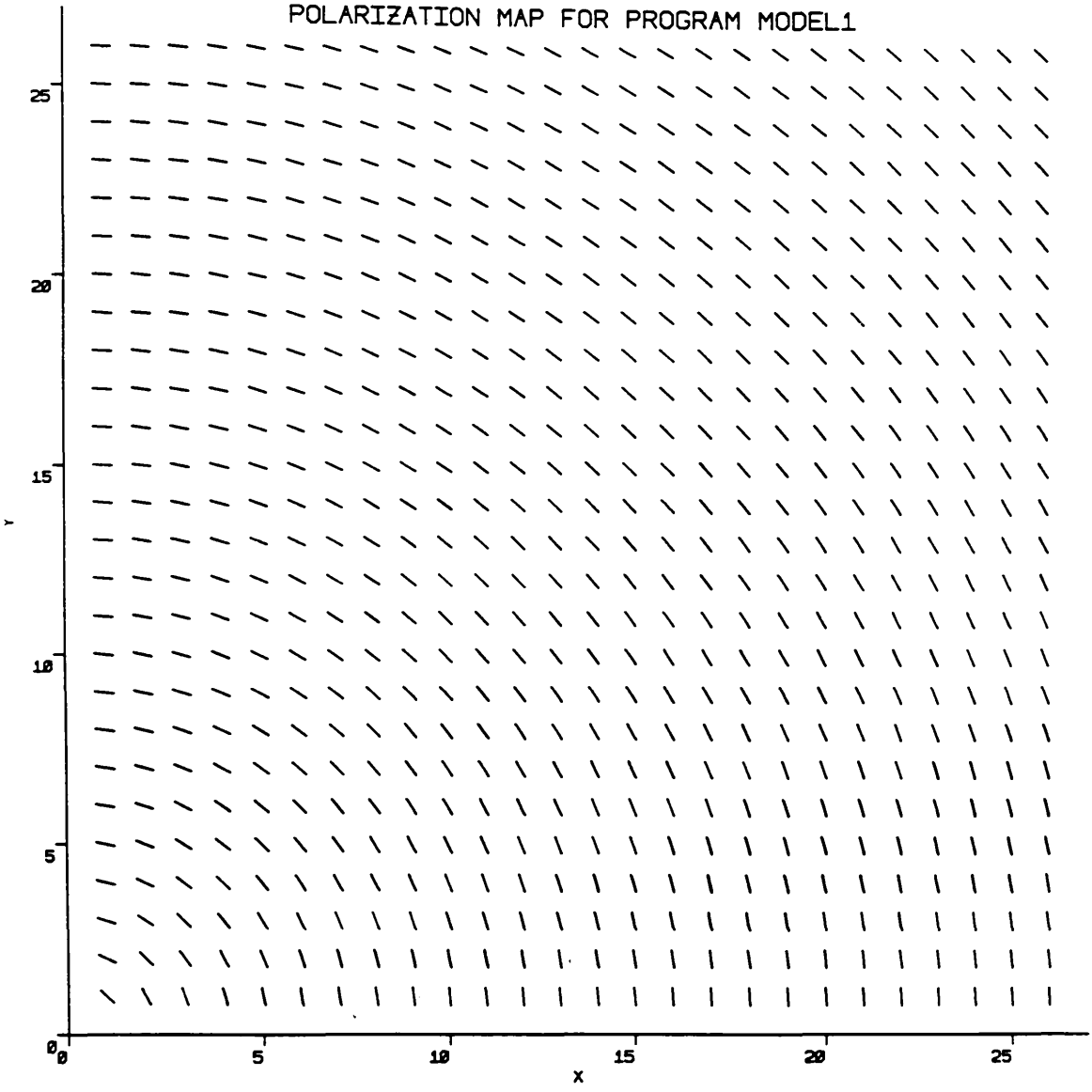

Figure 6.4: Polarization map produced by MODELPLOT.FOR from the results of program MODEL1.FOR. This diagram represents the polarization pattern which would be seen by an observer looking at the dipole magnetic field along the dipole axis z. The diagram only shows one quadrant of the whole field as the patterns in the other quadrants are simply reflections of this pattern about the axes, due to the rotational symmetry of the dipole magnetic field about z. The angle of polarization is represented as a rotation anti-clockwise from the vertical direction and the degree of polarization as the length of the line plotted. The maximum degree of polarization in polarization maps for all models in this thesis is 71% (derived from equation (3.74)).

calculates the angle and degree of polarization for an observer looking along the x-axis. We see from figure 6.5 that

$$B_{\perp} = (B_z^2 + B_y^2)^{\frac{1}{2}} \tag{6.17}$$

$$\tan \chi = \frac{B_z}{B_y} \tag{6.18}$$

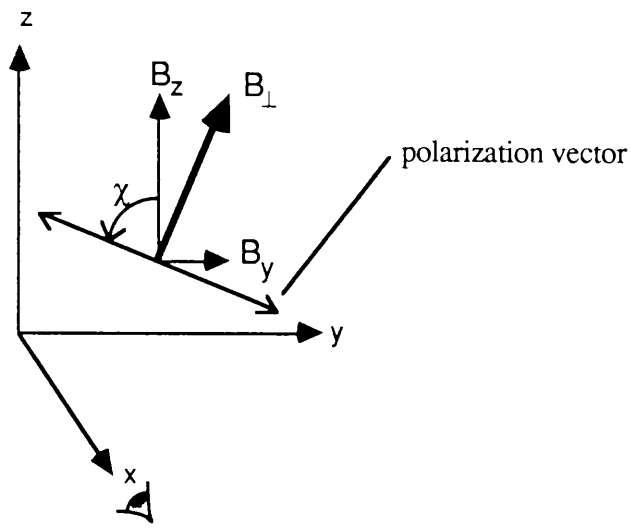

Figure 6.5: The geometry for an observer viewing along the x-axis.

If we expand equations (6.17) and (6.18) using equations (6.8) and (6.9) we obtain expressions for the component of the magnetic field perpendicular to the line of sight and the angle of polarization in Cartesian coordinates:

$$B_{\perp} = \frac{\mu_0 m}{4\pi r^5} (5z^2y^2+2x^2y^2-4x^2z^2+4z^4+x^4+y^4)^{\frac{1}{2}} \tag{6.16}$$

$$\tan \chi = \frac{(2z^2 - x^2 - y^2)}{3zy} \tag{6.17}$$

Here the angle of polarization varies with x and so must be integrated along the line

of sight x to allow for depolarization (see chapter 2, section 2.3). As we saw in chapter 2, the Stokes intensity parameters are linearly additive. Therefore, we can deal with the effects of depolarization along the line of sight in a straightforward way; we simply calculate the Stokes intensities integrated along the line of sight x and in doing this have taken the depolarization into account. The angle of polarization for any grid point is given by the ratio of I_U to $I_{Q,}$ as in equation (2.9), for that grid point. The degree of polarization is again calculated by use of equation (2.12).

The main difference between MODEL.FOR and MODEL1.FOR is that we must perform three integrations because of the dependence of the polarization angle on x. From half angle formulae (see equations (6.11) and (6.12)) and equation (6.17) we find that

$$\cos 2\chi = \left(\frac{13z^2y^2 - 4z^4 + 4x^2z^2 - 2x^2y^2 - x^4 - y^4}{5z^2y^2 + 4z^4 - 4x^2z^2 + 2x^2y^2 + x^4 + y^4}\right) \tag{6.18}$$

$$\sin 2\chi = \left(\frac{6zy\,(2z^2 - x^2 - y^2)}{5z^2y^2 + 4z^4 - 4x^2z^2 + 2x^2y^2 + x^4 + y^4}\right) \tag{6.19}$$

The expressions we integrate are then:

1) the expression for $B_\perp$ given by equation (6.16) but neglecting the constant term of $\mu_0 m/4\pi$. This integral is directly proportional to the intensity;

2) the expression which gives us an integral proportional to I_Q. We integrate the product of equations (6.16) and (6.18);

3) the expression which gives us an integral proportional to I_U. We integrate the product of equations (6.16) and (6.19).

The polarization pattern seen by the observer in this case is shown in figure 6.6.

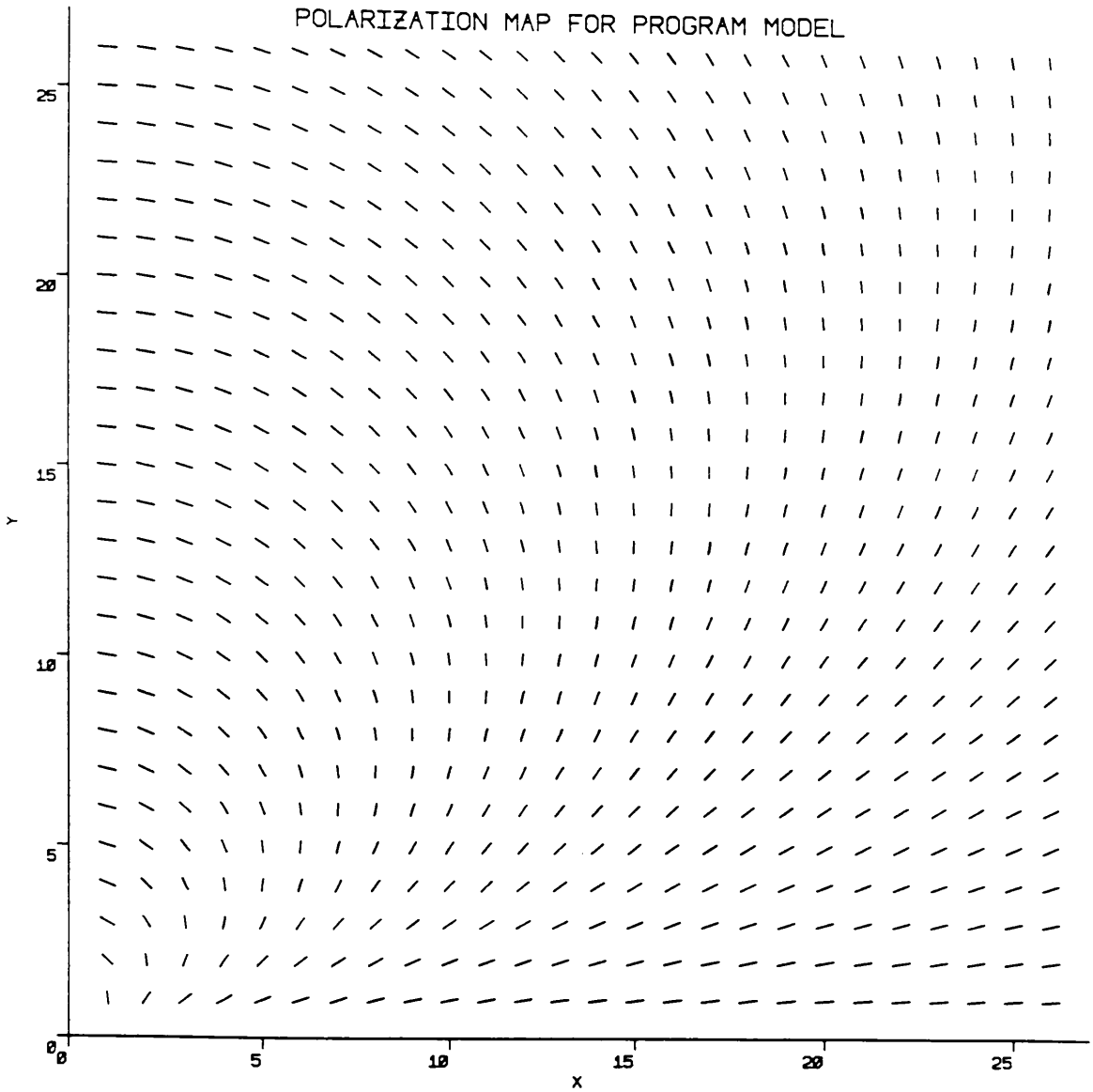

Figure 6.6: Polarization map produced by MODELPLOT.FOR from the results of program MODEL.FOR. This diagram represents the polarization pattern which would be seen by an observer looking at the dipole magnetic field from the side. As in figure 6.4, the diagram only shows one quadrant of the whole field. The angle of polarization is represented as a rotation anti-clockwise from the vertical direction and the degree of polarization as the length of the line plotted.

6.5 The Case for an Observer at an Arbitrary Angle of Inclination to the Dipole Axis

We do not know the angle of inclination of the Crab nebula's magnetic field to our line of sight at the times when the observational data used in this thesis were gathered. Therefore, we want to construct a program which will calculate the polarization pattern for an observer at any angle of inclination to the dipole axis so that we would eventually be able to compare the model with the observational data. We need only consider inclination of the observer's line of sight to the dipole axis z. As we saw in the model above the inherent rotational symmetry of the dipole field around z means that the polarization pattern is the same for any line of sight in the (x,y) plane. Figure 6.7 shows the axes of the dipole system and those of the observer's system. This model scans a grid which is perpendicular to the observer's line of sight in the (x_i,y_i) plane (this is the same procedure as in the first two models). Any line of sight in the (x_i,y) plane would give the same polarization pattern as any other because of the rotational symmetry of the magnetic field about z. Calculation of the perpendicular component of the magnetic field, $B_\perp$, and the Stokes intensity parameters can either use the inclined coordinate system (x_i,y_i,z_i) directly or can convert the grid values of the inclined system to their corresponding values in the non-inclined system (x,y,z). Program MODEL3.FOR uses the non-inclined system of coordinates for its calculations whereas, MODEL4.FOR uses the inclined system of coordinates. Both these programs ultimately produce the same polarization vector pattern for any given angle of inclination of the observer, i. Neither program can produce results if $i = 0°$ because of problems with dividing by zero within the program. The programs can, however, handle any value of i between 0.001° (which gives results almost exactly the same as $i = 0°$) and 90°.

We already have a set of equations for B_x, B_y and B_z (equations (6.4), (6.5) and (6.6)) and we can see from figure 6.7 that:

$$B_{x_i} = B_x \tag{6.20}$$

$$B_{y_i} = B_y \cos i + B_z \sin i \tag{6.21}$$

$$B_{z_i} = B_z \cos i - B_y \sin i \tag{6.22}$$

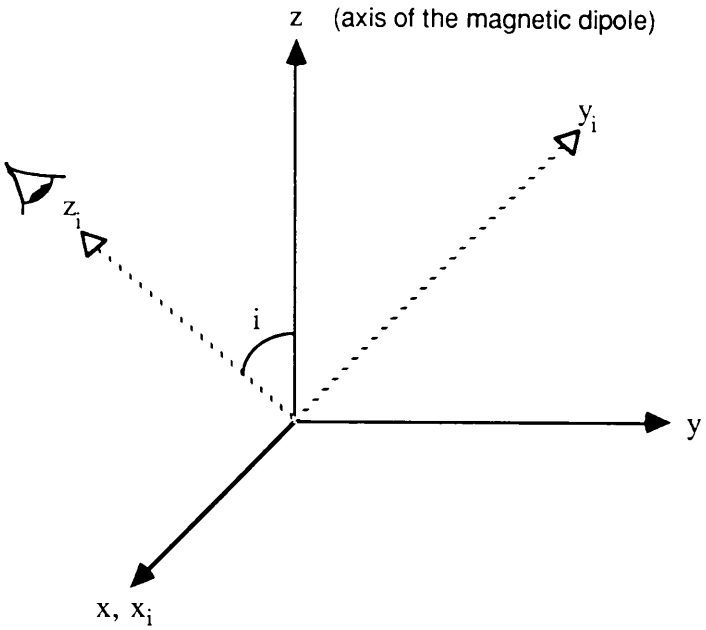

Figure 6.7 : Axes for the magnetic dipole field (x,y,z) and for an observer at an angle of inclination i to the dipole axis z (x_i,y_i,z_i). The observer's line of sight is along z_i.

So, using the non-inclined system of coordinates as in MODEL3.FOR, an observer looking along z_i will see a component of the magnetic field perpendicular to his line of sight

$$B_{\perp} = (B_{x_i}^2 + B_{y_i}^2)^{\frac{1}{2}} \tag{6.23}$$

The angle of polarization in this coordinate system is given by the equation

$$\tan \chi = \frac{B_{y_i}}{B_{x_i}} \tag{6.24}$$

So, we use equations (6.20) and (6.21) to substitute for B_{xi} and B_{yi} in equations (6.23) and (6.24), obtaining

$$B_{\perp} = (B_x^2 + (B_y \sin i + B_z \cos i)^2)^{\frac{1}{2}} \tag{6.25}$$

$$\tan\chi = \frac{B_y \cos i + B_z \sin i}{B_x} \tag{6.26}$$

Then using equations (6.4), (6.5) and (6.6) we have;

$$B_{\perp} = \left[\frac{9\kappa^2 x^2 z^2}{r^{10}} + \left(\frac{3\kappa yz}{r^5} \cos i + \frac{\kappa}{r^5} (2z^2 - x^2 - y^2) \sin i \right)^2 \right]^{\frac{1}{2}}$$

$$B_{\perp} = \frac{\kappa}{r^5} \left[9x^2 z^2 + (3yz \cos i + (2z^2 - x^2 - y^2) \sin i)^2 \right]^{\frac{1}{2}} \tag{6.27}$$

and

$$\tan\chi = \frac{\frac{3\kappa yz}{r^5} \cos i + \frac{\kappa(2z^2 - x^2 - y^2) \sin i}{r^5}}{\frac{3\kappa xz}{r^5}}$$

$$\tan\chi = \frac{3yz \cos i + (2z^2 - x^2 - y^2) \sin i}{3xz} \tag{6.28}$$

As in program MODEL.FOR, in MODEL3.FOR we have three integrations to perform. The integration for the intensity uses equation (6.27) as the integrand.

Equation (6.28) is used to find the expressions for $\cos 2\chi$ and $\sin 2\chi$ which are needed in the other two integrands. If the angle of inclination is 0° or 90° equations (6.27) and (6.28) revert to their special case forms; which are given in equations (6.7), (6.8), (6.16) and (6.17).

For MODEL4.FOR we want to find the expressions for $B_\perp$ and $\tan\chi$ in terms of (x_i, y_i, z_i). The coordinate transformations

$$x = x_i$$

$$y = y_i \cos i - z_i \sin i$$

$$z = z_i \cos i + y_i \sin i$$

follow directly from figure 6.7. Using these transformations equations (6.4), (6.5) and (6.6) become

$$B_x = \frac{3\kappa x_i (z_i \cos i + y_i \sin i)}{(x_i^2 + y_i^2 + z_i^2)^{\frac{5}{2}}} \tag{6.29}$$

$$B_y = \frac{3\kappa y_i (z_i \cos i + y_i \sin i)}{(x_i^2 + y_i^2 + z_i^2)^{\frac{5}{2}}} \tag{6.30}$$

$$B_z = \frac{\kappa \left(2(z_i \cos i + y_i \sin i)^2 - x_i^2 - (y_i \cos i - z_i \sin i)^2\right)}{(x_i^2 + y_i^2 + z_i^2)^{\frac{5}{2}}} \tag{6.31}$$

We now use equations (6.29), (6.30) and(6.31) to express B_{xi} (equation (6.20)) and B_{yi} (equation (6.21)) in terms of x_i, y_i and z_i

$$B_{xi} = \frac{3\kappa x_i (z_i \cos i + y_i \sin i)}{(x_i^2 + y_i^2 + z_i^2)^{\frac{5}{2}}} \tag{6.32}$$

$$B_{yi} = \frac{\kappa\left[y_i \cos i(z_i \cos i + y_i \sin i) + \sin i(2(z_i \cos i + y_i \sin i)^2 - x_i^2 - (y_i \cos i - z_i \sin i)^2)\right]}{(x_i^2 + y_i^2 + z_i^2)^{\frac{1}{2}}} \tag{6.33}$$

If we let

$$A = (2y_i^2 - x_i^2 - z_i^2) \quad , \quad C = 3x_i y_i \quad , \quad D = 3x_i z_i \quad , \quad E = 3y_i z_i$$

we can simplify (6.32) and (6.33) to

$$B_{xi} = \frac{\kappa}{r^5}(C \sin i + D \cos i)$$

$$B_{yi} = \frac{\kappa}{r^5}(A \sin i + E \cos i)$$

where $r^2 = (x_i^2 + y_i^2 + z_i^2)$.

Now, from equation (6.23)

$$B_{\perp} = \frac{\kappa}{r^5}\left[(C \sin i + D \cos i)^2 + (A \sin i + E \cos i)^2 \right]^{\frac{1}{2}} \tag{6.34}$$

and equation (6.24)

$$\tan\chi = \frac{(A \sin i + E \cos i)}{(C \sin i + D \cos i)} \tag{6.35}$$

So, we have the necessary expressions for the integrands required in program MODEL4.FOR. The program MODEL5.FOR was then developed. This program is

essentially the same as MODEL4.FOR but the program user does not need to set the value of the angle of inclination for the program. MODEL5.FOR performs the calculations for models with i from 0° to 90° at 10° intervals and stores the results for each value of i in a separate file. This program takes a long time to run but can run unattended and produce the same results as ten separate runs of MODEL4.FOR. A series of polarization vector plots from the results of MODEL5.FOR are shown in figures 6.8-6.12.

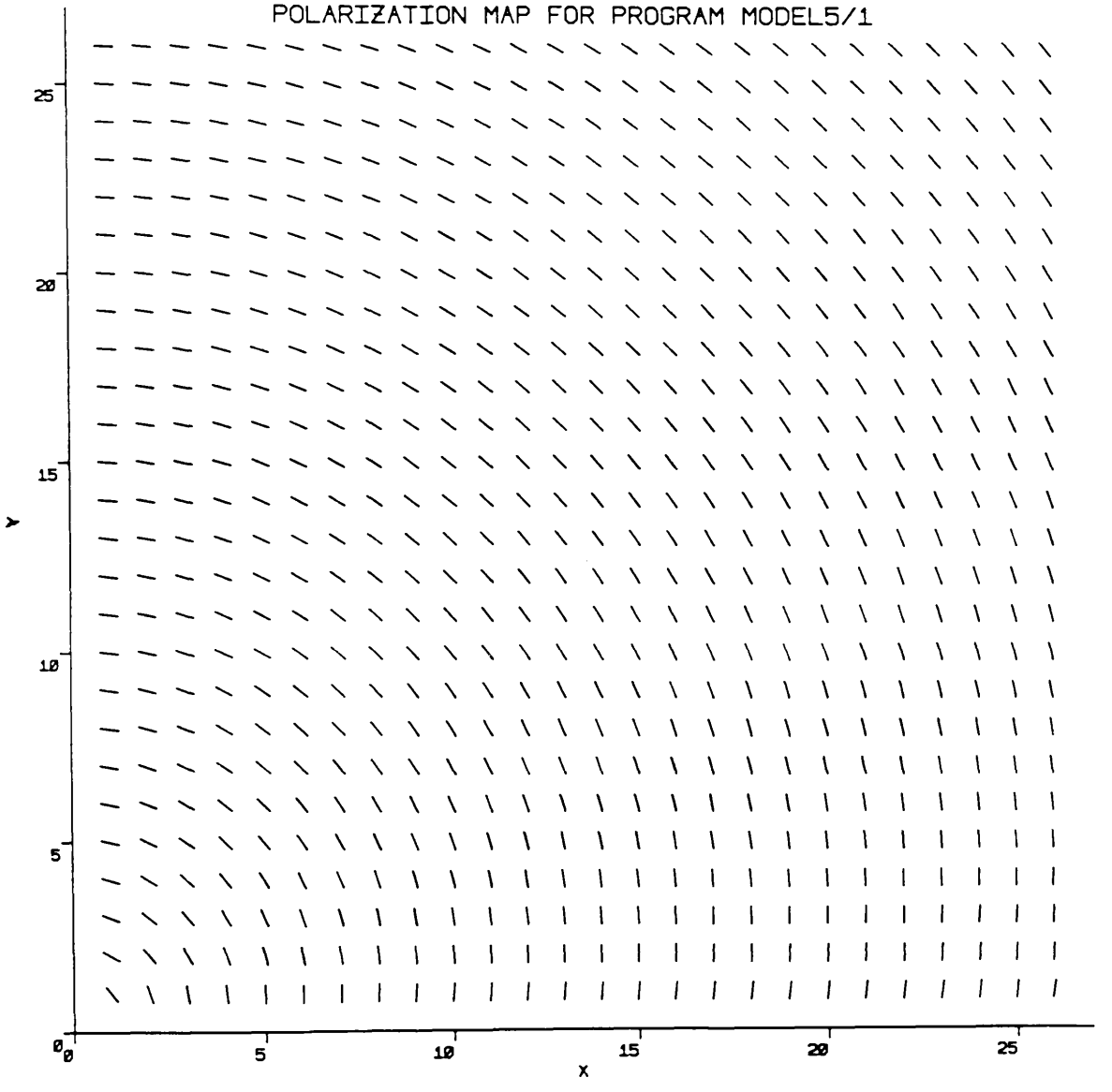

Figure 6.8: Polarization vector plot for a dipole magnetic field viewed at an angle of inclination of the observer of i = 10°.

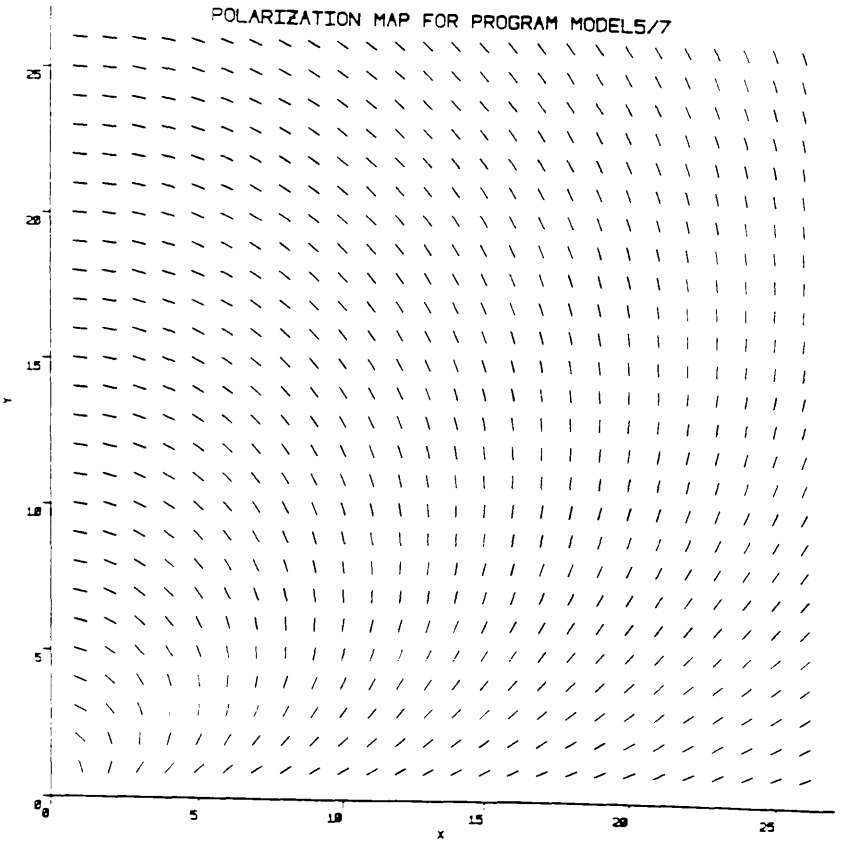

Figure 6.9: Polarization vector plot for a dipole magnetic field viewed at an angle of inclination of the observer of i = 70°.

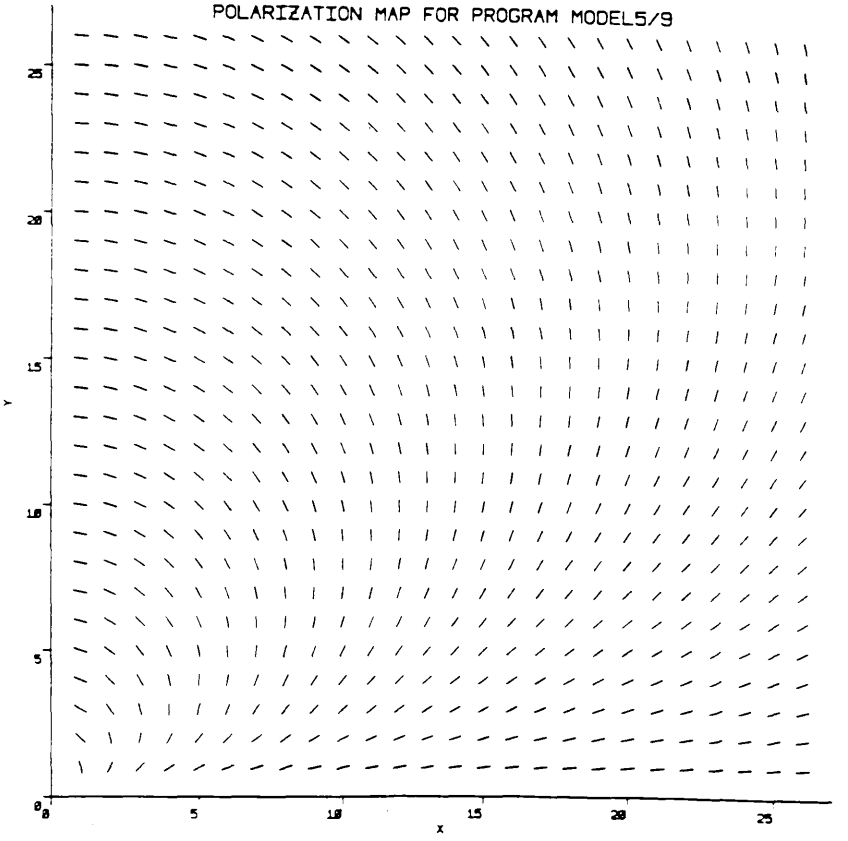

Figure 6.10: Polarization vector plot for a dipole magnetic field viewed at an angle of inclination of the observer of i = 90°.

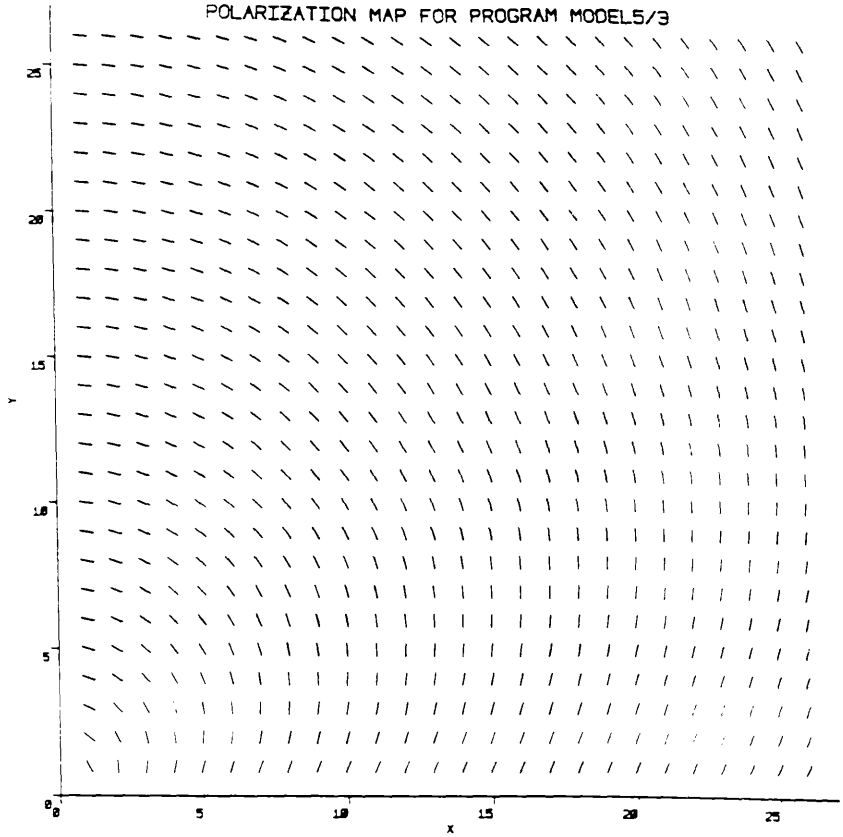

Figure 6.11: Polarization vector plot for a dipole magnetic field viewed at an angle of inclination of the observer of i = 30°.

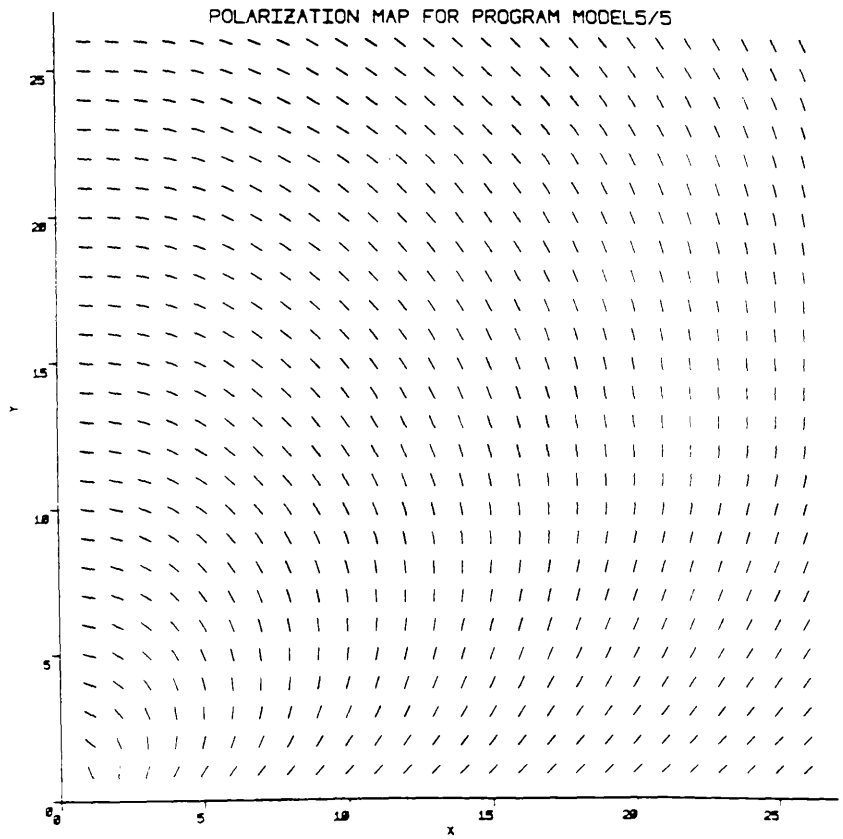

Figure 6.12: Polarization vector plot for a dipole magnetic field viewed at an angle of inclination of the observer of i = 50°.

6.6 Model for an Inclined Dipole Field with an Added Component in the ϕ-Direction

Again we consider figure 6.2. If the dipole rotated about its axis we would expect there to be some form of differential rotation effects if the dipole were situated in a plasma [41,46,55]. The main effect of this differential rotation would be the "winding-up" of the magnetic field lines, causing a component of the field in the ϕ-direction to be generated. As we saw in section 6.2 B_ϕ is zero for a simple dipole field. As an investigation of the effect of such a component on the polarization pattern a B_ϕ component proportional to r^{-4} was added to the dipole model.

For the addition of a component in the ϕ-direction we modify equations (6.4), (6.5) and (6.6) as below:

$$B_r = \frac{2\mu_0 m}{4\pi r^3} \cos\theta$$

$$B_\theta = \frac{\mu_0 m}{4\pi r^3} \sin\theta$$

$$B_\phi = \frac{\text{rat}\,\kappa}{r^4}$$

where rat is the factor which reduces or enhances the effect of B_ϕ relative to B_r and B_θ. Conversion to Cartesian coordinates (see figure 6.2) gives us:

$$B_x = \frac{3\kappa xz}{r^5} - \frac{\text{rat}\,\kappa y}{r^4(x^2+y^2)^{\frac{1}{2}}} \qquad (6.36)$$

$$B_y = \frac{3\kappa yz}{r^5} - \frac{\text{rat}\,\kappa y}{r^4(x^2+y^2)^{\frac{1}{2}}} \qquad (6.37)$$

$$B_z = \frac{\kappa}{r^5}(2z^2 - x^2 - y^2) \qquad (6.38)$$

We are using an inclined coordinate system as in figure 6.7 so we require expressions for B_{xi} and B_{yi} and $B_{\perp}$ and $\tan\chi$ as given by equations (6.23) and (6.24) in this case. Using equations (6.20) and (6.21) we obtain

$$B_{xi} = \frac{\kappa}{r^4}\left(\frac{3xz}{r} - \frac{rat\ y}{(x^2+y^2)^{\frac{1}{2}}}\right) \tag{6.39}$$

$$B_{yi} = \left(\frac{3\kappa zy}{r^5} + \frac{rat\ \kappa y}{r^4(x^2+y^2)^{\frac{1}{2}}}\right)\cos i + \left(\frac{\kappa}{r^5}(2z^2 - x^2 - y^2)\sin i\right) \tag{6.40}$$

Equations (6.39) and (6.40) are then used to find expressions for $B_{\perp}$ and $\tan\chi$ by substituting for x, y and z in terms of x_i, y_i and z_i. We can then find the relevant expressions for the integrands used to calculate I, I_Q and I_U as in the previous analyses. Program MODEL6.FOR generates the Stokes intensities for values of rat of 10, 100 and 1000 and for i between 0° and 90° at intervals of 10°. MODEL7.FOR generates results for the same range of i but for rat=50.

Two considerations make this model unrealistic in comparison to the postulated theoretical model of the Crab nebula (chapter 4, section 4.3). First, the Crab pulsar is an oblique rotator and so the dipole axis is not the axis of rotation. The axis of rotation lies almost in the (x,y) plane of the dipole and the field which is generated by the rotation is most likely to add to the B_r and B_θ components of the magnetic field, as it originates from the open field lines which lie close to the z-axis. The second drawback with the B_ϕ component is that we have not allowed for a variation in the component other than an r^{-4} fall-off as compared to the r^{-3} fall off of the other components. We have not allowed for a toroidal nature of the B_ϕ component by restricting its height relative to the z-axis or for a central zone where only the dipole field exists. Nevertheless, this model, generated by MODEL6.FOR and MODEL7.FOR, yields an interesting result. From consideration of figures

6.13-6.20 we find that the extra component only becomes evident in the polarization patterns for this model when the extra component is of the order of 10 times greater than the other components of the magnetic field. When B_ϕ is more than 100 times greater than either the B_r or B_θ components, it begins to dominate the polarization pattern. We therefore know that a component of between 10 to 100 times the existing component must be generated before we can see an effect in a polarization vector plot of this scale. The next step in improving this model would be to add components in B_r and B_θ of a reasonable size to investigate their effects on polarization. This would bring the computer generated model much closer to the theoretical model and may make comparisons with the observational data worthwhile.

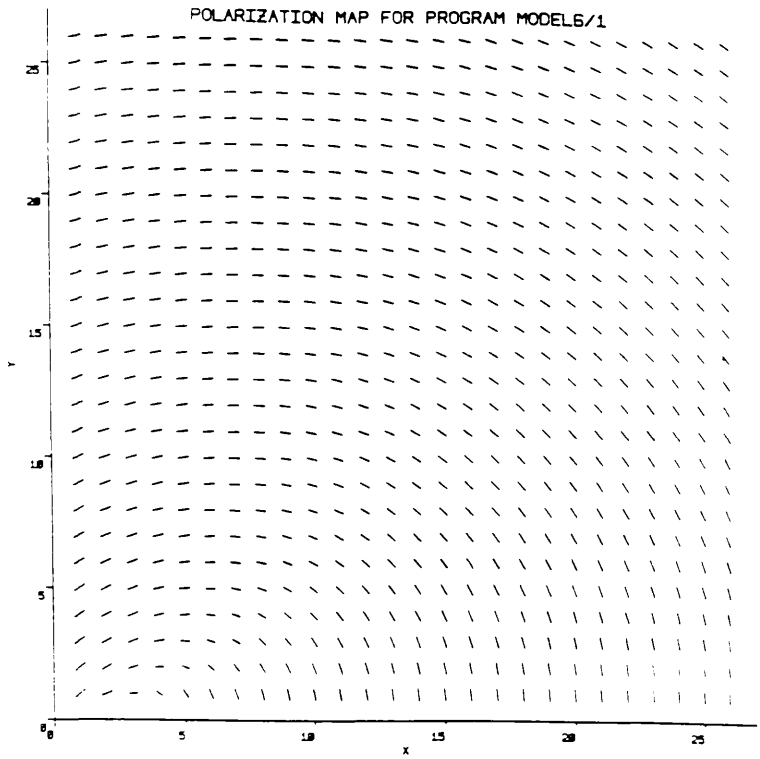

Figure 6.13: Polarization vector plot for a dipole magnetic field with an added component in the ϕ-direction which has a ratio of 10 to the other field components. This field structure viewed at an angle of inclination of the observer's line of sight to the dipole axis of $i = 0°$.

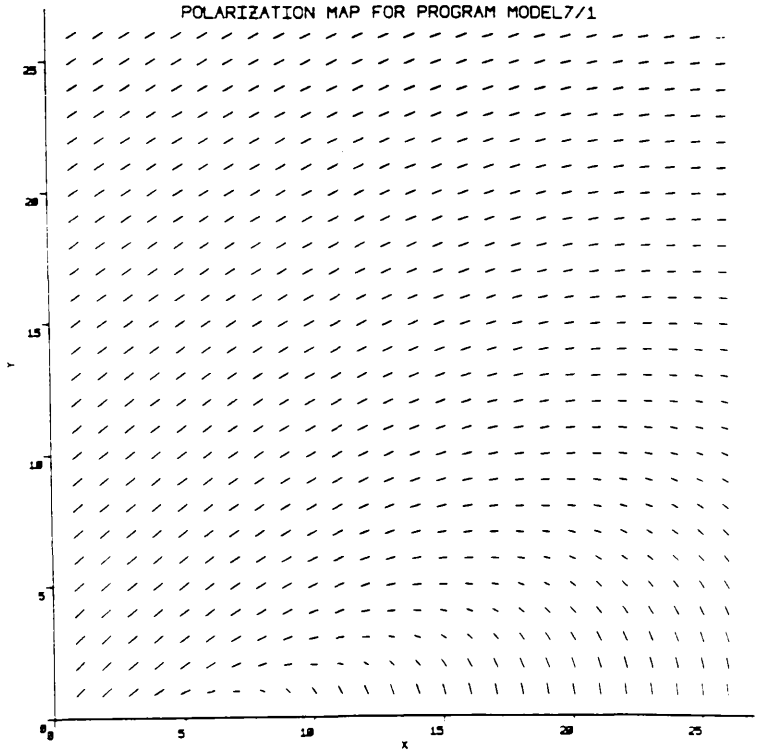

Figure 6.14: Polarization vector plot for a dipole magnetic field with an added component in the ϕ-direction which has a ratio of 50 to the other field components. This field structure viewed at an angle of inclination of the observer's line of sight to the dipole axis of $i = 0°$.

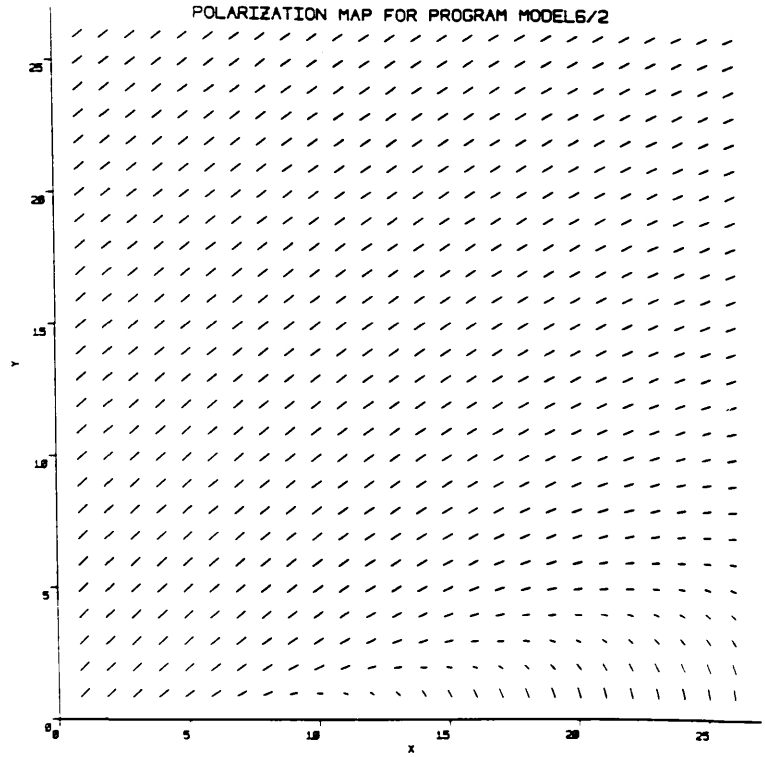

Figure 6.15: Polarization vector plot for a dipole magnetic field with an added component in the ϕ-direction which has a ratio of 100 to the other field components. This field structure viewed at an angle of inclination of the observer's line of sight to the dipole axis of $i = 0°$.

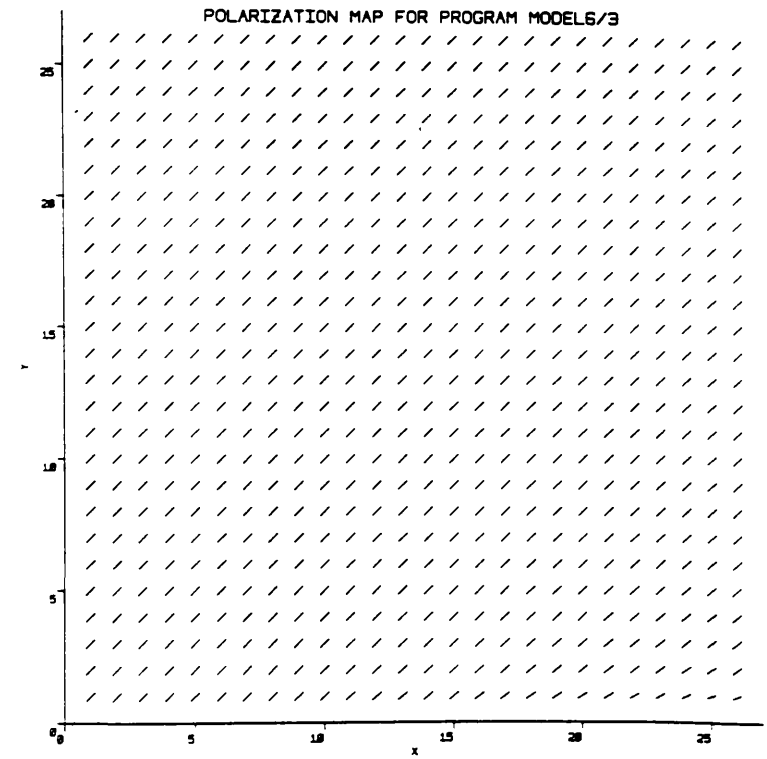

Figure 6.16: Polarization vector plot for a dipole magnetic field with an added component in the ϕ-direction which has a ratio of 1000 to the other field components. This field structure viewed at an angle of inclination of the observer's line of sight to the dipole axis of $i = 0°$.

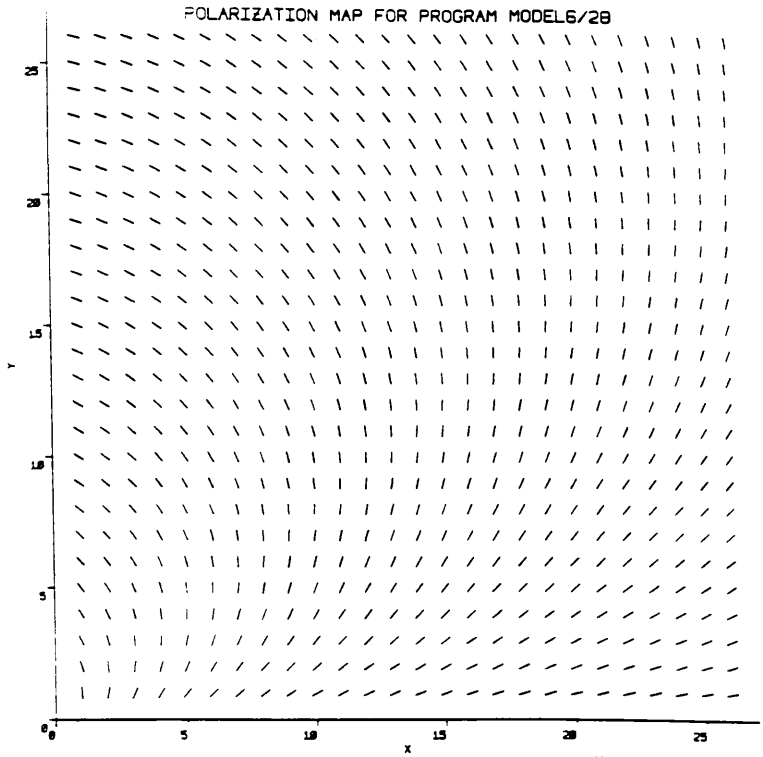

Figure 6.17: Polarization vector plot for a dipole magnetic field with an added component in the ϕ-direction which has a ratio of 10 to the other field components. This field structure viewed at an angle of inclination of the observer's line of sight to the dipole axis of i = 90°.

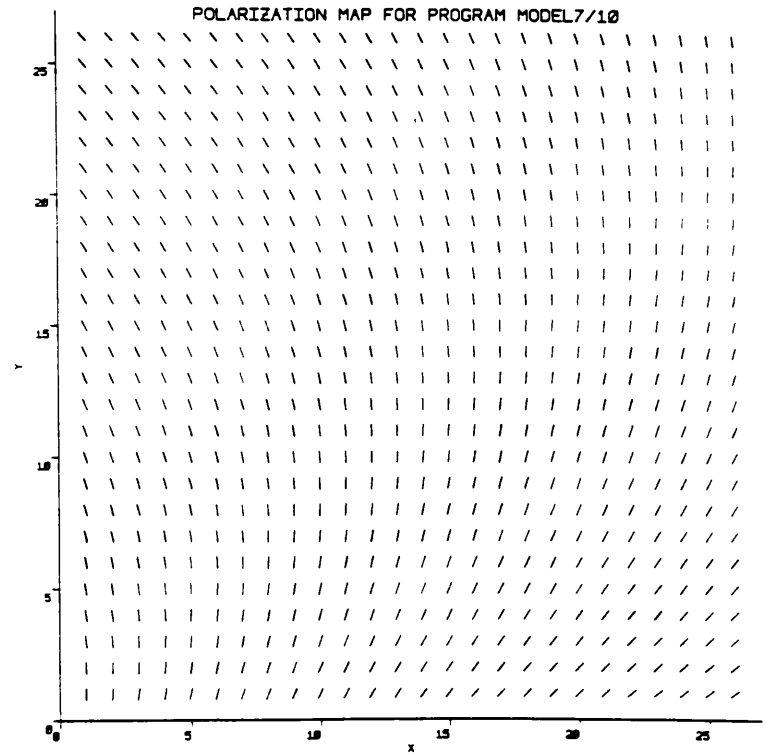

Figure 6.18: Polarization vector plot for a dipole magnetic field with an added component in the ϕ-direction which has a ratio of 50 to the other field components. This field structure viewed at an angle of inclination of the observer's line of sight to the dipole axis of i = 90°.

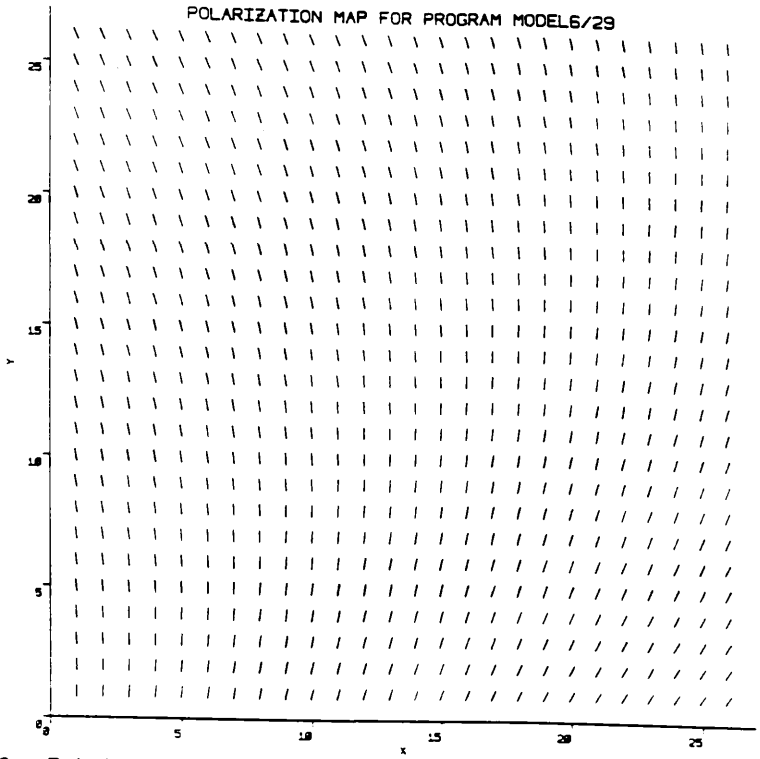

Figure 6.19: Polarization vector plot for a dipole magnetic field with an added component in the ϕ-direction which has a ratio of 100 to the other field components. This field structure viewed at an angle of inclination of the observer's line of sight to the dipole axis of i = 90°.

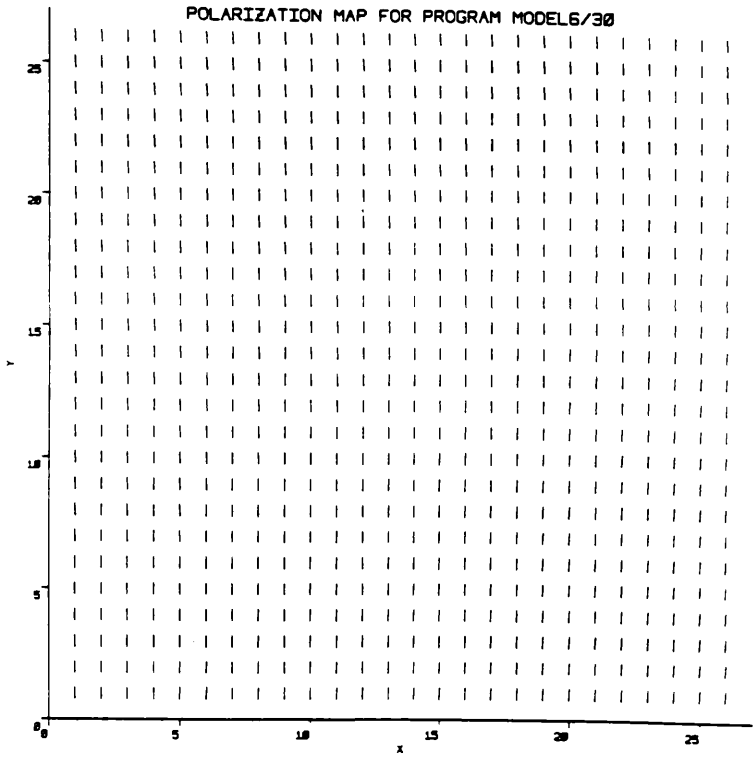

Figure 6.20: Polarization vector plot for a dipole magnetic field with an added component in the ϕ-direction which has a ratio of 1000 to the other field components. This field structure viewed at an angle of inclination of the observer's line of sight to the dipole axis of i = 90°.

Chapter 7

Conclusions

From the analysis of the two sets of polarimetric data [1,2], discussed in chapter 5, we have seen that there has been some change in the direction of the magnetic field in the northern part of the nebula. The average change in polarization angle is a rotation in the anti-clockwise direction of $11° \pm 5°$ (at a confidence level of 95%). A more detailed study of the nebula, on a pixel to pixel basis, would require complicated reduction of the resolution of McLean, Aspin and Reitsema's data [2] so that it matched exactly the resolution achieved by Woltjer [1]. Such an operation would involve writing special codes to perform the reduction and would be very time intensive. Such data reduction codes require much specialised study and knowledge if they are to produce the best results. Such work was not within the scope of this project but may be possible using STARLINK software packages which were not used in this project. The results from the centre finding programs were good for McLean, Aspin and Reitsema's data, but did not give a conclusive result for Woltjer's data. Therefore, unfortunately, we could not investigate the possibility of a change in the centre of polarization or intensity of the nebula with time.

Although the results from the data analysis have not proved as conclusive as one might have hoped, the theoretical computer modelling, discussed in chapter 6, produced some interesting results. The development of a computer model which would produce the polarization map which would be observed for a given magnetic field structure was a significant part of this project. The initial intention was to develop a computer generated model of the Crab nebula which could be compared with the data. Direct comparison of such a model to the data sets used in this work could tell us much about the structure of the Crab nebula magnetic field. To obtain the best results from such a comparison the model presented in this thesis requires further modifications. A useful modification would be the addition of a disk

component of the magnetic field lying in the same plane as the dipole axis in order to simulate the effect of a toroidal field component as suggested in several theoretical studies [e.g. 41,53,55].

Development of the computer model led to a consideration of the plasma theory of the Crab nebula magnetic field (see chapter 4). Treatment of the Crab nebula as a plasma is not a new concept but is necessary if any theoretical model is to be a realistic representation of the nebula. As have seen in chapter 4, previous work which tried to determine the magnetic field structure of the Crab nebula from the ideal magnetohydrodynamic equations (chapter 4, section 4.1) has not been sound and this is an area which requires further investigation. A solution of the frozen-in field equation would facilitate further computer modelling of the magnetic field structure of the Crab nebula as it would give us an expression for the magnetic field component generated by the pulsar rotation.

The main conclusion of this thesis is that there remain many unanswered questions about the Crab nebula's magnetic field structure, as well as many other aspects of its behaviour which were not mentioned in detail in this work. The key to progress in this field is the study of the plasma behaviour of the nebula and the solution of the frozen-in field equation. Initially we need a solution for the static case but perhaps eventually a solution will be found for the non-static case where the magnetic field evolves with time.

References

Key to Abbreviations

B.A.N.	Bulletins of the Astronomical Institutes of the Netherlands
Ann. Rev. Ast. Ap.	Annual Review of Astronomy and Astrophysics
Ap. J.	Astrophysical Journal
Ap. J. Lett.	Astrophysical Journal Letters
Ast. J.	Astronomical Journal
M.N.R.A.S.	Monthly Notices of the Royal Astronomical Society
P.A.S.P.	Publications of the Astronomical Society of the Pacific
Proc. Nat. Acad. Sci.	Proceedings of the National Academy of Science
Aust. J. Phys.	Australian Journal of Physics
Sov. Ast.	Soviet Astronomy
Ast. Ap.	Astronomy and Astrophysics
Ap. Sp. Sci.	Astrophysics and Space Science

References

[1] L. Woltjer (1957) B.A.N., 13, 478, 301.

[2] I.S. McLean, C. Aspin and H. Reitsema (1983) Nature, 304, 243.

[3] K. Davidson and R. Fesen (1985) Ann. Rev. Ast. Ap., 23, 119.

[4] C.F. Kennel and F.V. Coroniti (1984) Ap. J., 283, 694.

[5] V. Trimble (1968) Ast. J., 73, 7, 535.

[6] D.H. Clark, P. Murdin, R. Wood, R. Gilmozzi, J. Danziger and A.W. Furr (1983) M.N.R.A.S., 204, 415.

[7] V. Trimble (1985) in "*The Crab Nebula and Related Supernova Remnants*", ed. M.C. Kafatos and R.B.C. Henry, Cambridge University Press.

[8] A. van Maanen (1928) Mt. Wilson Contributions, No. 356.

[9] W. Baade (1956) B.A.N., 12, 462, 312.

[10] I.S. Shapiro and S.A. Teukolsky (1983) in "*Black Holes, White Dwarfs and Neutron Stars*", chapters 9 and 10, Wiley.

[11] J.H. Oort and Th. Walraven (1956) B.A.N.,12, 462, 285.

[12] D.E. Osterbrock (1957) P.A.S.P., 69, 227.

[13] C.F. Kennel and F.V. Coroniti (1984) Ap. J., 283, 710.

[14] I.A.U. Symp. No. 46, "*The Crab Nebula*", ed. R.D. Davies and F.G. Smith, Reidel.

[15] "*The Crab Nebula and Related Supernova Remnants*" (1985), ed. M.C. Kafatos and R.B.C. Henry, Cambridge University Press.

[16] K.E. Lundmark (1921) P.A.S.P., 33, 225.

[17] J.C. Duncan (1921) Proc. Nat. Acad. Sci., 7, 179.

[18] C.O. Lampland (1921) P.A.S.P., 33, 79.

[19] V.M. Slipher (1916) P.A.S.P., 28, 191.

[20] W. Baade (1942) Ap. J., 96, 188.

[21] R. Minkowski (1942) Ap. J., 96, 199.

[22] I.S. Shklovskii (1953) Doklady Akad. Nauk. U.S.S.R., 90, 983.

[23] V.A. Dombrowsky (1954) Doklady Akad. Nauk. U.S.S.R., 90, 1021.

[24] M.A. Vashakidze (1954) Astronomy Circulars, No. 147.

[25] Th. Walraven (1957) B.A.N., 13, 478, 293.

[26] V. Trimble (1973) P.A.S.P., 85, 579.

[27] V. Trimble and L. Woltjer (1971) Ap. J. Lett., 163, L97.

[28] G.D. Schmidt, J.R.P. Angel and E.A. Beaver (1979) Ap. J., 227, 106.

[29] C.H. Mayer, T.P. McCullough and R.M. Sloanaker (1964) Ast. J., 139, 248.

[30] L.I. Matveenko and V.I. Kostenko (1979) Aust. J. Phys., 32, 105.

[31] A.S. Wilson (1972) M.N.R.A.S., 157, 229.

[32] A.S. Wilson (1972) M.N.R.A.S., 160, 355.

[33] A.S. Wilson (1972) M.N.R.A.S., 160, 373.

[34] E. Swinbank (1980) M.N.R.A.S., 193, 451.

[35] E. Swinbank and G. Pooley (1979) M.N.R.A.S., 186, 775.

[36] T. Velusamy (1985) M.N.R.A.S., 212, 359.

[37] M. Longair (1981) pages 248-249, 254-256, in "*High Energy Astrophysics*", Cambridge University Press.

[38] D.H. Staelin and E.C. Reifinstein III (1968) Science, 162,1481.

[39] W.J. Cocke, M.J. Disney and D.J. Taylor (1969) Nature, 221, 525.

[40] P. Sturrock (1971) Ap. J., 164, 529.

[41] M.J. Rees and J.E. Gunn (1974) M.N.R.A.S., 167, 1.

[42] J.H. Piddington (1957) Aust. J. Phys., 10, 350.

[43] A.J. Deutsch (1955) Annales d'Astrophysique, 18, 1.

[44] A.A. Korchakov and S.I. Syrovatskii (1961) Sov. Ast., 5, 5, 678.

[45] B. Aschenbach and W. Brinkmann (1975) Ast. Ap., 41, 147.

[46] N.S. Kardashev (1965) Sov. Ast., 8, 5, 643.

[47] J.E. Gunn and J.P. Ostriker (1971) Ast. J., 165, 523.

[48] J.D. Landstreet and J.R.P. Angel (1971) Nature, 230, 103.

[49] P.G. Martin, R. Illing and J.R.P. Angel (1972) M.N.R.A.S., 159, 191.

[50] G. Benford, G. Bodo and A. Ferrari (1978) Ast. Ap., 70, 815.

[51] M.A. Ruderman and P.G. Sutherland (1975) Ap. J., 196, 51.

[52] A. Greve and A.M. van Genderen (1982) Ast. Ap., 115, 79.

[53] J.J. Barnard (1986) Ap. J., 303, 280.

[54] J. Kristian, N. Visvanathan, J.A. Westphal and G.H. Snellen (1970) Ap. J., 162, 415.

[55] E.G. Tsikarishvili, G.D. Chagelishvili, O.V. Chedia, J.G. Lominadze and Z.A. Sokhadze (1988) Ap. Sp. Sci., November, 255.

[56] G.B. Rybicki and A.P. Lightman (1979) "*Radiative Processes in Astrophysics*", Wiley.

[57] J.C. Brown, I.J.D. Craig and D.B. Melrose (1983) Ap. Sp. Sci., 92, 105.

[58] M. Abramowitz and I.A. Stegun (1965) "*Handbook of Mathematical Functions*", Dover.

[59] J.A. Bittencourt (1986) "*Fundamentals of Plasma Physics*", Pergamon.

[60] L. Woltjer (1958) B.A.N., 14, 483, 39.

[61] J.D. Scargle (1969) Ap. J., 156, 401.

[62] S.H. Pravdo and P. Serlemitsos (1981) Ap. J., 246, 484.

[63] G.D. Walraven, R.D. Hall, C.A. Meegan, P.L. Coleman, D.H. Shelton and R.C. Haymes (1975) Ap. J., 202, 502.

[64] G.L. Grasdalen (1979) P.A.S.P., 91, 436.

[65] C.C. Wu (1981) Ap. J., 245, 581.

[66] P. Lorrain and D.R. Corson (1962) "*Electromagnetic Fields and Waves*", Freeman.

Appendix A

```
c       Program FILLCRAB.FOR

        open(unit=3,status='old',name='crabxy.dat')
        open(unit=4,status='old',name='crabiqu.dat')
        open(unit=5,status='new',name='fullcrab.dat')
        do 1 l=0,36
        read(3,*) x1,x2
        m=x2-x1
        do 2 j=0,50
        if (j.lt.x1) then
         n=1
         I=-1
         Q=0.0
         U=0.0
         write (5,*) n,I,Q,U
        else
        if (j.eq.x1) then
         do 3 k=0,m
         read(4,*) n,I,Q,U
         write (5,*) n,I,Q,U
    3   continue
        else
        if (j.gt.x2) then
         n=1
         I=-1
         Q=0.0
         U=0.0
         write (5,*) n,I,Q,U
        end if
        end if
        end if
    2   continue
    1   continue
        stop
        end
```

```
c   Program IQUPROG calculates I,Q,U from X,P,I...Woltjer's data

      pi=4.*atan(1.)
      open(unit=1,status='old',name='crabxpi.dat')
      open(unit=2,status='new',name='crabiqu.dat')
      do 1 j=1,1101
      read(1,*) n,X,P,I
      X=X*pi/180.
      if (X.lt.0.) then
       Q=0.
       U=0.
       I=-1
      else
       U=P*sin(2.*X)
       Q=P*cos(2.*X)
      end if
      write(2,20) n,I,Q,U
20    format(I2,I4,2F10.5)
1     continue
      stop
      end
```

```
c       Program CRABPLOT.FOR

        dimension x(2),y(2)
        open(unit=2,status='old',name='crabxy.dat')
        open(unit=3,status='old',name='crabxpi.dat')
        pi=4.*atan(1.)
        call gopks(6,-1)
        call gopwk(2,1,4014)
        call gacwk(2)
        call gswn (1,0.0,50.0,0.0,40.0)
        call gselnt (1)
        do 1 j=1,37
        read(2,*) x1,x2
        m=x2-x1
        x1=x1+2
         do 2 k=0,m
         read(3,*) n,chi,P,I
          if (chi.eq.-1) goto 2
         chi=(pi/2.)+chi*pi/180.
         a=P*cos(chi)
         a=a/50.
         b=P*sin(chi)
         b=b/50.
         xc=x1+k
         yc=39-j
         x(1)=xc-a/2
         y(1)=yc-b/2
         x(2)=xc+a/2
         y(2)=yc+b/2
         call gpl(2,x,y)
2       continue
1       continue
        call gdawk(2)
        call gclwk(2)
        call gclks
        stop
        end
```

```
c        program  FULLPLOT plots either Mclean or Woltjer's data

         dimension y(2),x(2)
         character*20 title
         print*,'Input filename?'
         read(6,99) title
         print*,'If using Woltjer data type 1, Mclean data type 0.'
         read(6,*) nn
         open(unit=3,status='old',name=title)
         pi=4.*atan(1.)
         call gopks(6,-1)
         call gopwk(2,1,4014)
         call gacwk(2)
         call gswn(1,0.0,52.0,0.0,40.0)
         call gselnt(1)
         do 1 j=1,37
          if(nn.eq.1) then
          yc=39-j
          else
          yc=j+1
          end if
          do 2 k=1,51
          read(3,*) n,I,Q,U

c        Test for the quadrant of the angle 2X.
          if(Q.eq.0.0.and.U.eq.0.0) then
           twochi=0.0
          else
          if(Q.gt.0.0.and.U.ge.0.0) then
           twochi=atan(U/Q)
          else
          if(Q.lt.0.0.and.U.ge.0.0) then
           twochi=pi+atan(U/Q)
          else
          if(Q.gt.0.0.and.U.le.0.0) then
           twochi=(2*pi)+atan(U/Q)
          else
          if(Q.lt.0.0.and.U.le.0.0) then
           twochi=pi+atan(U/Q)
          else
          if(Q.eq.0.0.and.U.gt.0.0) then
           twochi=pi/2.
          else
          if(Q.eq.0.0.and.U.lt.0.0) then
           twochi=(3./2.)*pi
          end if
          end if
          end if
          end if
          end if
          end if
          end if
          chi=(twochi/2.)+(pi/2.)
           P=(Q**2+U**2)**0.5
           a=P*cos(chi)
           b=P*sin(chi)
           if(nn.eq.1) then
           a=a/50.
           b=b/50.
           else
           a=a/2000.
           b=b/2000.
           end if
           xc=k
           x(1)=xc-a/2
           y(1)=yc-b/2
           x(2)=xc+a/2
           y(2)=yc+b/2
           call gpl(2,x,y)
2          continue
1         continue
          call gdawk(2)
          call gclwk(2)
          call gclks
99        format(a20)
          stop
          end
```

```
c        program highres (sorts Mclean et al's data in squares of 51x33 pixels
c        and produces 56 files of data in I,Q,U form)

        character*80 title
        open(unit=3,status='old',name='mccrab.dat')
        open(unit=4,status='old',name='names.dat')
        do 1 n=1,8
        do 2 m=1,7
        unitno=m+6
        read(4,99) title
        open(unit=unitno,status='new',name=title)
99      format(a80)
2       continue
        do 3 j=1,33
         do 4 k=1,357
         read(3,*) I,Q,U
         if (k.le.51) then
          write(7,*) I,Q,U
         else
         if (k.ge.52.and.k.le.102) then
          write(8,*) I,Q,U
         else
         if (k.ge.103.and.k.le.153) then
          write(9,*) I,Q,U
         else
         if (k.ge.154.and.k.le.204) then
          write(10,*) I,Q,U
         else
         if (k.ge.205.and.k.le.255) then
          write(11,*) I,Q,U
         else
         if (k.ge.256.and.k.le.306) then
          write(12,*) I,Q,U
         else
         if (k.ge.307.and.k.le.357) then
          write(13,*) I,Q,U
         end if
         end if
         end if
         end if
         end if
         end if
         end if
 4       continue
 3       continue
         close(13)
         close(12)
         close(11)
         close(10)
         close(9)
         close(8)
         close(7)
 1       continue
        stop
        end
```

```
c       program hrplot (plots Mclean et al's data in a selected 51x33 pixel box)
        dimension x(2),y(2)
        character*8 title
        print*, 'Which area do you want to plot?'
        print*, 'Areas number HR1.dat to HR56.dat, 7 across, 8 down.'
        print*, ' '
        read(5,99) title
99      format(a8)
        open(unit=3,status='old',name=title)
        call gopks(6,-1)
        call gopwk(2,1,4014)
        call gacwk(2)
        pi=4.*atan(1.)
        print*, title
        call gswn(1,0.0,54.0,0.0,36.0)
        call gselnt(1)
        do 1 j=2,34
         yc=j
         do 2 k=2,52
         read(3,*) I,Q,U
         if(I.le.0) goto 2

c       Test for the quadrant of the angle 2X.
         if(Q.eq.0.0.and.U.eq.0.0) then
          chi=0.0
         else
         if(Q.gt.0.0.and.U.ge.0.0) then
          chi=(atan(U/Q))/2.
         else
         if(Q.lt.0.0.and.U.ge.0.0) then
          chi=(pi+atan(U/Q))/2.
         else
         if(Q.gt.0.0.and.U.le.0.0) then
          chi=pi+(atan(U/Q)/2.)
         else
         if(Q.lt.0.0.and.U.le.0.0) then
          chi=(pi+atan(U/Q))/2.
         else
         if(Q.eq.0.0.and.U.gt.0.0) then
          chi=pi/4.
         else
         if(Q.eq.0.0.and.U.lt.0.0) then
          chi=(3./4.)*pi
         end if
         end if
         end if
         end if
         end if
         end if
         end if
         chi=chi+(pi/2.)
         P=(Q**2+U**2)**0.5
         a=P*cos(chi)/50.
         b=P*sin(chi)/50.
         xc=k
         x(1)=xc-a/2
         y(1)=yc-b/2
         x(2)=xc+a/2
         y(2)=yc+b/2
         call gpl(2,x,y)
 2       continue
 1      continue
        call gdawk(2)
        call gclwk(2)
        call gclks
        stop
        end
```

```
c       program highres (sorts Mclean et al's data in squares of 21x22 pixels
c       and produces 204 files of data in I,Q,U form)
      character*20 title
      open(unit=3,status='old',name='mccrab.dat')
      open(unit=4,status='old',name='names.dat')
      do 1 n=1,12
      do 2 m=1,17
      unitno=n+6
      read(4,99) title
      open(unit=unitno,status='new',name=title)
99    format(a20)
2     continue
      do 3 j=1,22
       do 4 k=1,357
       read(3,*) I,Q,U
       if (k.le.21) then
        write(7,*) I,Q,U
       else
       if (k.ge.22.and.k.le.42) then
        write(8,*) I,Q,U
       else
       if (k.ge.43.and.k.le.63) then
        write(9,*) I,Q,U
       else
       if (k.ge.64.and.k.le.84) then
        write(10,*) I,Q,U
       else
       if (k.ge.85.and.k.le.105) then
        write(11,*) I,Q,U
       else
       if (k.ge.106.and.k.le.126) then
        write(12,*) I,Q,U
       else
       if (k.ge.127.and.k.le.147) then
        write(13,*) I,Q,U
       else
       if (k.ge.148.and.k.le.168) then
        write(14,*) I,Q,U
       else
       if (k.ge.169.and.k.le.189) then
        write(15,*) I,Q,U
       else
       if (k.ge.190.and.k.le.210) then
        write(16,*) I,Q,U
       else
       if (k.ge.211.and.k.le.231) then
        write(17,*) I,Q,U
       else
       if (k.ge.232.and.k.le.252) then
        write(18,*) I,Q,U
       else
       if (k.ge.253.and.k.le.273) then
        write(19,*) I,Q,U
       else
       if (k.ge.274.and.k.le.294) then
        write(20,*) I,Q,U
       else
       if (k.ge.295.and.k.le.315) then
        write(21,*) I,Q,U
       else
       if (k.ge.316.and.k.le.336) then
        write(22,*) I,Q,U
       else
       if (k.ge.337) then
        write(23,*) I,Q,U
       end if
       end if
       end if
       end if
       end if
       end if                                    close(18)
       end if                                    close(14)
       end if                                    close(13)
       end if                                    close(12)
       end if                                    close(11)
       end if                                    close(10)
       end if                                    close(9)
       end if                                    close(8)
       end if                                    close(7)
       end if                              1     continue
       end if                                    stop
       end if                                    end
4      continue
3      continue
       close(23)
       close(22)
       close(21)
       close(20)
       close(19)
       close(18)
       close(17)
```

```
c       program hr2plot(plots Mclean et al's data in a selected 21x22 pixel box)

        dimension x(2),y(2)
        character*10 title
        print*, 'Which area do you want to plot?'
        print*, 'Areas number HR1.dat to HR204.dat, 17 across, 12 down.'
        print*, ' '
        read(5,99) title
99      format(a10)
        open(unit=3,status='old',name=title)
        call gopks(6,-1)
        call gopwk(2,1,4014)
        call gacwk(2)
        pi=4.*atan(1.)
        print*, title
        call gswn(1,0.0,24.0,0.0,25.0)
        call gselnt(1)
        do 1 j=2,23
         yc=j
         do 2 k=2,22
         read(3,*) I,Q,U
         if(I.le.0) goto 2

c       Test for the quadrant of the angle 2X.
         if(Q.eq.0.0.and.U.eq.0.0) then
          chi=0.0
         else
         if(Q.gt.0.0.and.U.ge.0.0) then
          chi=(atan(U/Q))/2.
         else
         if(Q.lt.0.0.and.U.ge.0.0) then
          chi=(pi+atan(U/Q))/2.
         else
         if(Q.gt.0.0.and.U.le.0.0) then
          chi=pi+(atan(U/Q)/2.)
         else
         if(Q.lt.0.0.and.U.le.0.0) then
          chi=(pi+atan(U/Q))/2.
         else
         if(Q.eq.0.0.and.U.gt.0.0) then
          chi=pi/4.
         else
         if(Q.eq.0.0.and.U.lt.0.0) then
          chi=(3./4.)*pi
         end if
         end if
         end if
         end if
         end if
         end if
         end if
         chi=chi+(pi/2.)
         P=(Q**2+U**2)**0.5
         a=P*cos(chi)/50
         b=P*sin(chi)/50
         xc=k
         x(1)=xc-a/2
         y(1)=yc-b/2
         x(2)=xc+a/2
         y(2)=yc+b/2
         call gpl(2,x,y)
2        continue
1       continue
        call gdawk(2)
        call gclwk(2)
        call gclks
        stop
        end
```

```
c       program highres3 (sorts Mclean et al's data in squares of 7x8 pixels
c       and produces 1683 files of data in I,Q,U form)

c       To do this we must first divide the data into subsets of 21x24 pixels
c       which is a similar procedure to highres2.for.
      character*20 title,output
      open(unit=3,status='old',name='mccrab.dat')
      open(unit=4,status='old',name='names.dat')
      do 1 n=1,11
      do 2 m=1,17
      unitno=m+6
      read(4,99) title
      open(unit=unitno,status='new',name=title)
2     continue
      do 3 j=1,24
       do 4 k=1,357
       read(3,*) I,Q,U
       if (k.le.21) then
        write(7,*) I,Q,U
       else
       if (k.ge.22.and.k.le.42) then
        write(8,*) I,Q,U
       else
       if (k.ge.43.and.k.le.63) then
        write(9,*) I,Q,U
       else
       if (k.ge.64.and.k.le.84) then
        write(10,*) I,Q,U
       else
       if (k.ge.85.and.k.le.105) then
        write(11,*) I,Q,U
       else
       if (k.ge.106.and.k.le.126) then
        write(12,*) I,Q,U
       else
       if (k.ge.127.and.k.le.147) then
        write(13,*) I,Q,U
       else
       if (k.ge.148.and.k.le.168) then
        write(14,*) I,Q,U
       else
       if (k.ge.169.and.k.le.189) then
        write(15,*) I,Q,U
       else
       if (k.ge.190.and.k.le.210) then
        write(16,*) I,Q,U
       else
       if (k.ge.211.and.k.le.231) then
        write(17,*) I,Q,U
       else
       if (k.ge.232.and.k.le.252) then
        write(18,*) I,Q,U
       else
       if (k.ge.253.and.k.le.273) then
        write(19,*) I,Q,U
       else
       if (k.ge.274.and.k.le.294) then
        write(20,*) I,Q,U
       else
       if (k.ge.295.and.k.le.315) then
        write(21,*) I,Q,U
       else
       if (k.ge.316.and.k.le.336) then
        write(22,*) I,Q,U
       else
       if (k.ge.337) then
        write(23,*) I,Q,U
       end if
       end if
       end if
       end if
       end if
       end if
       end if
       end if
       end if
       end if
       end if
       end if
       end if
       end if
       end if
       end if
       end if
       end if
       end if
       end if
4      continue
3      continue
       close(23)
       close(22)
       close(21)
       close(20)
       close(19)
       close(18)
       close(17)
```

```
      close(15)
      close(14)
      close(13)
      close(12)
      close(11)
      close(10)
      close(9)
      close(8)
      close(7)
1     continue
      close(3)
      close(4)

c  Next we must divide each set of 21x24 pixels into sets of 7x8 pixels.

      open(unit=2,status='old',name='names.dat')
      open(unit=3,status='old',name='names2.dat')

c Open each file of 21x24 pixels in turn and divide into 9 blocks of 7x8 pixels.

      do 5 i=1,187
      read(2,99) title
      open(unit=4,status='old',name=title)
      do 6 nn=1,3
      do 7 mm=1,3
      number=6+mm
      read(3,99) output
      open(unit=number,status='new',name=output)
7     continue
      do 8 jj=1,8
      do 9 kk=1,21
      read(4,*) I,Q,U
      if (kk.le.7) then
       write(7,*) I,Q,U
      else
      if (kk.ge.8.and.kk.le.14) then
       write(8,*) I,Q,U
      else
      if (kk.ge.15.and.kk.le.21) then
       write(9,*) I,Q,U
      end if
      end if
      end if
9     continue
8     continue
      close(7)
      close(8)
      close(9)
6     continue
      close(4)
5     continue
99    format(a20)
      stop
      end
```

```
c       program hr3plot(plots Mclean et al's data in a selected 7x8 pixel box)

        dimension x(2),y(2)
        character*10 title
        print*, 'Which area do you want to plot?'
        print*, 'Areas number OP1.dat to OP1683.dat, 51 across, 33 down.'
        print*, ' '
        read(5,99) title
99      format(a10)
        open(unit=3,status='old',name=title)
        call gopks(6,-1)
        call gopwk(2,1,4014)
        call gacwk(2)
        pi=4.*atan(1.)
        print*, title
        call gswn(1,0.0,10.0,0.0,10.0)
        call gselnt(1)
        do 1 j=2,9
         yc=j
         do 2 k=2,8
         read(3,*) I,Q,U
         if(I.le.0) goto 2

c       Test for the quadrant of the angle 2X.
         if(Q.eq.0.0.and.U.eq.0.0) then
          chi=0.0
         else
         if(Q.gt.0.0.and.U.ge.0.0) then
          chi=(atan(U/Q))/2.
         else
         if(Q.lt.0.0.and.U.ge.0.0) then
          chi=(pi+atan(U/Q))/2.
         else
         if(Q.gt.0.0.and.U.le.0.0) then
          chi=pi+(atan(U/Q)/2.)
         else
         if(Q.lt.0.0.and.U.le.0.0) then
          chi=(pi+atan(U/Q))/2.
         else
         if(Q.eq.0.0.and.U.gt.0.0) then
          chi=pi/4.
         else
         if(Q.eq.0.0.and.U.lt.0.0) then
          chi=(3./4.)*pi
         end if
         end if
         end if
         end if
         end if
         end if
         end if
         chi=chi+(pi/2.)
         P=(Q**2+U**2)**0.5
         a=P*cos(chi)/50
         b=P*sin(chi)/50
         xc=k
         x(1)=xc-a/2
         y(1)=yc-b/2
         x(2)=xc+a/2
         y(2)=yc+b/2
         call gpl(2,x,y)
2        continue
1       continue
        call gdawk(2)
        call gclwk(2)
        call gclks
        stop
        end
```

```
c Wolfgram LOWRES.FOR reduces the resolution of Mclean's data to that of

      character*20 title
      open(unit=1,status='old',name='names3.dat')
      open(unit=2,status='new',name='lowres.dat')
      do 1 m=1,1683
      read(1,99) title
      open(unit=3,status='old',name=title)
      Isum=0
      Qsum=0.0
      Usum=0.0
      n=0
      do 2 k=1,56
      read(3,*) I,Q,U
      if (I.eq.0.and.Q.eq.0.0.and.U.eq.0.0) goto 2
      Isum=Isum+I
      Qsum=Qsum+Q
      Usum=Usum+U
      n=n+1
2     continue
      close(3)
      if (n.eq.0) then
      Ibar=0
      Qsum=0.0
      Usum=0.0
      else
      Ibar=Isum/n
c Do not need to divide Qsum and Usum by n because we only need a ratio
c between them. Also, dividing by n is not necessary to allow for depolarisation
      end if
      write(2,*) n,Ibar,Qsum,Usum
1     continue
      do jj=1,4
      do kk=1,51
      nn=0
      a=0.0
      write(2,*) nn,nn,a,a
      end do
      end do
99    format(a20)
      stop
      end
```

```
c        program lowresplot(plots Mclean et al's data at low resolution)
        dimension y(2),x(2)
        open(unit=3,status='old',name='lowres.dat')
        pi=4.*atan(1.)
        call gopks(6,-1)
        call gopwk(2,1,4014)
        call gacwk(2)
        call gswn(1,0.0,52.0,0.0,40.0)
        call gselnt(1)
        do 1 j=1,33
         yc=j+3
         do 2 k=1,51
         read(3,*) n,I,Q,U
         if (I.eq.0) goto 2

c       Test for the quadrant of the angle 2X.
         if(Q.eq.0.0.and.U.eq.0.0) then
          twochi=0.0
         else
         if(Q.gt.0.0.and.U.ge.0.0) then
          twochi=atan(U/Q)
         else
         if(Q.lt.0.0.and.U.ge.0.0) then
          twochi=pi+atan(U/Q)
         else
         if(Q.gt.0.0.and.U.le.0.0) then
          twochi=(2*pi)+atan(U/Q)
         else
         if(Q.lt.0.0.and.U.le.0.0) then
          twochi=pi+atan(U/Q)
         else
         if(Q.eq.0.0.and.U.gt.0.0) then
          twochi=pi/2.
         else
         if(Q.eq.0.0.and.U.lt.0.0) then
          twochi=(3./2.)*pi
         end if
         end if
         end if
         end if
         end if
         end if
         end if
         chi=(twochi/2.)+(pi/2.)
          P=(Q**2+U**2)**0.5
          a=P*cos(chi)
          b=P*sin(chi)
          a=a/2000.
          b=b/2000.
          xc=k
          x(1)=xc-a/2
          y(1)=yc-b/2
          x(2)=xc+a/2
          y(2)=yc+b/2
          call gpl(2,x,y)
2        continue
1       continue
        call gdawk(2)
        call gclwk(2)
        call gclks
        stop
        end
```

```
c program BINS.FOR puts Woltjer's data into 5 degree bins.
      integer a,aa,b,bb,c,cc,d,dd,e,ee,f,ff,g,gg,h,hh
      integer p,r,s,t,v,w,pp,rr,ss,tt,vv,ww
      open(unit=1,status='old',name='fullcrab.dat')
      open(unit=2,status='new',name='bins.dat')
      pi=4.*atan(1.)
      do 1 j=1,1850
      read(1,*) n,I,QQ,UU
      if (I.le.0) goto 1

c     Test for the quadrant of the angle 2X.
       if(QQ.eq.0.0.and.UU.eq.0.0) then
        chi=0.0
       goto 99
       else
       if(QQ.gt.0.0.and.UU.ge.0.0) then
        chi=(atan(UU/QQ))/2.
       goto 99
       else
       if(QQ.lt.0.0.and.UU.ge.0.0) then
        chi=(pi+atan(UU/QQ))/2.
       goto 99
       else
       if(QQ.gt.0.0.and.UU.le.0.0) then
        chi=pi+(atan(UU/QQ)/2.)
       goto 99
       else
       if(QQ.lt.0.0.and.UU.le.0.0) then
        chi=(pi+atan(UU/QQ))/2.
       goto 99
       else
       if(QQ.eq.0.0.and.UU.gt.0.0) then
        chi=pi/4.
       goto 99
       else
       if(QQ.eq.0.0.and.UU.lt.0.0) then
        chi=(3./4.)*pi
       goto 99
       end if
       end if
       end if
       end if
       end if
       end if
       end if

 99    chi=(chi*180.)/pi

       if (chi.lt.5.) a=a+1
       if (chi.ge.5.0.and.chi.lt.10.) b=b+1
       if (chi.ge.10.0.and.chi.lt.15.) c=c+1
       if (chi.ge.15.0.and.chi.lt.20.) d=d+1
       if (chi.ge.20.0.and.chi.lt.25.) e=e+1
       if (chi.ge.25.0.and.chi.lt.30.) f=f+1
       if (chi.ge.30.0.and.chi.lt.35.) g=g+1
       if (chi.ge.35.0.and.chi.lt.40.) h=h+1
       if (chi.ge.40.0.and.chi.lt.45.) k=k+1
       if (chi.ge.45.0.and.chi.lt.50.) l=l+1
       if (chi.ge.50.0.and.chi.lt.55.) m=m+1
       if (chi.ge.55.0.and.chi.lt.60.) n=n+1
       if (chi.ge.60.0.and.chi.lt.65.) p=p+1
       if (chi.ge.65.0.and.chi.lt.70.) r=r+1
       if (chi.ge.70.0.and.chi.lt.75.) s=s+1
       if (chi.ge.75.0.and.chi.lt.80.) t=t+1
       if (chi.ge.80.0.and.chi.lt.85.) v=v+1
       if (chi.ge.85.0.and.chi.lt.90.) w=w+1
       if (chi.ge.90.0.and.chi.lt.95.) aa=aa+1
       if (chi.ge.95.0.and.chi.lt.100.) bb=bb+1
       if (chi.ge.100.0.and.chi.lt.105.) cc=cc+1
       if (chi.ge.105.0.and.chi.lt.110.) dd=dd+1
       if (chi.ge.110.0.and.chi.lt.115.) ee=ee+1
       if (chi.ge.115.0.and.chi.lt.120.) ff=ff+1
       if (chi.ge.120.0.and.chi.lt.125.) gg=gg+1
       if (chi.ge.125.0.and.chi.lt.130.) hh=hh+1
       if (chi.ge.130.0.and.chi.lt.135.) kk=kk+1
       if (chi.ge.135.0.and.chi.lt.140.) ll=ll+1
       if (chi.ge.140.0.and.chi.lt.145.) mm=mm+1
       if (chi.ge.145.0.and.chi.lt.150.) nn=nn+1
       if (chi.ge.150.0.and.chi.lt.155.) pp=pp+1
       if (chi.ge.155.0.and.chi.lt.160.) rr=rr+1
       if (chi.ge.160.0.and.chi.lt.165.) ss=ss+1
       if (chi.ge.165.0.and.chi.lt.170.) tt=tt+1
       if (chi.ge.170.0.and.chi.lt.175.) vv=vv+1
       if (chi.ge.175.0.and.chi.lt.180.) ww=ww+1
 1     continue
       write(2,*) a,b,c,d,e,f,g,h,k,l,m,n,p,r,s,t,v,w
       write(2,*) aa,bb,cc,dd,ee,ff,gg,hh,kk,ll,mm,nn,pp,rr,ss,tt,vv,ww
       stop
       end
```

```
c program BINS1.FOR puts McLean's data into 5 degree bins.
      integer a,aa,b,bb,c,cc,d,dd,e,ee,f,ff,g,gg,h,hh
      integer p,r,s,t,v,w,pp,rr,ss,tt,vv,ww
      open(unit=1,status='old',name='lowres.dat')
      open(unit=2,status='new',name='bins1.dat')
      pi=4.*atan(1.)
      do 1 j=1,1683
      read(1,*) n,I,QQ,UU
      if (I.le.0) goto 1

c     Test for the quadrant of the angle 2X.
       if(QQ.eq.0.0.and.UU.eq.0.0) then
        chi=0.0
       goto 99
       else
       if(QQ.gt.0.0.and.UU.ge.0.0) then
        chi=(atan(UU/QQ))/2.
       goto 99
       else
       if(QQ.lt.0.0.and.UU.ge.0.0) then
        chi=(pi+atan(UU/QQ))/2.
       goto 99
       else
       if(QQ.gt.0.0.and.UU.le.0.0) then
        chi=pi+(atan(UU/QQ)/2.)
       goto 99
       else
       if(QQ.lt.0.0.and.UU.le.0.0) then
        chi=(pi+atan(UU/QQ))/2.
       goto 99
       else
       if(QQ.eq.0.0.and.UU.gt.0.0) then
        chi=pi/4.
       goto 99
       else
       if(QQ.eq.0.0.and.UU.lt.0.0) then
        chi=(3./4.)*pi
       goto 99
       end if
       end if
       end if
       end if
       end if
       end if
       end if

 99    chi=(chi*180.)/pi

       if (chi.lt.5.) a=a+1
       if (chi.ge.5.0.and.chi.lt.10.) b=b+1
       if (chi.ge.10.0.and.chi.lt.15.) c=c+1
       if (chi.ge.15.0.and.chi.lt.20.) d=d+1
       if (chi.ge.20.0.and.chi.lt.25.) e=e+1
       if (chi.ge.25.0.and.chi.lt.30.) f=f+1
       if (chi.ge.30.0.and.chi.lt.35.) g=g+1
       if (chi.ge.35.0.and.chi.lt.40.) h=h+1
       if (chi.ge.40.0.and.chi.lt.45.) k=k+1
       if (chi.ge.45.0.and.chi.lt.50.) l=l+1
       if (chi.ge.50.0.and.chi.lt.55.) m=m+1
       if (chi.ge.55.0.and.chi.lt.60.) n=n+1
       if (chi.ge.60.0.and.chi.lt.65.) p=p+1
       if (chi.ge.65.0.and.chi.lt.70.) r=r+1
       if (chi.ge.70.0.and.chi.lt.75.) s=s+1
       if (chi.ge.75.0.and.chi.lt.80.) t=t+1
       if (chi.ge.80.0.and.chi.lt.85.) v=v+1
       if (chi.ge.85.0.and.chi.lt.90.) w=w+1
       if (chi.ge.90.0.and.chi.lt.95.) aa=aa+1
       if (chi.ge.95.0.and.chi.lt.100.) bb=bb+1
       if (chi.ge.100.0.and.chi.lt.105.) cc=cc+1
       if (chi.ge.105.0.and.chi.lt.110.) dd=dd+1
       if (chi.ge.110.0.and.chi.lt.115.) ee=ee+1
       if (chi.ge.115.0.and.chi.lt.120.) ff=ff+1
       if (chi.ge.120.0.and.chi.lt.125.) gg=gg+1
       if (chi.ge.125.0.and.chi.lt.130.) hh=hh+1
       if (chi.ge.130.0.and.chi.lt.135.) kk=kk+1
       if (chi.ge.135.0.and.chi.lt.140.) ll=ll+1
       if (chi.ge.140.0.and.chi.lt.145.) mm=mm+1
       if (chi.ge.145.0.and.chi.lt.150.) nn=nn+1
       if (chi.ge.150.0.and.chi.lt.155.) pp=pp+1
       if (chi.ge.155.0.and.chi.lt.160.) rr=rr+1
       if (chi.ge.160.0.and.chi.lt.165.) ss=ss+1
       if (chi.ge.165.0.and.chi.lt.170.) tt=tt+1
       if (chi.ge.170.0.and.chi.lt.175.) vv=vv+1
       if (chi.ge.175.0.and.chi.lt.180.) ww=ww+1
 1     continue
       write(2,*) a,b,c,d,e,f,g,h,k,l,m,n,p,r,s,t,v,w
       write(2,*) aa,bb,cc,dd,ee,ff,gg,hh,kk,ll,mm,nn,pp,rr,ss,tt,vv,ww
       stop
       end
```

```
c      Program ANGLE1.FOR tests for a preferred direction of polarization
c in the Crab Nebula (Woltjer data).
      dimension n(1101),X(1101),I(1101),Q(1101),U(1101)
      dimension Y(0:44),sum(0:44)
      pi=4.*atan(1.)
      open(unit=1,status='old',name='crabiqu.dat')
      open(unit=2,status='new',name='angle1.dat')
      do 1 j=1,1101
      read(1,*) n(j),I(j),Q(j),U(j)
1     continue
      do 2 m=0,43
      sum(m)=0.0
      Y(m)=m*5.
      do 3 j=1,1101
      QQ=Q(j)
      UU=U(j)
c      Test for the quadrant of the angle 2X.
       if(QQ.eq.0.0.and.UU.eq.0.0) then
        chi=0.0
       goto 99
       else
       if(QQ.gt.0.0.and.UU.ge.0.0) then
        chi=(atan(UU/QQ))/2.
       goto 99
       else
       if(QQ.lt.0.0.and.UU.ge.0.0) then
        chi=(pi+atan(UU/QQ))/2.
       goto 99
       else
       if(QQ.gt.0.0.and.UU.le.0.0) then
        chi=pi+(atan(UU/QQ)/2.)
       goto 99
       else
       if(QQ.lt.0.0.and.UU.le.0.0) then
        chi=(pi+atan(UU/QQ))/2.
       goto 99
       else
       if(QQ.eq.0.0.and.UU.gt.0.0) then
        chi=pi/4.
       goto 99
       else
       if(QQ.eq.0.0.and.UU.lt.0.0) then
        chi=(3./4.)*pi
       goto 99
       end if
       end if
       end if
       end if
       end if
       end if
       end if

 99    X(j)=(chi*180.)/pi
       diff=X(j)-Y(m)
       if (diff.lt.0.) diff=-diff
       if (diff.gt.90.) diff=180.-diff
       sum(m)=sum(m)+diff
 3     continue
       write(2,*) Y(m),sum(m)
 2     continue
       stop
       end
```

```
c      Program ANGLE1S.FOR tests for a preferred direction of polarization
c in the Crab Nebula (Woltjer data). Squared sum method.
      dimension n(1101),X(1101),I(1101),Q(1101),U(1101)
      dimension Y(0:180),sum(0:180)
      pi=4.*atan(1.)
      open(unit=1,status='old',name='crabiqu.dat')
      open(unit=2,status='new',name='angle1.dat')
      do 1 j=1,1101
      read(1,*) n(j),I(j),Q(j),U(j)
1     continue
      do 2 m=0,180
      sum(m)=0.0
      Y(m)=m*1.
      do 3 j=1,1101
      QQ=Q(j)
      UU=U(j)
c      Test for the quadrant of the angle 2X.
       if(QQ.eq.0.0.and.UU.eq.0.0) then
        chi=0.0
       goto 99
       else
       if(QQ.gt.0.0.and.UU.ge.0.0) then
        chi=(atan(UU/QQ))/2.
       goto 99
       else
       if(QQ.lt.0.0.and.UU.ge.0.0) then
        chi=(pi+atan(UU/QQ))/2.
       goto 99
       else
       if(QQ.gt.0.0.and.UU.le.0.0) then
        chi=pi+(atan(UU/QQ)/2.)
       goto 99
       else
       if(QQ.lt.0.0.and.UU.le.0.0) then
        chi=(pi+atan(UU/QQ))/2.
       goto 99
       else
       if(QQ.eq.0.0.and.UU.gt.0.0) then
        chi=pi/4.
       goto 99
       else
       if(QQ.eq.0.0.and.UU.lt.0.0) then
        chi=(3./4.)*pi
       goto 99
       end if
       end if
       end if
       end if
       end if
       end if
       end if

99     X(j)=(chi*180.)/pi
       diff=X(j)-Y(m)
       if (diff.lt.0.) diff=-diff
       if (diff.gt.90.) diff=180.-diff
       sum(m)=sum(m)+(diff**2)
3      continue
       write(2,*) Y(m),sum(m)
2      continue
       stop
       end
```

```
c      Program ANGLE2.FOR tests for a preferred direction of polarization
c in the Crab Nebula (Mclean data).
       dimension n(1683),X(1683),I(1683),Q(1683),U(1683)
       dimension Y(0:180),sum(0:180)
       pi=4.*atan(1.)
       open(unit=1,status='old',name='lowres.dat')
       open(unit=2,status='new',name='angle2.dat')
       do 1 j=1,1683
       read(1,*) n(j),I(j),Q(j),U(j)
 1     continue
       do 2 m=0,180
       sum(m)=0.0
       Y(m)=m*1.
       do 3 j=1,1683
       if (I(j).le.0) goto 3
       QQ=Q(j)
       UU=U(j)
c       Test for the quadrant of the angle 2X.
        if(QQ.eq.0.0.and.UU.eq.0.0) then
         chi=0.0
        goto 99
        else
        if(QQ.gt.0.0.and.UU.ge.0.0) then
         chi=(atan(UU/QQ))/2.
        goto 99
        else
        if(QQ.lt.0.0.and.UU.ge.0.0) then
         chi=(pi+atan(UU/QQ))/2.
        goto 99
        else
        if(QQ.gt.0.0.and.UU.le.0.0) then
         chi=pi+(atan(UU/QQ)/2.)
        goto 99
        else
        if(QQ.lt.0.0.and.UU.le.0.0) then
         chi=(pi+atan(UU/QQ))/2.
        goto 99
        else
        if(QQ.eq.0.0.and.UU.gt.0.0) then
         chi=pi/4.
        goto 99
        else
        if(QQ.eq.0.0.and.UU.lt.0.0) then
         chi=(3./4.)*pi
        goto 99
        end if
        end if
        end if
        end if
        end if
        end if
        end if

 99     X(j)=chi*180./pi
        diff=X(j)-Y(m)
        if (diff.lt.0.) diff=-diff
        if (diff.gt.90.) diff=180.-diff
        sum(m)=sum(m)+diff
 3      continue
        write(2,*) Y(m),sum(m)
 2      continue
        stop
        end
```

```
c      Program ANGLE2S.FOR tests for a preferred direction of polarization
c in the Crab Nebula (Mclean data). Squared sum method.
      dimension n(1683),X(1683),I(1683),Q(1683),U(1683)
      dimension Y(0:44),sum(0:44)
      pi=4.*atan(1.)
      open(unit=1,status='old',name='lowres.dat')
      open(unit=2,status='new',name='angle2.dat')
      do 1 j=1,1683
      read(1,*) n(j),I(j),Q(j),U(j)
1     continue
      do 2 m=0,43
      sum(m)=0.0
      Y(m)=m*5.
      do 3 j=1,1683
      if (I(j).le.0) goto 3
      QQ=Q(j)
      UU=U(j)
c      Test for the quadrant of the angle 2X.
       if(QQ.eq.0.0.and.UU.eq.0.0) then
        chi=0.0
       goto 99
       else
       if(QQ.gt.0.0.and.UU.ge.0.0) then
        chi=(atan(UU/QQ))/2.
       goto 99
       else
       if(QQ.lt.0.0.and.UU.ge.0.0) then
        chi=(pi+atan(UU/QQ))/2.
       goto 99
       else
       if(QQ.gt.0.0.and.UU.le.0.0) then
        chi=pi+(atan(UU/QQ)/2.)
       goto 99
       else
       if(QQ.lt.0.0.and.UU.le.0.0) then
        chi=(pi+atan(UU/QQ))/2.
       goto 99
       else
       if(QQ.eq.0.0.and.UU.gt.0.0) then
        chi=pi/4.
       goto 99
       else
       if(QQ.eq.0.0.and.UU.lt.0.0) then
        chi=(3./4.)*pi
       goto 99
       end if
       end if
       end if
       end if
       end if
       end if
       end if

99     X(j)=chi*180./pi
       diff=X(j)-Y(m)
       if (diff.lt.0.) diff=-diff
       if (diff.gt.90.) diff=180.-diff
       sum(m)=sum(m)+(diff**2)
3      continue
       write(2,*) Y(m),sum(m)
2      continue
       stop
       end
```

```
c Program COTRAN converts cartesian data set to radial coords centred on
c the pulsar.(Woltjer)

      open(unit=1,status='old',name='fullcrab.dat')
      open(unit=2,status='new',name='pulcent.dat')
      pi=4.*atan(1.)
      do 1 j=1,37
      y=22.-j
      do 2 k=1,51
      x=k-30.
      read(1,*) n,I,Q,U
      if (x.eq.0.0.and.y.eq.0.0) then
      theta=0.0
      goto 11
      else
      if (x.gt.0.0.and.y.ge.0.0) then
      theta=atan(y/x)
      goto 11
      else
      if (x.lt.0.0.and.y.ge.0.0) then
      theta=pi+atan(y/x)
      goto 11
      else
      if (x.lt.0.0.and.y.le.0.0) then
      theta=pi+atan(y/x)
      goto 11
      else
      if (x.gt.0.0.and.y.le.0.0) then
      theta=(2.*pi)+atan(y/x)
      goto 11
      else
      if (x.eq.0.0.and.y.gt.0.0) then
      theta=pi/2.
      goto 11
      else
      if (x.eq.0.0.and.y.lt.0.0) then
      theta=3.*pi/2.
      goto 11
      end if
      end if
      end if
      end if
      end if
      end if
      end if
 11   r=((x**2)+(y**2))**0.5
      theta=theta*180./pi
      write(2,*) n,r,theta,I,Q,U
      theta=0.0
 2    continue
 1    continue
      stop
      end
```

```
c Program COTRAN1 converts cartesian data set to radial coords centred on

c the pulsar. McLean's data

      open(unit=1,status='old',name='fullres.dat')
      open(unit=2,status='new',name='pulcent1.dat')
      pi=4.*atan(1.)
      do 1 j=1,37
      y=j-15.
      do 2 k=1,51
      x=k-30.
      read(1,*) n,I,Q,U
      if (x.eq.0.0.and.y.eq.0.0) then
      theta=0.0
      goto 11
      else
      if (x.gt.0.0.and.y.ge.0.0) then
      theta=atan(y/x)
      goto 11
      else
      if (x.lt.0.0.and.y.ge.0.0) then
      theta=pi+atan(y/x)
      goto 11
      else
      if (x.lt.0.0.and.y.le.0.0) then
      theta=pi+atan(y/x)
      goto 11
      else
      if (x.gt.0.0.and.y.le.0.0) then
      theta=(2.*pi)+atan(y/x)
      goto 11
      else
      if (x.eq.0.0.and.y.gt.0.0) then
      theta=pi/2.
      goto 11
      else
      if (x.eq.0.0.and.y.lt.0.0) then
      theta=3.*pi/2.
      goto 11
      end if
      end if
      end if
      end if
      end if
      end if
      end if
11    r=((x**2)+(y**2))**0.5
      theta=theta*180./pi
      write(2,*) n,r,theta,I,Q,U
      theta=0.0
2     continue
1     continue
      stop
      end
```

```
c  program SECTOR.FOR calculates preferred angle of polarization in a given
c sector or annulus, using Woltjer's data.

      real irad
      dimension n(1887),r(1887),theta(1887),I(1887),Q(1887),U(1887)
      dimension ang(0:180),sum(0:180)
      pi=4.*atan(1.)
      open(unit=1,status='old',name='pulcent.dat')
      open(unit=2,status='new',name='sector.dat')
      print*, 'Enter inner radius'
      print*, ' '
      read(6,*) irad
      print*, 'Enter outer radius (max=35.0)'
      print*, ' '
      read(6,*) orad
      print*,'Enter the limiting angles of the sector required'
      print*,' '
      read(6,*) alpha1,alpha2
      do 1 k=1,1887
      read(1,*) n(k),r(k),theta(k),I(k),Q(k),U(k)
1     continue
      write(2,*) irad,orad,alpha1,alpha2
      do 2 m=0,180
      ang(m)=m*1.
      sum(m)=0.0
      do 3 k=1,1887
      if (r(k).lt.irad) goto 3
      if (r(k).gt.orad) goto 3
      if (theta(k).lt.alpha1) goto 3
      if (theta(k).gt.alpha2) goto 3
      if (I(k).le.0) goto 3
      x=Q(k)
      y=U(k)
      if (x.eq.0.0.and.y.eq.0.0) then
      chi=0.0
      goto 99
      else
      if (x.eq.0.0.and.y.gt.0.0) then
      chi=pi/4.
      goto 99
      else
      if (x.eq.0.and.y.lt.0.0) then
      chi=3.*pi/4.
      goto 99
      else
      if (x.lt.0.0.and.y.ge.0.0) then
      chi=(pi+atan(y/x))/2.
      goto 99
      else
      if (x.gt.0.0.and.y.ge.0.0) then
      chi=(atan(y/x))/2.
      goto 99
      else
      if(x.lt.0.0.and.y.le.0.0) then
      chi=(pi+atan(y/x))/2.
      goto 99
      else
      if (x.gt.0.0.and.y.le.0.0) then
      chi=((2.0*pi)+atan(y/x))/2.
      goto 99
      end if
      end if
      end if
      end if
      end if
      end if
      end if
99    chi=(chi*180.0)/pi
      diff=chi-ang(m)
      if (diff.lt.0.0) diff=-diff
      if (diff.gt.90.) diff=180.-diff
      sum(m)=sum(m)+(diff**2)
3     continue
      average=average+sum(m)
      write(2,*) ang(m),sum(m)
2     continue
      average=average/181.
      write(2,*) average
      stop
      end
```

```
c  program SECTOR1.FOR calculates preferred angle of polarization in a given
c sector or annulus.(McLean data)
      real irad
      dimension n(1887),r(1887),theta(1887),I(1887),Q(1887),U(1887)
      dimension ang(0:180),sum(0:180)
      pi=4.*atan(1.)
      open(unit=1,status='old',name='pulcent1.dat')
      open(unit=2,status='new',name='sector1.dat')
      print*, 'Enter inner radius'
      print*, ' '
      read(6,*) irad
      print*, 'Enter outer radius (max=30.0)'
      print*, ' '
      read(6,*) orad
      print*,'Enter the limiting anglesof the sector required'
      print*,' '
      read(6,*) alpha1,alpha2
      do 1 k=1,1887
      read(1,*) n(k),r(k),theta(k),I(k),Q(k),U(k)
1     continue
      write(2,*) irad,orad,alpha1,alpha2
      do 2 m=0,180
      ang(m)=m*1.
      sum(m)=0.0
      do 3 k=1,1887
      if (r(k).lt.irad) goto 3
      if (r(k).gt.orad) goto 3
      if (theta(k).lt.alpha1) goto 3
      if (theta(k).gt.alpha2) goto 3
      if (I(k).le.0) goto 3
      x=Q(k)
      y=U(k)
      if (x.eq.0.0.and.y.eq.0.0) then
      chi=0.0
      goto 99
      else
      if (x.eq.0.0.and.y.gt.0.0) then
      chi=pi/4.
      goto 99
      else
      if (x.eq.0.and.y.lt.0.0) then
      chi=3.*pi/4.
      goto 99
      else
      if (x.lt.0.0.and.y.ge.0.0) then
      chi=(pi+atan(y/x))/2.
      goto 99
      else
      if (x.gt.0.0.and.y.ge.0.0) then
      chi=(atan(y/x))/2.
      goto 99
      else
      if(x.lt.0.0.and.y.le.0.0) then
      chi=(pi+atan(y/x))/2.
      goto 99
      else
      if (x.gt.0.0.and.y.le.0.0) then
      chi=((2.0*pi)+atan(y/x))/2.
      goto 99
      end if
      end if
      end if
      end if
      end if
      end if
      end if
99    chi=(chi*180.0)/pi
      diff=chi-ang(m)
      if (diff.lt.0.) diff=-diff
      if (diff.gt.90.) diff=180.-diff
      sum(m)=sum(m)+diff
3     continue
      average=average+sum(m)
      write(2,*) ang(m),sum(m)
2     continue
      average=average/181.
      write(2,*) average
      stop
      end
```

```
c Program NEWCEN.FOR  tests for the statistical likelihood of a nominated
c centre (Woltjer).

      dimension n(1887),I(1887),Q(1887),U(1887),IU(1887),IQ(1887)
      integer aen1,aen2,xc,yc
      open(unit=1,status='old',name='fullcrab.dat')
      print*,'Give the coordinates of the centre to be tested.'
      print*,'16 < xc < 35 and 10 < yc < 27'
      read(5,*) xc,yc
      num=9.60498e+5
      do m=1,1887
      read(1,*) n(m),I(m),Q(m),U(m)
      end do
      sum=0.
      do j=27-yc,47-yc
      do k=xc-16,xc+16
      aen1=(51*(j-1))+k
      aen2=(51*((2*(37-yc))-j-1))+((2*xc)-k)
      IQ(aen1)=I(aen1)*Q(aen1)
      IQ(aen2)=I(aen2)*Q(aen2)
      IQdiff=(IQ(aen1)-IQ(aen2))**2
      IU(aen1)=I(aen1)*U(aen1)
      IU(aen2)=I(aen2)*U(aen2)
      IUdiff=(IU(aen1)-IU(aen2))**2
      sum=sum+IQdiff+IUdiff
      end do
      end do
      sum=sum/num
      write(6,*) sum
99    format(a20)
      stop
      end


c Program NEWICEN.FOR  tests for the statistical likelihood of a nominated
c centre (Woltjer).

      dimension n(1887),I(1887)
      integer aen1,aen2,xc,yc
      open(unit=1,status='old',name='fullcrab.dat')
      open(unit=4,status='new',name='IcenW.dat')
      num=4.80249e+5
      do m=1,1887
      read(1,*) n(m),I(m)
      end do
      do l=1,11
      xc=23+l
      do ll=1,11
      yc=9+ll
      sum=0.
      do j=27-yc,47-yc
      do k=xc-16,xc+16
      aen1=(51*(j-1))+k
      aen2=(51*((2*(37-yc))-j-1))+((2*xc)-k)
      Idiff=(I(aen1)-I(aen2))**2
      sum=sum+Idiff
      end do
      end do
      sum=sum/num
      write(4,*) xc,yc,sum
      end do
      end do
99    format(a20)
      stop
      end
```

```
c Program NEWCEN1.FOR tests the statistical likelihood of a choosen centre
c of the nebula (McLean).

      dimension n(1887),I(1887),Q(1887),U(1887),IU(1887),IQ(1887)
      integer aen1,aen2,xc,yc
      open(unit=1,status='old',name='fullres.dat')
      print*,'Give the coordinates of the centre to be tested.'
      print*,'16 < xc < 35 and 10 < yc < 27'
      read(5,*) xc,yc
      do m=1,1887
      read(1,*) n(m),I(m),Q(m),U(m)
      end do
      num=9.60498e5
      sum=0.
      do j=yc-10,yc+10
      do k=xc-16,xc+16
      aen1=(51*(j-1))+k
      aen2=(51*((2*yc)-j-1))+((2*xc)-k)
      IQ(aen1)=I(aen1)*Q(aen1)/100.
      IQ(aen2)=I(aen2)*Q(aen2)/100.
      IQdiff=(IQ(aen1)-IQ(aen2))**2
      IU(aen1)=I(aen1)*U(aen1)/100.
      IU(aen2)=I(aen2)*U(aen2)/100.
      IUdiff=(IU(aen1)-IU(aen2))**2
      sum=sum+IQdiff+IUdiff
      end do
      end do
      sum=sum/num
      write(6,*) sum
      stop
      end


c Program NEWICEN1.FOR tests the statistical likelihood of a choosen centre
c of the nebula (McLean).

      dimension n(1887),I(1887)
      integer aen1,aen2,xc,yc
      open(unit=1,status='old',name='fullres.dat')
      open(unit=4,status='new',name='IcenM.dat')
      do m=1,1887
      read(1,*) n(m),I(m)
      end do
      num=4.80249e5
      do l=1,11
      xc=23+l
      do ll=1,11
      yc=9+ll
      sum=0.
      do j=yc-10,yc+10
      do k=xc-16,xc+16
      aen1=(51*(j-1))+k
      aen2=(51*((2*yc)-j-1))+((2*xc)-k)
      Idiff=(I(aen1)-I(aen2))**2
      sum=sum+Idiff
      end do
      end do
      sum=sum/num
      write(4,*) xc,yc,sum
      end do
      end do
      stop
      end
```

Appendix B

```
c       PROGRAM MODELPLOT.FOR
        dimension x(2),y(2)
        character*20 title
        pi=4.*atan(1.)
        print*, 'Input filename?'
        print*,' '
        read(5,99) title
        open(unit=2,status='old',name=title)
        call gopks(6,-1)
        call gopwk(2,1,4014)
        call gacwk(2)
        call gswn(1,0.0,30.0,0.0,30.0)
        call gselnt(1)
        do 1 j=1,676
        read(2,*) xc,yc,P,chi
        chi=(pi/2.)+(chi*pi/180.)
        a=P*cos(chi)
        b=P*sin(chi)
        x(1)=xc-a/2.
        y(1)=yc-b/2.
        x(2)=xc+a/2.
        y(2)=yc+b/2.
        call gpl(2,x,y)
1       continue
        call gdawk(2)
        call gclwk(2)
        call gclks
99      format(a20)
        stop
        end
```

```
c      PROGRAM MODEL1.FOR
       implicit double precision (A-I),(O-Z)
       real S14AAF,x1,x2,x3,x4,x,y
       integer LW,LIW,IW,IFAIL
       dimension W(1000),IW(300)
       external B
       common /xy/ x,y
       open(unit=2,status='new',name='model1.dat')
       pi=4.*atan(1.)

       ifail=0
       epsabs=0.0e0
       epsrel=1.0e-4
       a1=1.0d-10
       a2=100.d0
       LW=1000
       LIW=300

c First evaluate the modified Bessel functions F and G in terms of gamma fns.
       x1=2.163
       x2=0.496
       x3=1.663
       x4=0.9966
       gamma1=S14AAF(x1,ifail)
       gamma2=S14AAF(x2,ifail)
       gamma3=S14AAF(x3,ifail)
       gamma4=S14AAF(x4,ifail)
       F=(2/3.32)*(2**0.66)*gamma1*gamma2
       G=(2/3.32)*(2**0.66)*gamma3*gamma4

c      n0=function of x and y, constant in this prog so cancels and does not
c become part of the integral function B(y).

       do 1 k=0,25
       do 2 j=0,25
       x=k+1.0
       y=j+1.0
c cannot calculate values for the origin because of divide by zero!

       call D01AJF(B,a1,a2,epsabs,epsrel,result,abserr,W,LW,IW,LIW,ifail)
       I=result
       print*,I
       Q=result*((x**2-y**2)/(y**2+x**2))
       U=result*((2*x*y)/(y**2+x**2))
       degpol=(G/F)*(U**2+Q**2)**0.5/I
c leave G and F out of I,U,Q because they only appear in degpol as shown

       chi=atan(y/x)
c Convert chi into degrees
       chi=chi*180.0/pi
       write(2,*) x,y,degpol,chi

    2  continue
    1  continue
       stop
       end


       double precision function B(z)
       common /xy/ x,y
       B=(((3.d0*(((z**2.d0)*((x**2.d0)+(y**2.d0)))**0.5d0))/((((x**2.d0)
      $ +(y**2.d0)+(z**2.d0))**0.5)**5.d0)))**1.66d0
       return
       end
```

```
c     PROGRAM MODEL.FOR calculates the polarization parameters of synchrotron
c radiation for a side on view of a magnetic dipole field.
      implicit double precision (A-I),(O-Z)
      real S14AAF,x1,x2,x3,x4,y,z,x
      integer LW,LIW,IW,IFAIL
      dimension W(1000),IW(300)
c In order to perform the integration over the line of sight the values of the
c perpendicular magnetic field component, IQ and IU must be calculated by
c subroutines of the main program for each grid point and returned to the
c apropriate NAG routine.
      external B,BQ,BU
      common /yz/ y,z
      open(unit=2,status='new',name='model.dat')
      pi=4.d0*datan(1.d0)

c Set up limits and accuracy requirements for the integration routines.
      ifail=0
      epsabs=0.0e0
      epsrel=1.0e-04
      a1=1.d-10
      a2=1000.d0
      LW=1000
      LIW=300

c Evaluate the modified Bessel functions F and G in terms of gamma fns.
      x1=2.163
      x2=0.496
      x3=1.663
      x4=0.9966
      gamma1=S14AAF(x1,ifail)
      gamma2=S14AAF(x2,ifail)
      gamma3=S14AAF(x3,ifail)
      gamma4=S14AAF(x4,ifail)
      F=(2/3.32)*(2**0.66)*gamma1*gamma2
      G=(2/3.32)*(2**0.66)*gamma3*gamma4

      do 1 k=0,25
      do 2 j=0,25
      y=k+1.0
      z=j+1.0

c cannot calculate values for the origin because of divide by zero!

      call D01AJF(B,a1,a2,epsabs,epsrel,I,abserr,W,LW,IW,LIW,ifail)
      call D01AJF(BQ,a1,a2,epsabs,epsrel,Q,abserr,W,LW,IW,LIW,ifail)
      call D01AJF(BU,a1,a2,epsabs,epsrel,U,abserr,W,LW,IW,LIW,ifail)
      degpol=(G/F)*((U**2+Q**2)**0.5/I)
c leave G and F out of I,U,Q because they only appear in degpol as shown

c     Test for the quadrant of the angle 2X.
       if(Q.eq.0.d0.and.U.eq.0.d0) then
        chi=0.0
       else
       if(Q.gt.0.d0.and.U.ge.0.d0) then
        chi=datan(U/Q)/2.d0
       else
       if(Q.lt.0.d0.and.U.ge.0.d0) then
        chi=((pi+datan(U/Q)))/2.d0
       else
       if(Q.gt.0.d0.and.U.le.0.d0) then
        chi=((datan(U/Q)/2.d0))+pi
       else
       if(Q.lt.0.d0.and.U.le.0.d0) then
        chi=((pi+datan(U/Q)))/2.d0
       else
       if(Q.eq.0.d0.and.U.gt.0.d0) then
        chi=pi/4.d0
       else
       if(Q.eq.0.d0.and.U.lt.0.d0) then
        chi=0.75d0*pi
       end if
       end if
       end if
       end if
       end if
       end if
       end if

c Convert chi into degrees
      chi=chi*180.d0/pi
      write(2,*) y,z,degpol,chi

    2 continue
    1 continue
      stop
      end
```

```
function B(x)
common /yz/ y,z
P1=(5.d0*(y**2))+(4.d0*(z**2))-(4.d0*(x**2))
P2=((x**2)+(y**2))**2
B=(((((z**2)*P1)+P2)**0.5)/((((x**2)+(y**2)+(z**2))**0.5)**5))**1.66d0

return
end

function BQ(x)
common /yz/ y,z
P1=((5.d0*(y**2))+(4.d0*(z**2))-(4.d0*(x**2)))
P2=((x**2)+(y**2))**2
P3=(13.d0*(y**2))+(4.d0*(x**2))-(4.d0*(z**2))
B=(((((z**2)*P1)+P2)**0.5)/((((x**2)+(y**2)+(z**2))**0.5)**5))**1.66d0
BQ=B*(((P3*(z**2))-P2)/((P1*(z**2))+P2))
return
end

function BU(x)
common /yz/ y,z
P1=((5.d0*(y**2))+(4.d0*(z**2))-(4.d0*(x**2)))
P2=((x**2)+(y**2))**2
P4=(2.d0*(z**2))-(x**2)-(y**2)
B=(((((z**2)*P1)+P2)**0.5)/((((x**2)+(y**2)+(z**2))**0.5)**5))**1.66d0)
BU=B*((6.d0*z*y*P4)/((P1*(z**2))+P2))
return
end
```

```
c     PROGRAM MODEL3.FOR     model for an inclined dipole,using non-inclined
c coordinate system for the calculations i.e. convert xi,yi,zi to x,y,z.

      implicit double precision (A-I),(O-Z)
      real S14AAF,x1,x2,x3,x4
      integer LW,LIW,IW,IFAIL
      dimension W(1000),IW(300)
      external B,IQ,IU
      common /xz/ xi,zi,inc
      open(unit=1,status='old',name='inc.dat')
      open(unit=2,status='new',name='model3.dat')
      read(1,*) angle
      pi=4.d0*datan(1.d0)
      inc=(angle*pi)/180.d0

      ifail=0
      epsabs=0.0e0
      epsrel=1.0e-04
      a1=1.d-10
      a2=1000.d0
      LW=1000
      LIW=300

c First evaluate the modified Bessel functions F and G in terms of gamma fns.
      x1=2.163
      x2=0.496
      x3=1.663
      x4=0.9966
      gamma1=S14AAF(x1,ifail)
      gamma2=S14AAF(x2,ifail)
      gamma3=S14AAF(x3,ifail)
      gamma4=S14AAF(x4,ifail)
      F=(2/3.32)*(2**0.66)*gamma1*gamma2
      G=(2/3.32)*(2**0.66)*gamma3*gamma4

      do 1 k=0,25
      do 2 j=0,25
      xi=k+1.d0
      zi=j+1.d0

c cannot calculate values for the origin because of divide by zero!

      call D01AJF(B,a1,a2,epsabs,epsrel,I,abserr,W,LW,IW,LIW,ifail)
      call D01AJF(IQ,a1,a2,epsabs,epsrel,Q,abserr,W,LW,IW,LIW,ifail)
      call D01AJF(IU,a1,a2,epsabs,epsrel,U,abserr,W,LW,IW,LIW,ifail)
      degpol=(G/F)*((U**2+Q**2)**0.5/I)
c leave G and F out of I,U,Q because they only appear in degpol as shown

c      Test for the quadrant of the angle 2X.
       if(Q.eq.0.d0.and.U.eq.0.d0) then
        chi=0.0
       else
       if(Q.gt.0.d0.and.U.ge.0.d0) then
        chi=datan(U/Q)/2.d0
       else
       if(Q.lt.0.d0.and.U.ge.0.d0) then
        chi=((pi+datan(U/Q)))/2.d0
       else
       if(Q.gt.0.d0.and.U.le.0.d0) then
        chi=((datan(U/Q)/2.d0))+pi
       else
       if(Q.lt.0.d0.and.U.le.0.d0) then
        chi=((pi+datan(U/Q)))/2.d0
       else
       if(Q.eq.0.d0.and.U.gt.0.d0) then
        chi=pi/4.d0
       else
       if(Q.eq.0.d0.and.U.lt.0.d0) then
        chi=0.75d0*pi
       end if
       end if
       end if
       end if
       end if
       end if
       end if

c Convert chi into degrees
      chi=chi*180.d0/pi
      write(2,*) xi,zi,degpol,chi

   2  continue
   1  continue
      stop
      end


      function B(yi)
      implicit double precision (A-I),(O-Z)
      common /xz/ xi,zi,inc
      x=(zi*dcos(inc))-(yi*dsin(inc))
      z=(zi*dsin(inc))+(yi*dcos(inc))
      y=xi
      A=2.d0*(z**2)-(x**2)-(y**2)
      E=3.d0*z*y
      C=3.d0*x*z
      D=(A*dsin(inc))+(C*dcos(inc))
      R=((x**2)+(y**2)+(z**2))**5
      B=((((E**2)+(D**2))**0.5)/R)**1.66d0
      return
      end

      function IQ(yi)
      implicit double precision (A-I),(O-Z
      common /xz/ xi,zi,inc
      x=(zi*dcos(inc))-(yi*dsin(inc))
      z=(zi*dsin(inc))+(yi*dcos(inc))
      y=xi
      A=2.d0*(z**2)-(x**2)-(y**2)
      E=3.d0*z*y
      C=3.d0*x*z
      D=(A*dsin(inc))+(C*dcos(inc))
      R=((x**2)+(y**2)+(z**2))**5
      B=((((E**2)+(D**2))**0.5)/R)**1.66d
      IQ=B*((E**2)-(D**2))/((E**2)+(D**2),
      return
      end

      function IU(yi)
      implicit double precision (A-I),(O-Z)
      common /xz/ xi,zi,inc
      x=(zi*dcos(inc))-(yi*dsin(inc))
      z=(zi*dsin(inc))+(yi*dcos(inc))
      y=xi
      A=2.d0*(z**2)-(x**2)-(y**2)
      E=3.d0*z*y
      C=3.d0*x*z
      D=(A*dsin(inc))+(C*dcos(inc))
      R=((x**2)+(y**2)+(z**2))**5
      B=((((E**2)+(D**2))**0.5)/R)**1.66c
      IU=B*2.d0*E*D/((E**2)+(D**2))
      return
      end
```

```
c      PROGRAM MODEL4.FOR      model for an inclined dipole.

       implicit double precision (A-I),(O-Z)
       real S14AAF,x1,x2,x3,x4
       integer LW,LIW,IW,IFAIL
       dimension W(1000),IW(300)
       external B,IQ,IU
       common /xz/ xi,yi,inc
       open(unit=1,status='old',name='inc.dat')
       open(unit=2,status='new',name='model4.dat')
       read(1,*) angle
       pi=4.d0*datan(1.d0)
       inc=(angle*pi)/180.d0

       ifail=0
       epsabs=0.0e0
       epsrel=1.0e-4
       a1=1.d-10
       a2=5000.d0
       LW=1000
       LIW=300

c First evaluate the modified Bessel functions F and G in terms of gamma fns.
       x1=2.163
       x2=0.496
       x3=1.663
       x4=0.9966
       gamma1=S14AAF(x1,ifail)
       gamma2=S14AAF(x2,ifail)
       gamma3=S14AAF(x3,ifail)
       gamma4=S14AAF(x4,ifail)
       F=(2/3.32)*(2**0.66)*gamma1*gamma2
       G=(2/3.32)*(2**0.66)*gamma3*gamma4

       do 1 k=0,25
       do 2 j=0,25
       xi=k+1.d0
       yi=j+1.d0

c cannot calculate values for the origin because of divide by zero!

       call D01AJF(B,a1,a2,epsabs,epsrel,I,abserr,W,LW,IW,LIW,ifail)
       call D01AJF(IQ,a1,a2,epsabs,epsrel,Q,abserr,W,LW,IW,LIW,ifail)
       call D01AJF(IU,a1,a2,epsabs,epsrel,U,abserr,W,LW,IW,LIW,ifail)
       degpol=(G/F)*((U**2+Q**2)**0.5/I)
c leave G and F out of I,U,Q because they only appear in degpol as shown

c      Test for the quadrant of the angle 2X.
        if(Q.eq.0.d0.and.U.eq.0.d0) then
         chi=0.0
        else
        if(Q.gt.0.d0.and.U.ge.0.d0) then
         chi=datan(U/Q)/2.d0
        else
        if(Q.lt.0.d0.and.U.ge.0.d0) then
         chi=((pi+datan(U/Q)))/2.d0
        else
        if(Q.gt.0.d0.and.U.le.0.d0) then
         chi=((datan(U/Q)/2.d0))+pi
        else
        if(Q.lt.0.d0.and.U.le.0.d0) then
         chi=((pi+datan(U/Q)))/2.d0
        else
        if(Q.eq.0.d0.and.U.gt.0.d0) then
         chi=pi/4.d0
        else
        if(Q.eq.0.d0.and.U.lt.0.d0) then
         chi=0.75d0*pi
        end if
        end if
        end if
        end if
        end if
        end if
        end if

c Convert chi into degrees
       chi=chi*180.d0/pi
       write(2,*) xi,yi,degpol,chi

    2  continue
    1  continue
       stop
       end


       function B(zi)
       implicit double precision (A-I),(O-Z)
       common /xz/ xi,yi,inc
       A=(2.d0*(yi**2))-(xi**2)-(zi**2)
       E=3.d0*zi*yi
       C=3.d0*xi*yi
       D=3.d0*xi*zi
       AA=(A*dsin(inc))+(E*dcos(inc))
       BB=(C*dsin(inc))+(D*dcos(inc))
       R=((xi**2)+(yi**2)+(zi**2))**4.15d0
       B=(((AA**2)+(BB**2))**0.83d0)/R
       return
       end

       function IU(zi)
       implicit double precision (A-I),(O-Z
       common /xz/ xi,yi,inc
       A=(2.d0*(yi**2))-(xi**2)-(zi**2)
       E=3.d0*zi*yi
       C=3.d0*xi*yi
       D=3.d0*xi*zi
       AA=(A*dsin(inc))+(E*dcos(inc))
       BB=(C*dsin(inc))+(D*dcos(inc))

       R=((xi**2)+(yi**2)+(zi**2))**4.15d0
       B=(((AA**2)+(BB**2))**0.83d0)/R
       IU=B*2.d0*AA*BB/((BB**2)+(AA**2))
       return
       end

       function IQ(zi)
       implicit double precision (A-I),(O-Z)
       common /xz/ xi,yi,inc
       A=(2.d0*(yi**2))-(xi**2)-(zi**2)
       E=3.d0*zi*yi
       C=3.d0*xi*yi
       D=3.d0*xi*zi
       AA=(A*dsin(inc))+(E*dcos(inc))
       BB=(C*dsin(inc))+(D*dcos(inc))
       R=((xi**2)+(yi**2)+(zi**2))**4.15d0
       B=(((AA**2)+(BB**2))**0.83d0)/R
       IQ=B*((BB**2)-(AA**2))/((BB**2)+(AA*
       return
       end
```

```
c     PROGRAM MODEL5.FOR     model for an inclined dipole between 0 and

c  90 degrees in 10 degree intervals.

      implicit double precision (A-I),(O-Z)
      real S14AAF,x1,x2,x3,x4
      integer LW,LIW,IW,IFAIL
      dimension W(1000),IW(300)
      external B,IQ,IU
      common /xz/ xi,yi,inc

c First evaluate the modified Bessel functions F and G in terms of gamma fns.
      x1=2.163
      x2=0.496
      x3=1.663
      x4=0.9966
      gamma1=S14AAF(x1,ifail)
      gamma2=S14AAF(x2,ifail)
      gamma3=S14AAF(x3,ifail)
      gamma4=S14AAF(x4,ifail)
      F=(2/3.32)*(2**0.66)*gamma1*gamma2
      G=(2/3.32)*(2**0.66)*gamma3*gamma4

c     Work through angles from 0 to 90 degrees
      pi=4.d0*datan(1.d0)
      do 9 mm=0,9
      open(unit=2,status='new',name='model5.dat')
      if (mm.eq.0) then
      angle=0.001
      else
      angle=mm*10.d0
      end if
      inc=(angle*pi)/180.d0

      ifail=0
      epsabs=0.0e0
      epsrel=1.0e-4
      a1=1.d-10
      a2=5000.d0
      LW=1000
      LIW=300

      do 1 k=0,25
      do 2 j=0,25
      xi=k+1.d0
      yi=j+1.d0

c cannot calculate values for the origin because of divide by zero!

      call D01AJF(B,a1,a2,epsabs,epsrel,I,abserr,W,LW,IW,LIW,ifail)
      call D01AJF(IQ,a1,a2,epsabs,epsrel,Q,abserr,W,LW,IW,LIW,ifail)
      call D01AJF(IU,a1,a2,epsabs,epsrel,U,abserr,W,LW,IW,LIW,ifail)
      degpol=(G/F)*((U**2+Q**2)**0.5/I)
c leave G and F out of I,U,Q because they only appear in degpol as shown

c     Test for the quadrant of the angle 2X.
       if(Q.eq.0.d0.and.U.eq.0.d0) then
        chi=0.0
       else
       if(Q.gt.0.d0.and.U.ge.0.d0) then
        chi=datan(U/Q)/2.d0
       else
       if(Q.lt.0.d0.and.U.ge.0.d0) then
        chi=((pi+datan(U/Q)))/2.d0
       else
       if(Q.gt.0.d0.and.U.le.0.d0) then
        chi=((datan(U/Q)/2.d0))+pi
       else
       if(Q.lt.0.d0.and.U.le.0.d0) then
        chi=((pi+datan(U/Q)))/2.d0
       else
       if(Q.eq.0.d0.and.U.gt.0.d0) then
        chi=pi/4.d0
       else
       if(Q.eq.0.d0.and.U.lt.0.d0) then
        chi=0.75d0*pi
       end if
       end if
       end if
       end if
       end if
       end if
       end if

c Convert chi into degrees
      chi=chi*180.d0/pi
      write(2,*) xi,yi,degpol,chi

    2 continue
    1 continue
      close(2)
    9 continue
      stop
```

```
end

function B(zi)
implicit double precision (A-I),(O-Z)
common /xz/ xi,yi,inc
A=(2.d0*(yi**2))-(xi**2)-(zi**2)
E=3.d0*zi*yi
C=3.d0*xi*yi
D=3.d0*xi*zi
AA=(A*dsin(inc))+(E*dcos(inc))
BB=(C*dsin(inc))+(D*dcos(inc))
R=((xi**2)+(yi**2)+(zi**2))**4.15d0
B=(((AA**2)+(BB**2))**0.83d0)/R
return
end

function IU(zi)
implicit double precision (A-I),(O-Z)
common /xz/ xi,yi,inc
A=(2.d0*(yi**2))-(xi**2)-(zi**2)
E=3.d0*zi*yi
C=3.d0*xi*yi
D=3.d0*xi*zi
AA=(A*dsin(inc))+(E*dcos(inc))
BB=(C*dsin(inc))+(D*dcos(inc))
R=((xi**2)+(yi**2)+(zi**2))**4.15d0
B=(((AA**2)+(BB**2))**0.83d0)/R
IU=B*2.d0*AA*BB/((BB**2)+(AA**2))
return
end

function IQ(zi)
implicit double precision (A-I),(O-Z)
common /xz/ xi,yi,inc
A=(2.d0*(yi**2))-(xi**2)-(zi**2)
E=3.d0*zi*yi
C=3.d0*xi*yi
D=3.d0*xi*zi
AA=(A*dsin(inc))+(E*dcos(inc))
BB=(C*dsin(inc))+(D*dcos(inc))
R=((xi**2)+(yi**2)+(zi**2))**4.15d0
B=(((AA**2)+(BB**2))**0.83d0)/R
IQ=B*((BB**2)-(AA**2))/((BB**2)+(AA**2))
return
end
```

```
c     PROGRAM MODEL6.FOR     model for an inclined dipole with a toriodal field
c  component of varying ratio to the r and theta field components.
      implicit double precision (A-I),(O-Z)
      real S14AAF,x1,x2,x3,x4
      integer LW,LIW,IW,IFAIL
      dimension W(1000),IW(300)
      external B,IQ,IU
      common /xz/ xi,yi,inc,rat
      pi=4.d0*datan(1.d0)

      ifail=0
      epsabs=0.0e0
      epsrel=1.0e-4
      a1=1.d-10
      a2=5000.d0
      LW=1000
      LIW=300
c First evaluate the modified Bessel functions F and G in terms of gamma fns.
      x1=2.163
      x2=0.498
      x3=1.663
      x4=0.9966
      gamma1=S14AAF(x1,ifail)
      gamma2=S14AAF(x2,ifail)
      gamma3=S14AAF(x3,ifail)
      gamma4=S14AAF(x4,ifail)
      F=(2/3.32)*(2**0.66)*gamma1*gamma2
      G=(2/3.32)*(2**0.66)*gamma3*gamma4

c     Work through angles from 0 to 90 degrees
      do 9 mm=0,9
      if(mm.eq.0) then
      angle=0.001d0
      else
      angle=mm*10.d0
      end if
      inc=(angle*pi)/180.d0
c     Work through ratios from 10 to 1000
      do hi=1,3
      rat=10**hi
      open(unit=2,status='new',name='model6.dat')

      do 1 k=0,25
      do 2 j=0,25
      xi=k+1.d0
      yi=j+1.d0

c cannot calculate values for the origin because of divide by zero!

      call D01AJF(B,a1,a2,epsabs,epsrel,I,abserr,W,LW,IW,LIW,ifail)
      call D01AJF(IQ,a1,a2,epsabs,epsrel,Q,abserr,W,LW,IW,LIW,ifail)
      call D01AJF(IU,a1,a2,epsabs,epsrel,U,abserr,W,LW,IW,LIW,ifail)
      degpol=(G/F)*((U**2+Q**2)**0.5/I)
c leave G and F out of I,U,Q because they only appear in degpol as shown

c     Test for the quadrant of the angle 2X.
       if(Q.eq.0.d0.and.U.eq.0.d0) then
        chi=0.0
       else
       if(Q.gt.0.d0.and.U.ge.0.d0) then
        chi=datan(U/Q)/2.d0
       else
       if(Q.lt.0.d0.and.U.ge.0.d0) then
        chi=((pi+datan(U/Q)))/2.d0
       else
       if(Q.gt.0.d0.and.U.le.0.d0) then
        chi=((datan(U/Q)/2.d0))+pi
       else
       if(Q.lt.0.d0.and.U.le.0.d0) then
        chi=((pi+datan(U/Q)))/2.d0
       else
       if(Q.eq.0.d0.and.U.gt.0.d0) then
        chi=pi/4.d0
       else
       if(Q.eq.0.d0.and.U.lt.0.d0) then
        chi=0.75d0*pi
       end if
       end if
       end if
       end if
       end if
       end if
       end if

c Convert chi into degrees
      chi=chi*180.d0/pi
      write(2,*) xi,yi,degpol,chi

    2 continue
```

```
1  continue
   close(2)
   end do
9  continue
   stop
   end


   function B(zi)
   implicit double precision (A-I),(O-Z)
   common /xz/ xi,yi,inc,rat
   x=xi
   y=(yi*dcos(inc))-(zi*dsin(inc))
   z=(zi*dcos(inc))+(yi*dsin(inc))
   rr=((x**2)+(y**2)+(z**2))**0.5d0
   a=3*x*z/rr
   c=(rat*y)/(((x**2)+(y**2))**0.5d0)
   d=3*z*y/rr
   e=(2.d0*(z**2)-(x**2)-(y**2))/rr
   w=((d+c)*dcos(inc))+(e*dsin(inc))
   R=((x**2)+(y**2)+(z**2))**3.32d0
   B=((((a-c)**2)+(w**2))**0.83d0)/R
   return
   end

   function IU(zi)
   implicit double precision (A-I),(O-Z)
   common /xz/ xi,yi,inc,rat
   x=xi
   y=(yi*dcos(inc))-(zi*dsin(inc))
   z=(zi*dcos(inc))+(yi*dsin(inc))
   rr=((x**2)+(y**2)+(z**2))**0.5d0
   a=3*x*z/rr
   c=(rat*y)/(((x**2)+(y**2))**0.5d0)
   d=3*z*y/rr
   e=(2.d0*(z**2)-(x**2)-(y**2))/rr
   w=((d+c)*dcos(inc))+(e*dsin(inc))
   R=((x**2)+(y**2)+(z**2))**3.32d0
   B=((((a-c)**2)+(w**2))**0.83d0)/R
   CC=((a-c)**2)+(w**2)
   DD=2*w*(a-c)
   IU=B*DD/CC
   return
   end

   function IQ(zi)
   implicit double precision (A-I),(O-Z)
   common /xz/ xi,yi,inc,rat
   x=xi
   y=(yi*dcos(inc))-(zi*dsin(inc))
   z=(zi*dcos(inc))+(yi*dsin(inc))
   rr=((x**2)+(y**2)+(z**2))**0.5d0
   a=3*x*z/rr
   c=(rat*y)/(((x**2)+(y**2))**0.5d0)
   d=3*z*y/rr
   e=(2.d0*(z**2)-(x**2)-(y**2))/rr
   w=((d+c)*dcos(inc))+(e*dsin(inc))
   R=((x**2)+(y**2)+(z**2))**3.32d0
   B=((((a-c)**2)+(w**2))**0.83d0)/R
   AA=((a-c)**2)-(w**2)
   CC=((a-c)**2)+(w**2)
   IQ=B*AA/CC
   return
   end
```

```
c     PROGRAM MODEL7.FOR      model for an inclined dipole with a toriodal field

c  component of ratio 50 to the r and theta field components.

      implicit double precision (A-I),(O-Z)
      real S14AAF,x1,x2,x3,x4
      integer LW,LIW,IW,IFAIL
      dimension W(1000),IW(300)
      external B,IQ,IU
      common /xz/ xi,yi,inc,rat
      pi=4.d0*datan(1.d0)
      rat=50.

      ifail=0
      epsabs=0.0e0
      epsrel=1.0e-4
      a1=1.d-10
      a2=5000.d0
      LW=1000
      LIW=300

c First evaluate the modified Bessel functions F and G in terms of gamma fns.
      x1=2.163
      x2=0.496
      x3=1.663
      x4=0.9966
      gamma1=S14AAF(x1,ifail)
      gamma2=S14AAF(x2,ifail)
      gamma3=S14AAF(x3,ifail)
      gamma4=S14AAF(x4,ifail)
      F=(2/3.32)*(2**0.66)*gamma1*gamma2
      G=(2/3.32)*(2**0.66)*gamma3*gamma4


c     Work through angles from 0 to 90 degrees
      do 9 mm=0,9
      if(mm.eq.0) then
      angle=0.001d0
      else
      angle=mm*10.d0
      end if
      inc=(angle*pi)/180.d0
      open(unit=2,status='new',name='model7.dat')

      do 1 k=0,25
      do 2 j=0,25
      xi=k+1.d0
      yi=j+1.d0

c cannot calculate values for the origin because of divide by zero!

      call D01AJF(B,a1,a2,epsabs,epsrel,I,abserr,W,LW,IW,LIW,ifail)
      call D01AJF(IQ,a1,a2,epsabs,epsrel,Q,abserr,W,LW,IW,LIW,ifail)
      call D01AJF(IU,a1,a2,epsabs,epsrel,U,abserr,W,LW,IW,LIW,ifail)
      degpol=(G/F)*((U**2+Q**2)**0.5/I)
c leave G and F out of I,U,Q because they only appear in degpol as shown

c     Test for the quadrant of the angle 2X.
       if(Q.eq.0.d0.and.U.eq.0.d0) then
        chi=0.0
       else
       if(Q.gt.0.d0.and.U.ge.0.d0) then
        chi=datan(U/Q)/2.d0
       else
       if(Q.lt.0.d0.and.U.ge.0.d0) then
        chi=((pi+datan(U/Q)))/2.d0
       else
       if(Q.gt.0.d0.and.U.le.0.d0) then
        chi=((datan(U/Q)/2.d0))+pi
       else
       if(Q.lt.0.d0.and.U.le.0.d0) then
        chi=((pi+datan(U/Q)))/2.d0
       else
       if(Q.eq.0.d0.and.U.gt.0.d0) then
        chi=pi/4.d0
       else
       if(Q.eq.0.d0.and.U.lt.0.d0) then
        chi=0.75d0*pi
       end if
       end if
       end if
       end if
       end if
       end if
       end if

c Convert chi into degrees
      chi=chi*180.d0/pi
      write(2,*) xi,yi,degpol,chi

    2 continue
    1 continue
```

```
9  continue
   stop
   end


   function B(zi)
   implicit double precision (A-I),(O-Z)
   common /xz/ xi,yi,inc,rat
   x=xi
   y=(yi*dcos(inc))-(zi*dsin(inc))
   z=(zi*dcos(inc))+(yi*dsin(inc))
   rr=((x**2)+(y**2)+(z**2))**0.5d0
   a=3*x*z/rr
   c=(rat*y)/(((x**2)+(y**2))**0.5d0)
   d=3*z*y/rr
   e=(2.d0*(z**2)-(x**2)-(y**2))/rr
   w=((d+c)*dcos(inc))+(e*dsin(inc))
   R=((x**2)+(y**2)+(z**2))**3.32d0
   B=((((a-c)**2)+(w**2))**0.83d0)/R
   return
   end

   function IU(zi)
   implicit double precision (A-I),(O-Z)
   common /xz/ xi,yi,inc,rat
   x=xi
   y=(yi*dcos(inc))-(zi*dsin(inc))
   z=(zi*dcos(inc))+(yi*dsin(inc))
   rr=((x**2)+(y**2)+(z**2))**0.5d0
   a=3*x*z/rr
   c=(rat*y)/(((x**2)+(y**2))**0.5d0)
   d=3*z*y/rr
   e=(2.d0*(z**2)-(x**2)-(y**2))/rr
   w=((d+c)*dcos(inc))+(e*dsin(inc))
   R=((x**2)+(y**2)+(z**2))**3.32d0
   B=((((a-c)**2)+(w**2))**0.83d0)/R
   CC=((a-c)**2)+(w**2)
   DD=2*w*(a-c)
   IU=B*DD/CC
   return
   end

   function IQ(zi)
   implicit double precision (A-I),(O-Z)
   common /xz/ xi,yi,inc,rat
   x=xi
   y=(yi*dcos(inc))-(zi*dsin(inc))
   z=(zi*dcos(inc))+(yi*dsin(inc))
   rr=((x**2)+(y**2)+(z**2))**0.5d0
   a=3*x*z/rr
   c=(rat*y)/(((x**2)+(y**2))**0.5d0)
   d=3*z*y/rr
   e=(2.d0*(z**2)-(x**2)-(y**2))/rr
   w=((d+c)*dcos(inc))+(e*dsin(inc))
   R=((x**2)+(y**2)+(z**2))**3.32d0
   B=((((a-c)**2)+(w**2))**0.83d0)/R
   AA=((a-c)**2)-(w**2)
   CC=((a-c)**2)+(w**2)
   IQ=B*AA/CC
   return
   end
```